6-2015

Acclimatization to High-Altitude, Long-Term Hypoxia Alters BK Channel Structure and Function

Xiaoxiao Tao

LOMA LINDA UNIVERSITY
School of Medicine
in conjunction with the
Faculty of Graduate Studies

Acclimatization to High-Altitude, Long-Term Hypoxia Alters BK Channel Structure and Function

by

Xiaoxiao Tao

A Dissertation submitted in partial satisfaction of
the requirements for the degree of
Doctor of Philosophy in Pharmacology

June 2015

Each person whose signature appears below certifies that this dissertation in his/her opinion is adequate, in scope and quality, as a dissertation for the degree Doctor of Philosophy.

_____, Chairperson

David A. Hessinger, Professor of Physiology and Pharmacology, of Biochemistry and Natural Sciences

_____

John N. Buchholz, Professor of Physiology and Pharmacology

_____

Lawrence D. Longo, Distinguished Professor of Gynecology and Obstetrics, of Physiology and Pharmacology, and of Biochemistry

_____

Subburaman Mohan, Research Professor of Medicine, Biochemistry and Physiology

_____

Kylie J. Watts, Assistant professor of Microbiology and Molecular Genetics

_____

Lubo Zhang, Professor of Physiology and Pharmacology

ACKNOWLEDGEMENTS

I would like to express my deepest gratitude to Dr. Hessinger who provided a great opportunity for me to learn the things that I have always wanted to learn. His way of thinking science and his way of doing science inspired me to continue to discover its secrets. I want to thank you for all of your time, money, energy and passion that you have invested in me, and hope that you will be satisfied with and be proud of the scientist you have carved with your efforts.

I would also like to thank all my committee members for their advice and direction. And Dr. Longo, for his motto, persevere, that kept me going.

To Dr. Thorington, our special lab member, thank you for all the help that will always be remembered. To those in the Hessinger laboratory with whom I have collaborated or worked with during all those years, thank you for your time, support, and efforts.

To my dear mother in heaven, Xiaosu Shu, I want to dedicate this to you as my sincere present, wish you could understand me and all those psychological struggles and fights that you had been putting up with me. I do love you more than anything else in this world. I do cherish all those years, all those memories and all the endless support.

And finally, I would like to thank God for providing me the undeserved opportunity to study His creation and marvel in its complexity. And all Your guidance that came along with me and made me believe and have faith in that there will always be lights at the end of the tunnel that shined upon by You.

CONTENTS

TABLES

Tables Page

Chapter 2

Chapter 3

FIGURES

Figures Page

Chapter 1

Chapter 2

Chapter 3

ABSTRACT OF THE DISSERTATION

Acclimatization to High-Altitude, Long-Term Hypoxia
Alters BK Channel Structure and Function

Xiaoxiao Tao

Doctor of Philosophy, Graduate Program in Pharmacology
Loma Linda University, June 2015
Dr. David A. Hessinger, Chairperson

We examined the major possible mechanisms for the left shift of the BK channel I-V relationship in native basilar artery myocytes from the two LTH groups. These mechanisms included: differential expression of the accessary BK β-1 subunit; differential phosphorylation of the BKα subunit; and splice variation of the BKα subunit. Using molecular cloning, heterologous expression, and patch-clamp electrophysiology techniques, we elucidated a mechanism that, at least in part, contributes to the differences we observed between channels from native normoxic and LTH myocytes.

CHAPTER ONE

INTRODUCTION

BK Channel

BK Channel Structure

Large-conductance, calcium-activated potassium channels (BK channels) were first functionally observed in snail neurons as a calcium-dependent potassium current (47). Subsequently, they were observed and cloned from various organisms (3,12,13,61).

BK channels, like many membrane proteins, undergo transcriptional and post-transcriptional regulation. The BK channel is a tetrameric assembly of both α and β subunits. BK channel α subunits are polypeptides of 120-140 kDa encoded by a single gene *Slo* or KCNMA1, which can be spliced at several sites. Unique among potassium channels, BK α comprises seven transmembrane domains (S0-S6), placing the smaller N-terminus extracellularly and the large C-terminus intracellularly. The intracellular domain contains four hydrophobic segments (S7-S10), two regulating conductance of potassium domains (RCK-high affinity and low affinity), a stretch of aspartate residures are known as the calcium bowl (5, 52), and a conserved c type heme binding motif (CKACH) (70) (Fig 1).

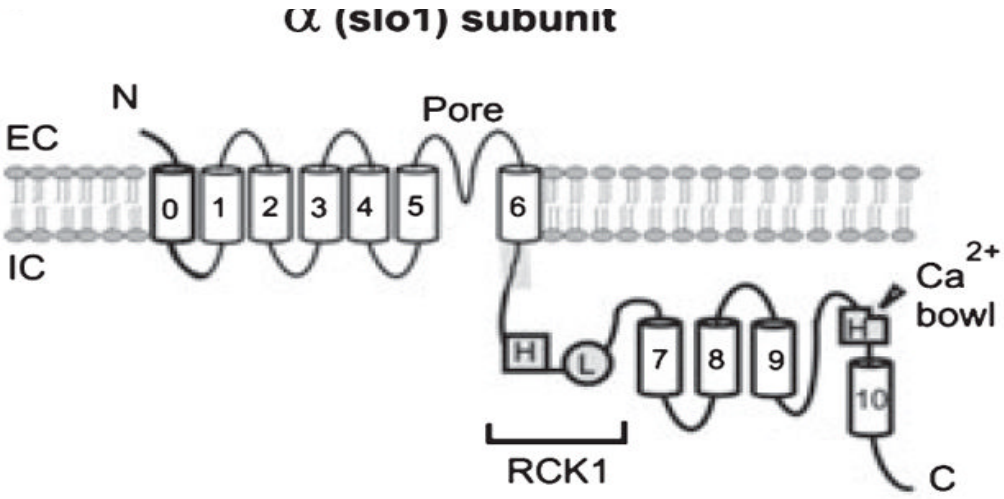

Figure 1. BK α has seven transmembrane domains (S0-S6), and four intracellular hydrophobic regions (S7-S10). The pore domain, the calcium bowl and RCK1 H (high affinity) and L (low affinity) are also shown. EC, Extracellular; IC, Intracellular.

Auxiliary Subunit

BK channel β subunits are auxiliary components of BK channels. They are a small group of highly conserved proteins with two transmembrane domains, short intracellular N- and C-termini and a large extracellular region and a molecular weight of about 25-30 kDa. Expressions of four subtypes have been identified (β1, β2, β3 and β4) in various tissue types (4, 30, 48, 74). In general, as an auxiliary subunit, the β subunit interacts with the channel-forming α subunit in several ways: interacting with the STREX exon (58); and β4 subunits down regulate α subunits (74). The principal action of the β subunit is to increase channel burst duration, which results in an apparent increase in calcium sensitivity (59). For vascular smooth muscle cells, the major subtype of β subunit is β1 (23). Estradiol (estrogen) activates BK channels via the β1 subunit (73) and regulates β1 gene expression (53).

Electrophysiologically, β1 subunit increases the apparent calcium sensitivity of the BK α subunit (48). In genetic hypertension, diabetes, and aging, the β1 subunits are down regulated in vascular smooth muscle cells (1, 42, 55), so β1 subunit expression may protect against some types of hypertension (54).

Regulation of BK Channel

Posttranslational Modification of BK Channel Protein

Phosphorylation and glycosylation (17) are the two major forms of BK channel post-translational modification. Phosphorylation of ion channels is one of the most dynamic regulatory mechanisms for controlling ion channel function under various circumstances.

One example is that PKA can confer totally different effects on two alternatively spliced *Slo* variants in *Aplysia* neuron (82). Our lab's previous finding suggests that developmentally regulated BK channel-associated phosphatases and kinases can differentially phosphorylate this channel and, thereby, modulate calcium affinity (37, 38, 39).

PKA, PKG and PKC all regulate BK channel function by phosphorylating the channel protein (71, 75, 83, 84, 85, 86). PKA activates the BK channel, as does PKG (38, 39). However, PKC inhibits BK channel in rat pituitary tumor (GH3) cells (65), and reduces the BK current in rat tail artery smooth muscle cells (62).

Alternative Splicing

Alternative splicing is a selective, post-transcriptional mechanism by which a gene can be translated into isoforms of varied functions. The BK a subunit (BK α) is highly alternatively spliced. Alternatively spliced transcripts can be species specific or tissue specific. Splice variants show distinct channel properties, including changes in conductance, open probability, calcium sensitivity (34), channel kinetics (66).

Regulators of splicing can be modulated by phosphorylation and nuclear-cytoplasmic redistribution (45). One of the regulators, PTB, is a RNA binding protein that is inversely correlated with specific splicing events (15). PTB levels are high in the late embryonic stage and decline with time. *Slo* splice variants can also alter BKα and BKβ surface expression (29, 80, 81).

Alternative splicing is one of the major mechanisms for generating protein diversity in the course of evolution (14). The BK channel, which responds to a wide

variety of physiological and environmental stimuli, is a good candidate for this regulatory mechanism. Evolutionary convergence of alternative splicing in voltage-gated sodium channels, calcium channels, and BK channels occurred independently in different lineages despite the fact that they share tandem exon duplications. Splicing makes channel modification faster at the post-transcriptional stage and more precise than repression of whole genes (9).

One of the most studied alternatively spliced exons of BK is STREX, which when present, is a cysteine rich domain within the C-terminal region (60) that increases the voltage sensitivity of the channel. The expression of the STREX insert in BK channels can be induced by androgens, and inhibited by glucocorticoids in bovine chromaffin cells (35). Testosterone, (43) estrogen, progesterone, pregnancy (87), stress (36, 78, 46), and development (41) can regulate the expression of the STREX exon. Hair cells from rat (33) and from turtle (25, 26, 27) show the greatest numbers of BK splice variants, which are used to tune the frequency the inner ear.

RNA Editing

RNA editing, unlike alternative splicing, is a more subtle change in protein structure, generally involving single nucleotide changes (28). There are growing numbers of receptors and ion channels that have been identified as highly edited isoforms (*e.g.* glycine receptors (49), NMDA receptors (24), AMPA receptors, serotonin receptors, Na/K ATPase, and squid Kv channels) (63, 64). The major form of RNA editing is A-to-I editing (63), which is catalyzed by adenosine deaminases acting on RNA (ADARs). ADARs can also modulate siRNA and miRNA pathways. Thus, ADARs can influence

gene expression by several distinct pathways and mechanisms (22, 57). Although single-nucleotide polymorphisms (SNPs) in vascular BK channels have been reported both for α and β subunits (31), there is currently no literature suggesting that BK channel RNA is edited. SNPs can cause loss- or gain-of-function of the channels. Epigenetic mechanism can influence the post-transcriptional expression of BK channels (72), which could explain that under LTH conditions, SNPs can be induced or mediated by low oxygen levels. Single amino acid mutation may be attributed to the opposing ethanol effects in BK channels from vascular smooth muscle cell and neuron. (40)

Transcriptional Control of BK channel Expression

Work done by Atkinson's group using *Drosophila* suggests that tissue-specific expression of splice variants are modulated by development using different promoters and various transcriptional factors (2, 6, 7, 8). These studies indicate that BK channels are alternatively spliced at different developmental stages (79) in conjunction with multiple promoters and transcriptional start sites (32), which potentially make the BK channel a much more diversified molecule. This property might give rise to different channel isoforms even in the same tissue (*e.g.* vascular smooth muscle), but in different locations (*e.g.* basilar *vs.* mid cerebral *vs.* pulmonary arteries) in mammals.

Significance

Cerebral Circulation, BK Channel and High Altitude Hypoxia

The brain is the least tolerant of hypoxia of all the organs. Interruption of cerebral blood flow for a few seconds causes unconsciousness. Hypoxia persisting for a few

minutes will cause irreversible brain damage. The basilar artery, one of the major arteries that supply blood to the brain, specifically the brain stem and pons, has a high density of large conductance, calcium activated potassium channels (BK channels) in its smooth muscle myocytes compared to peripheral vessels e.g. pulmonary artery (unpublished findings). BK channels have been reported to be able to sense oxygen indirectly (76). During brain hypoxia, either acute or long term, the cerebral vasculature adapts to maintain adequate blood flow to the brain. Thus, cerebral vasculature BK channels are crucial during hypoxia regulation of the brain circulation. .

Basilar artery is one of the major arteries that supply oxygen to the brain. The two vertebral arteries and the basilar artery are sometimes together called the vertebrobasilar system, which supplies blood to the posterior part of circle of Willis and anastomoses with blood supplied to the anterior part of the circle of Willis from the carotid arteries including brain stem and pons. Ischemia or hemorrhage of the basilar artery can cause locked-in syndrome in which a patient is aware and awake, but cannot move or communicate verbally due to complete paralysis of nearly all voluntary muscles in the body except for the eyes. The more critical condition is that hypoxia and ischemia of the brainstem can lead to death.

Long-term hypoxia, such as occurs in high altitude adaptation by humans, has fundamental physiological and clinical implications, especially in perinatal biology. Millions of people currently live at altitudes higher than 2500 meters, where oxygen supply is limited. At such high altitude and above, a series of physiological events occur, in which cerebral blood flow velocity decreases, in particular, in the basilar artery in children and adolescents (19). Research done at Himalayan high-altitudes (4200m)

showed that cerebral autoregulation becomes critically impaired (21). Research also suggested that cerebral vascular responses might be impaired in Andean high altitudes dwellers (56). However, little is known about the molecular mechanisms by which the developing brain adapts under such hypoxic conditions.

Molecules That Target BK channels

The BK channel is a major regulatory ion channel in excitable cells, including muscle and neurons. In vascular smooth muscle cells, it is a major regulator of vascular tone (68). BK channels couple membrane potential and intracellular calcium concentration. Once activated by an increase in intracellular calcium, BK channels give rise to an efflux of potassium which hyperpolarizes the membrane potential (5). Because of its important roles, the BK channel is a highly regulated cellular target. It can be directly regulated by heme (70), reactive oxygen species (69), carbon monoxide (20, 77), nitric oxide (67) and estrogen (73). Clinically, recombinant BK channels have been used to treat erectile dysfunction (50). Also, BK channel openers have been shown to have protective effects in stroke (16). In addition, BK channels, along with GABA receptors (18), glycine receptors (44, 51) and NMDA receptors and other ion channels are considered to be pharmacological targets of ethanol (10). BK channels show the highest sensitivity to ethanol and all ethanol-resistant mutants of *C. elegans* have BK channel loss-of-function mutations (11). These findings suggest that BK channel is the most susceptible target, especially at lower, physiologically relevant levels of ethanol.

Hypothesis

My working hypothesis is that observed functional differences between the BK channels of LTH and NX basilar artery smooth muscle cells are due to splice variation of the BKα subunit.

References

1. Amberg GC, Santana LF. Downregulation of the BK channel beta1 subunit in genetic hypertension. Circ Res. 2003 Nov 14;93(10):965-71.

2. Atkinson NS, Brenner R, Chang W, Wilbur J, Larimer JL, Yu J. Molecular separation of two behavioral phenotypes by a mutation affecting the promoters of a Ca-activated K channel. J Neurosci. 2000 Apr 15;20(8):2988-93.

3. Atkinson NS, Robertson GA, Ganetzky B. A component of calcium-activated potassium channels encoded by the Drosophila slo locus. Science. 1991 Aug 2;253(5019):551-5.

4. Behrens R, Nolting A, Reimann F, Schwarz M, Waldschütz R, Pongs O. hKCNMB3 and hKCNMB4, cloning and characterization of two members of the large-conductance calcium-activated potassium channel beta subunit family. FEBS Lett. 2000 May 26;474(1):99-106.

5. Berkefeld H, Fakler B, Schulte U. Ca^{2+}-activated K^{+} channels: from protein complexes to function. Physiol Rev. 2010 Oct;90(4):1437-59.

6. Bohm RA, Wang B, Brenner R, Atkinson NS. Transcriptional control of $Ca^{(2+)}$-activated $K^{(+)}$ channel expression: identification of a second, evolutionarily conserved, neuronal promoter. J Exp Biol. 2000 Feb;203(Pt 4):693-704.

7. Brenner R, Atkinson N. Developmental- and eye-specific transcriptional control elements in an intronic region of a $Ca^{(2+)}$-activated $K^{(+)}$ channel gene. Dev Biol. 1996 Aug 1;177(2):536-43.

8. Chang WM, Bohm RA, Strauss JC, Kwan T, Thomas T, Cowmeadow RB, Atkinson NS. Muscle-specific transcriptional regulation of the slowpoke $Ca^{(2+)}$-activated $K^{(+)}$ channel gene. J Biol Chem. 2000 Feb 11;275(6):3991-8.

9. Copley RR. Evolutionary convergence of alternative splicing in ion channels. Trends Genet. 2004 Apr;20(4):171-6.

10. Crowder CM. Ethanol targets: a BK channel cocktail in C. elegans. Trends Neurosci. 2004 Oct;27(10):579-82.

11. Davies AG, Pierce-Shimomura JT, Kim H, VanHoven MK, Thiele TR, Bonci A, Bargmann CI, McIntire SL. A central role of the BK potassium channel in behavioral responses to ethanol in C. elegans. Cell. 2003 Dec 12;115(6):655-66.

12. Elkins T, Ganetzky B. The roles of potassium currents in Drosophila flight muscles. J Neurosci. 1988 Feb;8(2):428-34.

13. Elkins T, Ganetzky B, Wu CF. A Drosophila mutation that eliminates a calcium-dependent potassium current. Proc Natl Acad Sci U S A. 1986 Nov;83(21):8415-9.

14. Ermakova EO, Nurtdinov RN, Gelfand MS. Fast rate of evolution in alternatively spliced coding regions of mammalian genes. BMC Genomics. 2006 Apr 18;7:84.

15. Grabowski PJ, Black DL. Alternative RNA splicing in the nervous system. Prog Neurobiol. 2001 Oct;65(3):289-308.

16. Gribkoff VK, Starrett JE Jr, Dworetzky SI, Hewawasam P, Boissard CG, Cook DA, Frantz SW, Heman K, Hibbard JR, Huston K, Johnson G, Krishnan BS, Kinney GG, Lombardo LA, Meanwell NA, Molinoff PB, Myers RA, Moon SL, Ortiz A, Pajor L, Pieschl RL, Post-Munson DJ, Signor LJ, Srinivas N, Taber MT, Thalody G, Trojnacki JT, Wiener H, Yeleswaram K, Yeola SW. Targeting acute ischemic stroke with a calcium-sensitive opener of maxi-K potassium channels. Nat Med. 2001 Apr;7(4):471-7.

17. Hagen BM, Sanders KM. Deglycosylation of the beta1-subunit of the BK channel changes its biophysical properties. Am J Physiol Cell Physiol. 2006 Oct;291(4):C750-6.

18. Hanchar HJ, Dodson PD, Olsen RW, Otis TS, Wallner M. Alcohol-induced motor impairment caused by increased extrasynaptic GABA(A) receptor activity. Nat Neurosci. 2005 Mar;8(3):339-45.

19. Hogan AM, Virues-Ortega J, Botti AB, Bucks R, Holloway JW, Rose-Zerilli MJ, Palmer LJ, Webster RJ, Baldeweg T, Kirkham FJ. Development of aptitude at altitude. Dev Sci. 2010 May;13(3):533-44.

20. Jaggar JH, Leffler CW, Cheranov SY, Tcheranova D, E S, Cheng X. Carbon monoxide dilates cerebral arterioles by enhancing the coupling of Ca2+ sparks to Ca2+-activated K+ channels. Circ Res. 2002 Oct 4;91(7):610-7.

21. Jansen GF, Basnyat B. Brain blood flow in Andean and Himalayan high-altitude populations: evidence of different traits for the same environmental constraint. J Cereb Blood Flow Metab. 2010 Aug 25.

22. Jepson JE, Reenan RA. RNA editing in regulating gene expression in the brain. Biochim Biophys Acta. 2007

23. Jiang Z, Wallner M, Meera P, Toro L. Human and rodent MaxiK channel beta-subunit genes: cloning and characterization. Genomics. 1999 Jan 1;55(1):57-67.

24. Jin C, Woodward JJ. Effects of 8 different NR1 splice variants on the ethanol inhibition of recombinant NMDA receptors. Alcohol Clin Exp Res. 2006 Apr;30(4):673-9.

25. Jones EM, Gray-Keller M, Art JJ, Fettiplace R. The functional role of alternative splicing of $Ca^{(2+)}$-activated K^+ channels in auditory hair cells. Ann N Y Acad Sci. 1999 Apr 30;868:379-85.

26. Jones EM, Gray-Keller M, Fettiplace R. The role of Ca^{2+}-activated K^+ channel spliced variants in the tonotopic organization of the turtle cochlea. J Physiol. 1999 Aug 1;518 (Pt 3):653-65.

27. Jones EM, Laus C, Fettiplace R. Identification of $Ca^{(2+)}$-activated K^+ channel splice variants and their distribution in the turtle cochlea. Proc Biol Sci. 1998 Apr 22;265(1397):685-92.

28. Keegan LP, Gallo A, O'Connell MA. The many roles of an RNA editor. Nat Rev Genet. 2001 Nov;2(11):869-78. Review.

29. Kim EY, Ridgway LD, Zou S, Chiu YH, Dryer SE. Alternatively spliced C-terminal domains regulate the surface expression of large conductance calcium-activated potassium channels. Neuroscience. 2007 Jun 8;146(4):1652-61.

30. Knaus HG, Garcia-Calvo M, Kaczorowski GJ, Garcia ML. Subunit composition of the high conductance calcium-activated potassium channel from smooth muscle, a representative of the mSlo and slowpoke family of potassium channels. J Biol Chem. 1994 Feb 11;269(6):3921-4.

31. Köhler R. Single-nucleotide polymorphisms in vascular Ca2+-activated K+-channel genes and cardiovascular disease. Pflugers Arch. 2010 Jul;460(2):343-51.

32. Kundu P, Alioua A, Stefani E, Toro L. Regulation of mouse Slo gene expression: multiple promoters, transcription start sites, and genomic action of estrogen. J Biol Chem. 2007 Sep 14;282(37):27478-92.

33. Langer P, Gründer S, Rüsch A. Expression of Ca^{2+}-activated BK channel mRNA and its splice variants in the rat cochlea. J Comp Neurol. 2003 Jan 6;455(2):198-209.

34. Lagrutta A, Shen KZ, North RA, Adelman JP. Functional differences among alternatively spliced variants of Slowpoke, a Drosophila calcium-activated potassium channel. J Biol Chem. 1994 Aug 12;269(32):20347-51.

35. Lai GJ, McCobb DP. Opposing actions of adrenal androgens and glucocorticoids on alternative splicing of Slo potassium channels in bovine chromaffin cells. Proc Natl Acad Sci U S A. 2002 May 28;99(11):7722-7.

36. Lai GJ, McCobb DP. Regulation of alternative splicing of Slo K+ channels in adrenal and pituitary during the stress-hyporesponsive period of rat development. Endocrinology. 2006 Aug;147(8):3961-7.

37. Lin MT, Hessinger DA, Pearce WJ, Longo LD. Developmental differences in Ca^{2+}-activated K^+ channel activity in ovine basilar artery. Am J Physiol Heart Circ Physiol. 2003 Aug;285(2):H701-9. Epub 2003.

38. Lin MT, Hessinger DA, Pearce WJ, Longo LD. Modulation of BK channel calcium affinity by differential phosphorylation in developing ovine basilar artery myocytes. Am J Physiol Heart Circ Physiol. 2006 Aug;291(2):H732-40.

39. Lin MT, Longo LD, Pearce WJ, Hessinger DA. Ca^{2+}-activated K^+ channel-associated phosphatase and kinase activities during development. Am J Physiol Heart Circ Physiol. 289(1):H414-25, 2005

40. Liu J, Asuncion-Chin M, Liu P, Dopico AM. CaM kinase II phosphorylation of slo Thr107 regulates activity and ethanol responses of BK channels. Nat Neurosci. 2006 Jan;9(1):41-9.

41. MacDonald SH, Ruth P, Knaus HG, Shipston MJ. Increased large conductance calcium-activated potassium (BK) channel expression accompanied by STREX variant downregulation in the developing mouse CNS. BMC Dev Biol. 2006 Jul 27;6:37.

42. McGahon MK, Dash DP, Arora A, Wall N, Dawicki J, Simpson DA, Scholfield CN, McGeown JG, Curtis TM. Diabetes downregulates large-conductance $Ca^{(2+)}$-activated potassium beta 1 channel subunit in retinal arteriolar smooth muscle. Circ Res. 2007 Mar 16;100(5):703-11.

43. Mahmoud SF, McCobb DP. Regulation of Slo potassium channel alternative splicing in the pituitary by gonadal testosterone. J Neuroendocrinol. 2004 Mar;16(3):237-43.

44. Mascia MP, Wick MJ, Martinez LD, Harris RA. Enhancement of glycine receptor function by ethanol: role of phosphorylation. Br J Pharmacol. 1998 Sep;125(2):263-70.

45. Matlin AJ, Clark F, Smith CW. Understanding alternative splicing: towards a cellular code. Nat Rev Mol Cell Biol. 2005 May;6(5):386-98.

46. McCobb DP, Hara Y, Lai GJ, Mahmoud SF, Flügge G. Subordination stress alters alternative splicing of the Slo gene in tree shrew adrenals. Horm Behav. 2003 Jan;43(1):180-6.

47. Meech RW. The sensitivity of Helix aspersa neurones to injected calcium ions. J Physiol. 1974 Mar;237(2):259-77.

48. Meera P, Wallner M, Toro L. A neuronal beta subunit (KCNMB4) makes the large conductance, voltage- and $Ca^{(2+)}$-activated K^+ channel resistant to charybdotoxin and iberiotoxin. Proc Natl Acad Sci U S A. 2000 May 9;97(10):5562-7.

49. Meier JC, Henneberger C, Melnick I, Racca C, Harvey RJ, Heinemann U, Schmieden V, Grantyn R. RNA editing produces glycine receptor alpha3(P185L), resulting in high agonist potency. Nat Neurosci. 2005 Jun;8(6):736-44. Epub 2005 May 15.

50. Melman A, Bar-Chama N, McCullough A, Davies K, Christ G. The first human trial for gene transfer therapy for the treatment of erectile dysfunction: preliminary results. Eur Urol. 2005 Aug;48(2):314-8.

51. Mihic SJ, Ye Q, Wick MJ, Koltchine VV, Krasowski MD, Finn SE, Mascia MP, Valenzuela CF, Hanson KK, Greenblatt EP, Harris RA, Harrison NL. Sites of alcohol and volatile anaesthetic action on GABA(A) and glycine receptors. Nature. 1997 Sep 25;389(6649):385-9.

52. Mulholland PJ, Hopf FW, Bukiya AN, Martin GE, Liu J, Dopico AM, Bonci A, Treistman SN, Chandler LJ. Sizing up ethanol-induced plasticity: the role of small and large conductance calcium-activated potassium channels. Alcohol Clin Exp Res. 2009 Jul;33(7):1125-35.

53. Nagar D, Liu XT, Rosenfeld CR. Am J Physiol Heart Circ Physiol. Estrogen regulates {beta}1-subunit expression in $Ca^{(2+)}$-activated K^+ channels in arteries from reproductive tissues. 2005 Oct;289(4):H1417-27. Epub 2005 May 27.

54. Nelson MT, Bonev AD. The beta1 subunit of the Ca^{2+}-sensitive K^+ channel protects against hypertension. J Clin Invest. 2004 Apr;113(7):955-7.

55. Nishimaru K, Eghbali M, Lu R, Marijic J, Stefani E, Toro L. Functional and molecular evidence of MaxiK channel beta1 subunit decrease with coronary artery ageing in the rat. J Physiol. 2004 Sep 15;559(Pt 3):849-62.

56. Norcliffe LJ, Rivera-Ch M, Claydon VE, Moore JP, Leon-Velarde F, Appenzeller O, Hainsworth R. Cerebrovascular responses to hypoxia and hypocapnia in high-altitude dwellers. J Physiol. 2005 Jul 1;566(Pt 1):287-94.

57. O'Connell MA. RNA editing: rewriting receptors. Curr Biol. 1997 Jul 1;7(7):R437-9.

58. Petrik D, Brenner R. Regulation of STREX exon large conductance, calcium-activated potassium channels by the beta4 accessory subunit. Neuroscience. 2007 Nov 23;149(4):789-803.

59. Ramanathan K, Michael TH, Fuchs PA. beta subunits modulate alternatively spliced, large conductance, calcium-activated potassium channels of avian hair cells. J Neurosci. 2000 Mar 1;20(5):1675-84.

60. Saito M, Nelson C, Salkoff L, Lingle CJ. A cysteine-rich domain defined by a novel exon in a slo variant in rat adrenal chromaffin cells and PC12 cells. J Biol Chem. 1997 May 2;272(18):11710-7.

61. Salkoff LB, Wyman RJ. Ion currents in Drosophila flight muscles. J Physiol. 1983 Apr;337:687-709.

62. Schubert R, Noack T, Serebryakov VN. Protein kinase C reduces the K_{Ca} current of rat tail artery smooth muscle cells. Am J Physiol. 1999 Mar;276(3 Pt 1):C648-58.

63. Seeburg PH. A-to-I editing: new and old sites, functions and speculations. Neuron. 2002 Jul 3;35(1):17-20.

64. Seeburg PH, Hartner J. Regulation of ion channel/neurotransmitter receptor function by RNA editing. Curr Opin Neurobiol. 2003 Jun;13(3):279-83.

65. Shipston MJ, Armstrong DL. Activation of protein kinase C inhibits calcium-activated potassium channels in rat pituitary tumour cells. J Physiol. 1996 Jun 15;493 (Pt 3):665-72.

66. Silberberg SD, Lagrutta A, Adelman JP, Magleby KL. Wanderlust kinetics and variable $^{Ca(2+)}$-sensitivity of Drosophila, a large conductance $Ca^{(2+)}$-activated K^+ channel, expressed in oocytes. Biophys J. 1996 Jun;70(6):2640-51.

67. Silva JM, Lewis DL. Nitric oxide enhances $Ca^{(2+)}$-activated K^+ channel activity in rat carotid body cells. Pflugers Arch. 2002 Mar;443(5-6):671-5.

68. Szado T, McLarnon M, Wang X, van Breemen C. Role of sarcoplasmic reticulum in regulation of tonic contraction of rabbit basilar artery. Am J Physiol Heart Circ Physiol. 2001 Oct;281(4):H1481-9.

69. Tang XD, Garcia ML, Heinemann SH, Hoshi T. Reactive oxygen species impair Slo1 BK channel function by altering cysteine-mediated calcium sensing. Nat Struct Mol Biol. 2004 Feb;11(2):171-8. Epub 2004 Jan 25.

70. Tang XD, Xu R, Reynolds MF, Garcia ML, Heinemann SH, Hoshi T. Haem can bind to and inhibit mammalian calcium-dependent Slo1 BK channels. Nature. 2003 Oct 2;425(6957):531-5.

71. Tian L, Coghill LS, MacDonald SH, Armstrong DL, Shipston MJ. Leucine zipper domain targets cAMP-dependent protein kinase to mammalian BK channels. J Biol Chem. 2003 Mar 7;278(10):8669-77.

72. Treistman SN, Martin GE. BK Channels: mediators and models for alcohol tolerance. Trends Neurosci. 2009 Dec;32(12):629-37.

73. Valverde MA, Rojas P, Amigo J, Cosmelli D, Orio P, Bahamonde MI, Mann GE, Vergara C, Latorre R. Acute activation of Maxi-K channels (hSlo) by estradiol binding to the beta subunit. Science. 1999 Sep 17;285(5435):1929-31.

74. Weiger TM, Holmqvist MH, Levitan IB, Clark FT, Sprague S, Huang WJ, Ge P, Wang C, Lawson D, Jurman ME, Glucksmann MA, Silos-Santiago I, DiStefano PS,

Curtis R. A novel nervous system beta subunit that downregulates human large conductance calcium-dependent potassium channels. J Neurosci. 2000 May 15;20(10):3563-70.

75. Widmer HA, Rowe IC, Shipston MJ. Conditional protein phosphorylation regulates BK channel activity in rat cerebellar Purkinje neurons. J Physiol. 2003 Oct 15;552(Pt 2):379-91.

76. Williams SE, Wootton P, Mason HS, Bould J, Iles DE, Riccardi D, Peers C, Kemp PJ. Hemoxygenase-2 is an oxygen sensor for a calcium-sensitive potassium channel. Science. 2004 Dec 17;306(5704):2093-7.

77. Xi Q, Tcheranova D, Parfenova H, Horowitz B, Leffler CW, Jaggar JH. Carbon monoxide activates KCa channels in newborn arteriole smooth muscle cells by increasing apparent Ca^{2+} sensitivity of alpha-subunits. Am J Physiol Heart Circ Physiol. 2004 Feb;286(2):H610-8.

78. Xie J, McCobb DP. Control of alternative splicing of potassium channels by stress hormones. Science. 1998 Apr 17;280(5362):443-6.

79. Xing Y, Lee CJ. Protein modularity of alternatively spliced exons is associated with tissue-specific regulation of alternative splicing. PLoS Genet. 2005 Sep;1(3):e34.

80. Zarei MM, Eghbali M, Alioua A, Song M, Knaus HG, Stefani E, Toro L. An endoplasmic reticulum trafficking signal prevents surface expression of a voltage- and Ca^{2+}-activated K^+ channel splice variant. Proc Natl Acad Sci U S A. 2004 Jul 6;101(27):10072-7.

81. Zarei MM, Zhu N, Alioua A, Eghbali M, Stefani E, Toro L. A novel MaxiK splice variant exhibits dominant-negative properties for surface expression. J Biol Chem. 2001 May 11;276(19):16232-9.

82. Zhang Y, Joiner WJ, Bhattacharjee A, Rassendren F, Magoski NS, Kaczmarek LK. The appearance of a protein kinase A-regulated splice isoform of slo is associated with the maturation of neurons that control reproductive behavior. J Biol Chem. 2004 Dec 10;279(50):52324-30. Epub 2004 Sep 16.

83. Zhou XB, Ruth P, Schlossmann J, Hofmann F, Korth M. Protein phosphatase 2A is essential for the activation of Ca^{2+}-activated K^+ currents by cGMP-dependent protein kinase in tracheal smooth muscle and Chinese hamster ovary cells. J Biol Chem. 1996 Aug 16;271(33):19760-7.

84. Zhou XB, Schlossmann J, Hofmann F, Ruth P, Korth M. Regulation of stably expressed and native BK channels from human myometrium by cGMP- and cAMP-dependent protein kinase. Pflugers Arch. 1998 Oct;436(5):725-34.

85. Zhou XB, Wang GX, Ruth P, Hüneke B, Korth M. BK(Ca) channel activation by membrane-associated cGMP kinase may contribute to uterine quiescence in pregnancy. Am J Physiol Cell Physiol. 2000 Dec;279(6):C1751-9.

86. Zhou XB, Arntz C, Kamm S, Motejlek K, Sausbier U, Wang GX, Ruth P, Korth M. A molecular switch for specific stimulation of the BKCa channel by cGMP and cAMP kinase. J Biol Chem. 2001 Nov 16;276(46):43239-45.

87. Zhu N, Eghbali M, Helguera G, Song M, Stefani E, Toro L. Alternative splicing of Slo channel gene programmed by estrogen, progesterone and pregnancy. FEBS Lett. 2005 Aug 29;579(21):4856-60.

CHAPTER TWO

ACCLIMATIZATION TO LONG-TERM HYPOXIA INCREASES CA^{2+}–ACTIVATED K^+ (BK) CHANNEL ACTIVITY IN FETAL AND ADULT OVINE BASILAR ARTERIES

XIAOXIAO TAO[1], MIKE T. LIN[2,4], GLYNE U. THORINGTON[2], SEAN M. WILSON[1,3], LAWRENCE D. LONGO[2,3], AND DAVID A. HESSINGER[1,2]

[1]Division of Pharmacology, [2]Division of Physiology, [3]Center for Perinatal Biology, School of Medicine, Loma Linda University, Loma Linda, California 92350 USA, [4]Department of Physiology, University of South Alabama, Alabama 36688 USA

Abstract

Acclimatization to high-altitude, long-term hypoxia (LTH) alters cerebral artery contraction-relaxation responses associated with changes in K^+ channel activity. We hypothesized that to maintain adequate oxygen perfusion during acclimatization to LTH, basilar arteries (BA) in the ovine near-term fetus would show increased smooth myocyte large-conductance Ca^{2+} activated potassium (BK) channel activity. To measure BK channel activity, expression, and cell surface distribution in isolated fetal and adult BA myocytes, we used patch-clamp electrophysiology, flow cytometry, and confocal microscopy. Several features distinguished BK channels of LTH acclimatized vessels from normoxic controls: 1) BK channel Ca^{2+} set points for both adult and fetal LTH sheep were lower, making LTH channels more sensitive to Ca^{2+} activation; 2) BK channels in LTH myocytes appeared more dephosphorylated; 3) BK channel half-activating voltages of LTH animals were left shifted ~30 mV independently of phosphorylation state; and 4) BK channel dwell times from LTH near-term fetus were longer and more sensitive to changes in phosphorylation state. In addition, the LTH fetus exhibited increased BK b-1 subunit surface expression. Furthermore, both the LTH and normoxic fetuses showed increased BK channel clustering and co-localization to lipid rafts compared to adults, making them more sensitive to Ca^{2+} activation from internal stores.

Key Words: Development, Ca^{2+} signaling, high altitude.

Abbreviations. Apase, alkaline phosphatase; BA, basilar artery; BK, large-conductance, Ca^{2+}–activated K^+ channel; Ca_0, Ca^{2+} set point; CBF; cerebral blood flow; ChTx, cholera toxin; FGR, fetal growth restricted, LTH, long-term hypoxia; PKA, cAMP-dependent

protein kinase; PKG, c-GMP-dependent protein kinase; RT, room temperature; $V_{1/2}$, membrane potential that half activates channels; WGA, wheat germ agglutinin.

Introduction

At high altitude, non-acclimatized adults and the developing fetuses may experience dysregulation of cerebral blood flow (CBF). Infants subjected to hypoxia *in utero* or born prematurely may exhibit decreased auto-regulation of CBF resulting in intraventricular hemorrhage, germinal matrix hemorrhage, or related problems (16). Such developmental complications can result in long-term neurologic sequelae such as cerebral palsy, mental retardation, and epilepsy (13, 41, 58, 63). In non-acclimatized adults, acute mountain sickness (62) and/or high altitude cerebral edema (18) may result. In addition, other clinical disorders feature long-term hypoxia (LTH), including cardiac and vascular disease (15, 54), impaired wound healing (5), cancer (11, 21, 40), and problems in pregnancy, such as an increased prevalence of preeclampsia (57). Thus, LTH can adversely affect fetal and adult health.

Because of its high metabolic activity and oxygen (O_2) requirement, with little or no O_2 stores, the brain is particularly vulnerable to hypoxia. The cerebral vasculature regulates CBF according to the brain's metabolic needs, and maintenance of adequate oxygenated CBF is vital because the brain regulates a myriad of essential physiological processes, as well as consciousness and behavior. During acute, short-term hypoxia, the cerebral vasculature dilates to increase CBF (24), and may contribute to development of cerebral edema and other central neurological disorders associated with high altitude. There is conflicting evidence, however, regarding the nature of cerebrovascular regulation under conditions of long-term hypoxia.

In adult humans at high altitude, CBF generally returns to normal following a transitional period of increased CBF (25, 56). In high-altitude, long-term acclimatized

sheep, middle cerebral artery vascular segments from both LTH adults and near-term fetuses showed significant differences in *ex vivo* contractility (17, 36). Arterial cerebrovascular segments of LTH adults showed significant increases in Ca^{2+} sensitivity, while those of LTH fetuses showed reduced large-conductance, Ca^{2+}-activated K^+ (BK) channel-mediated vasorelaxation (14, 35). Several physiological mechanisms have been proposed to account for the acclimatization response of developing cerebrovascular smooth muscle to long-term hypoxia, including decreased vascular resistance and increased vasodilator release (36). Regarding the LTH fetus, our previous work has suggested that chronic hypoxia may decrease channel density or sensitivity to Ca^{2+} (14). Related to this, A7r5 rat aorta cells cultured under 20-h hypoxia exhibited decreased BK channel open probability and mean open dwell times attributable to decreased BK β-1 subunit mRNA levels, and decreased cell surface BK β-1 expression as measured by flow cytometry (39). These results from LTH fetal sheep and cultured A7r5 rat aorta cells were at odds with the observations that CBF in the LTH fetal lambs did not differ from normoxic controls (26, 46, 60) and seemed counter-intuitive to our assumption that acclimatization of cerebral vasculature to LTH must ensure adequate perfusion to the brain. Because of these disparities between *in vitro* and *in vivo* data, we compared the intrinsic functional properties of natively expressed cerebrovascular BK channels from LTH and normoxic adult and near-term fetal sheep.

Our previous work with normoxic near-term fetal BA in sheep showed that increased BK channel activity was attributable to their higher affinity for Ca^{2+} ions (lower calcium set point, Ca_o) compared to adult (31). On this basis, we hypothesized that cerebrovascular acclimatization to the demands of LTH will involve increased BK

channel activity due to increased channel affinity to Ca^{2+} compared to normoxic controls. In the present study, we show that BK channel activities are increased in both LTH adult and fetal BA myocytes due, in part, to increased BK channel Ca^{2+}affinity. In addition, the near-term fetal myocytes exhibit increased BK β-1 subunit surface expression and BK channel clustering, allowing these channels to detect intracellular Ca^{2+} released from internal stores.

Methods

Experimental Animals

All surgical and experimental procedures were performed within the regulations of the Animal Welfare Act, the National Institutes of Health's Guide for the Care and Use of Laboratory Animals, "The Guiding Principles in the Care and use of Animals" approved by the Council of the American Physiological Society, and the Animal Care and Use Committee of Loma Linda University. Nonpregnant and time-dated pregnant ewes of mixed Western breed were divided between normoxic control (n = 8) and long-term hypoxic (LTH; n = 8) groups. All pregnant and nonpregnant ewes originated from the Nebeker Ranch (Lancaster, CA; elevation 720 m) where they were maintained at near sea level (normoxia) until 30 days gestation. At this time, some of the pregnant and nonpregnant ewes were transported to the Barcroft Laboratory, White Mountain Research Station, Bishop, CA (3,801 m; hypoxia; maternal arterial PO_2: 60 ± 3 Torr; fetal arterial PO_2: 19 ± 2 Torr) for the final 110 days of gestation. At this time, the ewes were transported to Loma Linda University (a 6 to 7 hr trip) for study. After arrival at Loma Linda University Medical Center Animal Research Facility (elevation: 346 m), LTH

ewes were surgically implanted with arterial and tracheal catheters. The adult PO_2 was maintained at approximately 60 Torr by adjusting humidified nitrogen gas flow through the tracheal catheter for several hours to days, as previously described (26), until the animal was euthanized for surgery. Normoxic control pregnant and nonpregnant ewes were maintained near sea level (~300 m) throughout gestation.

At the time of study, ewes were sedated with thiopental sodium (10 mg/kg, iv), and following intubation, anesthesia was maintained with inhalation of 1% isoflurane in O_2 throughout surgery. Following delivery of the fetus by hysterotomy, the fetus and ewes were euthanized with an overdose of Euthacol [pentobarbital sodium (100 mg/kg) and phenytoin sodium (10 mg, kg), Virbao, Ft. Worth, TX]. Fetal or adult brains were removed, placed in iced saline, and basilar arteries were rapidly dissected out.

Artery and Cell Isolation

Arteries were selected from the same anatomic segments of adult and fetal BA to approximate segments of similar function and embryonic origin. Consequently, the adult and fetal arteries were of different diameter (~300 mm vs. 200 mm, respectively). To determine the extent to which arteries of different size within age groups have the same current densities, we sampled current densities from proximal and distal segments of both adult and fetal basilar arteries. We observed no significant differences in current densities within age groups for arteries of different diameter. As described previously, BA smooth muscle cells were enzymatically dissociated and isolated (31).

Whole Cell Current Recordings

Vascular smooth muscle cells adhering to pre-cleaned glass cover slips were mounted in a perfusion chamber containing cell isolation solution for 15 min on the stage of an inverted microscope (Axiovert 35M, Carl Zeiss Instruments). The cell isolation solution then was exchanged for the bathing medium. Normoxic controls and LTH smooth myocytes showed characteristic elongated shapes with axial ratios of about 10:1 for adult, and 5:1 for the fetus.

Positive outward currents were measured in conventional and perforated-patch (23) whole-cell voltage-clamp configurations using an Axopatch 200B amplifier with Clampex 8 (Axon Instruments, Foster City CA). Currents were filtered at 1 kHz, using an Axopatch 200B internal 4-pole low-pass Bessel filter, and digitized at 2 kHz. For perforated-patch recordings, patch pipettes were back-filled with pipette solution containing amphotericin B (see *Reagents and solutions*, below). Due to differences in adult and fetal cell size, as well as within age groups, whole-cell currents were normalized with cell capacitance to obtain current density. An agar salt-bridge was used to minimize the solution junction potential differences.

Single-Channel Recordings

Single-channel currents were recorded from inside-out membrane patches of isolated arterial myocytes (19). Patch pipettes were fabricated using a programmable Flaming-Brown pipette puller and standardized fire polishing procedures. Because the patch pipettes so produced had similar tip resistances (≈15 MΩ), the area of contact with each membrane was also similar (51). Currents were filtered at 2 KHz and digitized at

10 KHz. The number of channels present in any given excised patch (N) was estimated from all-points histograms. Channel activity, NP_o, was calculated by using equation 1.

Equation 1 is $NP_o = \sum_{i=0}^{N} i \cdot Ai / \sum_{i=0}^{N} Ai$,

where i is the number of open channels (0 is the number for closed state), and A_i is the area associated with each channel state, as determined from curve-fit individual peak areas. The single-channel open probability (P_o) was then calculated from NP_o/N. The values for N were obtained by using high [Ca^{2+}] and/or depolarization to ascertain that less than three coincidental open events occurred during long recordings (>20 s) at a P_o higher than 0.8. Preparations with more than three channels present were discarded.

Dwell-Time Analysis

Single channel currents were analyzed with QuB software from SUNY, Buffalo NY (http://www.qub.buffalo.edu). For idealization, half-amplitude threshold analysis was used. Kinetic modeling of the idealized intervals used the maximum interval likelihood method. Dwell-time data were plotted with a logarithmic time x-axis and a square-root y-axis for the number of events in each bin. Bin density was 50 bins per decade.

Flow Cytometry

Freshly dissociated basilar myocytes were filtered in polystyrene round-bottom tubes fitted with cell-strainer caps (100-µm nylon mesh; Fisher Scientific, Chino, CA). Filtration separated the dispersed cells from larger debris and undigested arteries. The filtrate was centrifuged at 600 x g for 10 min at 4 °C. The supernatant was discarded and the pellet re-suspended in 300 µl PBS (in mM): NaCl (137), KCl (2.7), Na_2HPO_4 (10),

KH_2PO_4 (2), pH 7.4. To block non-specific binding, 15 µl of 1% intravenous immunoglobulin (1% solution of human serum IgG) in PBS was added to 100 µl of cell suspension and incubated at 4 ^{0}C for 15 min. After blocking, 1 µl of rabbit primary antibody to BKα-1 (1 mg/ml; cat. no. ab 587; Abcam Inc., Cambridge, MA) and 1µl of phycoerythrin-conjugated goat anti-rabbit IgG (secondary antibody cat. no. 20303; Imgenex Corp., San Diego, CA) were added for 15 min on ice. Cells were washed in 1 ml of PBS and centrifuged at 200 x g for 5 min at 4 ^{0}C. The supernatant was aspirated and the pellet was re-suspended in 200 µl of 1% paraformaldehyde in PBS and stored at 4 ^{0}C. Fixed cells were analyzed within three days. For each experiment, two controls were included consisting of untreated, fixed cells and fixed cells treated with secondary antibody only. For cytometric analysis, a FACsCalibur flow cytometer (BD Biosciences, Billerica, MA) equipped with the Cellquest Program was used.

Flow cytometric data were analyzed using FlowJo software (Tree Star, Ashland, OR), and image profiles were displayed as relative cell number against the log of fluorescence intensity. Histograms from representative experiments were expressed as geometric means ± SEM. Dead cells and debris were excluded (gated out) according to their forward and vertical scattering pattern. To provide sufficient numbers of cells for experiments, cells from two animals were pooled. For comparisons between adult and fetal groups, independent "*t*" tests were used. *P* values of <0.05 were considered to be statistically significant.

Confocal Microscopy Protocol and Analysis

Fresh basilar arteries excised from anesthetized, nonpregnant adult and near-term

fetal sheep were flash frozen with liquid nitrogen in OCT compound (Sakura Biotech, Torrance, CA) and stored at -80 ^{0}C. Frozen sections (10-mm thick) were cut using a cryostat (model CM3050S, Leica Microsystems, Wetzlar, Germany). Sections were air-dried at least 30 min, then fixed with ice-cold acetone for 10 min, followed by washing with room temperature (RT) PBS for 10 min. Sections were blocked with 1% BSA and 2% goat serum in PBS for 1 h, and then incubated with primary anti-BKα antibody (1:200; Cat. No. APC-151; Alomone Labs, Jerusalem, Israel) either at RT for 1 h or at 4 ^{0}C overnight (~ 16 h). Samples were then washed 3 times at RT in PBS for 10 min each. Then samples were incubated with goat anti-rabbit secondary antibody (1:300) conjugated with Alexa 488 (green; Cat. No. A11008, Life Technologies, Carlsbad, CA) at RT for 40 min in the dark. Sections were either counterstained for 15 min with wheat germ agglutinin conjugated to Alexa 594 (AF-594 conjugated WGA; 1:300), a general membrane marker, or with recombinant cholera toxin subunit B (ChTx) conjugated to Alexa 594 (5 mg/ml), a GM1 marker of lipid rafts (20, 38) (red; Cat. No. W11262 and V34777, respectively; Life Technologies) and then with Hoechst dye 33342 **(**0.01mg/ml; blue; Cat. No. H1399; Life Technologies) for 10 min to label cell nuclei. Coverslips (No. 1.5, VWR; 161.3 ± 1.25 mm thickness; n = 8) were then applied to samples.

Prepared slides were viewed and imaged with a LSM710 NLO Confocal system (Zeiss, Jena, Germany) equipped with 63x (n.a. 1.40) oil-immersion objective. Images were acquired with Zen software (Zeiss) at 1024 x 1024 pixels, where each pixel was 0.09 x 0.09 mm. To reduce background noise the pixel dwell time was 0.50 ms and four lines were averaged. To maximize imaging of intact myocytes, care was taken to image from the middle of cut sections. For cluster analysis, we used the particle analysis

function of ImageJ software (49; http://rsb.info.nih.gov/ij) with procedures similar to Kirby *et al.* (27). To measure BKα and ChTx clusters, we examined fluorescence at several incremental intensities above mean levels (52). Particle intensities were examined by converting from gray scale to binary images based on circularity and size criteria. Circularity criterion was set at > 0.1, where circularity (4π Area/Perimeter^2) can range from 0 (infinitely elongated polygon) to 1 (perfect circle). Size criterion was set at > 0.2 mm. Intensity data meeting criteria were collected, saved, and analyzed. Data were collected from an area of 20 x 40 mm per section. BKα and ChTx clusters were based on positive staining for BKα -like green and ChTx-like red fluorescence, respectively. For most purposes we used intensities 3.5-fold above mean intensities as the threshold to define "cluster" because it was the lowest threshold yielding significant differences between fetal and adult intensities. Statistical analysis used GraphPad Prism 5.0 (GraphPad Software, Inc., San Diego, CA). Two-way ANOVA with *post hoc* test comparison and unpaired t test of data sets were performed for each experiment.

For analysis of co-localization, threshold values were set using automated criteria within Coloc_2 software (http://fiji.sc/Coloc_2/), where pixels below threshold had null or anti-correlated intensities. This method gives a Pearson's correlation coefficient (r) of zero for the pixels below the threshold. The correlation coefficients for areas of overlapping expression of BK subunits with ChTx-positive fluorescence were then measured. For ChTx clusters, a threshold of 3-fold above mean was used, while for BKα clusters 3.5-fold was used.

Reagents and Solutions

Papain was obtained from Worthington Biochemical Corporation (Lakewood, NJ). Calcium standards and Fura-2 were obtained from Molecular Probes (Eugene, OR). Free calcium concentrations of patch-clamp solutions were first estimated with Max Chelator Sliders software (C. Patton; Stanford University; 45) and adjusted using fluorometric measurements with Fura-2 and Fura-6 and Ca^{2+} standard kits 2 and 3 (Molecular Probes) for calibration. All other chemicals were obtained from Sigma (St. Louis, MO). For cell isolation, the cell isolation solution contained (in mM): NaCl (55), Na^{+}-glutamate (80), KCl (5.6), $MgCl_2$ (2), glucose (10), and HEPES (10) adjusted to pH 7.3 with NaOH. For perforated-patch recording, the bathing solution contained (in mM): NaCl (134), KCl (6), $MgCl_2$ (1), glucose (10), $CaCl_2$ (2), and HEPES (10) adjusted to pH 7.4 with NaOH. The pipette solution for perforated-patch recordings contained (in mM): K^{+}-aspartate (110), KCl (30), NaCl (10), $MgCl_2$ (1), HEPES (10), and EGTA (0.05) adjusted to pH 7.2 with KOH, containing 200 mg/ml amphotericin B. For conventional whole-cell recording, the bathing solution contained (in mM): NaCl (140), KCl (5), $MgCl_2$ (1), glucose (10), $CaCl_2$ (1.5), and HEPES (10) adjusted to pH 7.4 with NaOH. The pipette solution for whole-cell recordings contained (in mM): K^{+}-gluconate (130), KCl (30), $MgCl_2$ (1), $CaCl_2$ (0.1), EGTA (0.5), and HEPES (5) adjusted to pH 7.2 with KOH. The single-channel bathing solution contained (in mM): KCl (140), Mg^{2+} (1), HEPES (10), and EGTA (5) adjusted to pH 7.2 with KOH with different free Ca^{2+} concentrations (~0.3, 1, 3, and 10 μM) measured fluorometrically using Fura-2. The single-channel pipette solution had the same composition as the bathing solution with ~3 μM free Ca^{2+}.

Data Analysis and Statistics

All values were calculated and displayed as means ± SEM. In all cases, *n* refers to the number of replicate cells. All statistical comparisons were performed at the 95% confidence level using two-sample, unpaired *t*-tests. A "P" value of < 0.05 was considered to be statistically significant. We verified all sample populations to be normally distributed. For comparisons of values that were not significantly different, power analyses were performed to confirm that statistical power was 0.7 and the probability of Type II errors was acceptably small. Curve fitting was performed with GraphPad Prism 5 (GraphPad Software, Inc.).

Results

Comparison of LTH adult and fetal whole-cell currents. In conventional whole-cell preparations, we recorded outward currents from LTH adult and fetal BA myocytes. Cell capacitances from LTH adult and fetal myocytes were 15.2 ± 0.9 pF (n = 6) and 8.3 ± 0.4 pF (n = 7), respectively ($P < 0.05$; Table 1). We recorded total outward currents from cells held at -60 mV followed by a series of depolarizing steps over the range of -60 to +60 mV. Because isolated adult myocytes present about 80% more plasma membrane surface area to the bathing medium than those of the fetus, we normalized raw whole-cell outward currents to membrane capacitance and present current measurements as current densities (Fig. 1A and B). The steady-state outward current density at +60 mV in LTH adult (54.2 ± 4.1 pA/pF; n = 7) was about twice that of fetal myocytes (24.8 ± 3.0 pA/pF; n = 8; $P < 0.01$; Fig. 1C; Table 1).

To determine the contribution of BK current to total whole-cell current density,

we applied paxilline (5×10^{-7} M) to inhibit BK current (53). Paxilline significantly reduced whole-cell current density. The paxilline-sensitive (*i.e.* BK) current density at +60 mV constituted about half (adult: 47.1%, $P < 0.001$ and fetus: 45.2%, $P < 0.001$) of the total outward current densities (Fig. 1C). Both paxilline-sensitive (Fig. 1D) and paxilline-resistant (Fig. 1E) current densities were two-fold greater in LTH adult than in fetal myocytes (Fig. 1C).

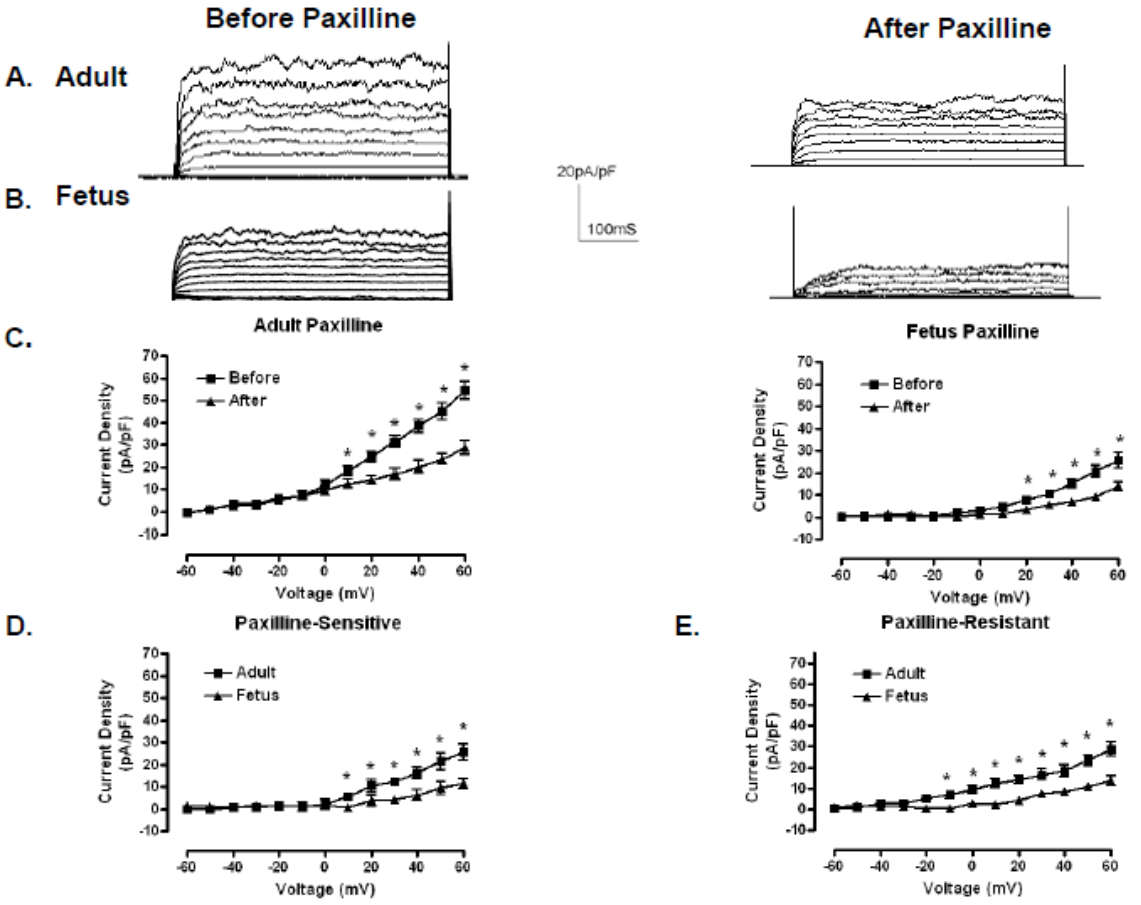

Figure 1. Whole-cell currents from LTH adult and fetal smooth muscle cells. A and B. Representative whole-cell outward membrane current density traces elicited by a series of 10-mV depolarizing steps (-60 to +60 mV) from a holding potential of -60 mV. Traces before (left) and after (right) paxilline application, are shown in typical isolated LTH adult (A) and fetal (B) basilar artery myocytes. Whole-cell current density is obtained from normalized whole cell currents to membrane capacitance to account for size differences between adult and fetal myocytes. C. Averaged steady-state current-voltage plot of outward current density in myocytes obtained from LTH adult (n = 6) and fetal (n = 7) basilar arteries before and after treatment with 5 x 10^{-7} M paxilline. D. Averaged steady-state paxilline-sensitive "BK" currents (left) and residual, paxilline-insensitive currents (right) obtained from digital subtraction of the individual traces such as in A and B. Asterisks (*) denote significant difference with $P < 0.05$.

Table 1. *Summary of conventional and perforated-patch recordings and analyses*.

	LTH		NX[a]	
	Adult	Fetus	Adult	Fetus
Capacitance (pF):				
Conventional whole-cell	15.2 ± 0.9 (6)	8.3 ± 0.4 (7)*	#	#
Perforated-patch	16.1 ± 1.3 (7)	9.4 ± 1.7 (6)*	15.7 ± 0.6	9.1 ± 0.6**
Current density (pA/pF):				
Conventional whole-cell[b]				
Outward current	54.2 ± 4.1 (7)	24.8 ± 3.0 (8)**	#	#
BK current	25.7 ± 3.4	11.2 ± 2.2*	#	#
Non-BK current	28.8 ± 3.2	13.6 ± 2.3*	~29[a]	~26[a]
Perforated-patch[b]				
Outward current	75.1 ± 5.9 (5)	71.6 ± 13 (6)	37.9 ± 1.8	57.9 ± 6.7*
BK current	46.3[c]	58.0[c]	10[a]	29[a]
BK channel parameters:				
Slope (mV/log $[Ca^{2+}]_i$)	65.9 ± 3.3	66.8 ± 3.8	67.1 ± 2.5	67.6 ± 2.7
Ca^{2+} set point (Ca_o, mM)	3.6	3.0	8.8	4.7
Hill coefficient (r_H)	3.3 ± 0.2	3.0 ± 0.3	2.9 ± 0.1	2.9 ± 0.2
Unitary conductance (pS)	215 ± 12	228 ± 7	221 ± 8	229 ± 5

Data are means ± SE, based on a sample size of (n). Conventional (Fig. 1) and perforated-patch (Fig. 9) whole-cell recording yield membrane capacitance and current density. Single-channel recording and analysis (Fig. 2) reveal BK channel parameters and properties. [a], from Lin *et al*. (33); [b], measured at +60 mV; [c], estimated by subtracting "Non-BK current" from perforated-patch "Outward current"; #, not measured;. Compared against adult of same treatment: * $P < 0.05$; ** $P < 0.01$.

Several factors could account for the difference in BK activities between LTH adult and fetal BA myocytes, including differences in channel affinity for Ca^{2+}, differential phosphorylation, and differential expression of BK subunits (*e.g.* α or a). Previously, in normoxic control animals, we showed that higher BK current density in the normoxic fetus was attributable to a higher intracellular affinity for Ca^{2+}, as compared to that of the adult (31). Consequently, we hypothesized that higher BK current density in LTH adult was due to a higher affinity for intracellular Ca^{2+}.

Effects of LTH on BK channel Ca^{2+} affinity. To compare the Ca^{2+} affinity of adult and fetal BK channels, we determined Ca^{2+} set points (Ca_0), where Ca_0 is the Ca^{2+} concentration that half-activates BK channels at 0 mV. The Ca_0 equals the K_d for Ca^{2+} at 0 mV (33). We recorded BK channel activity in inside out, excised patch preparations from LTH adult and fetal BA myocyte membranes (Fig. 2A) and plotted BK channel open probabilities at different voltages and Ca^{2+} concentrations (Fig. 2B). Data were fitted to the Boltzmann equation, and the membrane potential required for 50% activation of channels ($V_{1/2}$) and we plotted the $V_{1/2}$ values against log [Ca^{2+}] (Fig. 2C). From the equation for the line fitted to these data, we estimated the calcium sensitivities from the change in $V_{1/2}$ for a 10-fold change in Ca^{2+} concentration ($\Delta V_{1/2}$) (Table 1). The calcium sensitivities of these two age groups did not differ significantly, nor did they differ significantly from their normoxic controls (Table 1). The Ca_0 values estimated by linear regression were found to be 3.6 μM for LTH adult and 3.0 μM Ca^{2+} for fetal BK channels. However, both were lower than their corresponding normoxic controls (Table 1). Of note, similar Ca_0 values, Hill coefficients, and unitary conductances (Table 1) for LTH adult and fetal BK channels could not account for the two-fold difference in their whole-cell BK channel current densities.

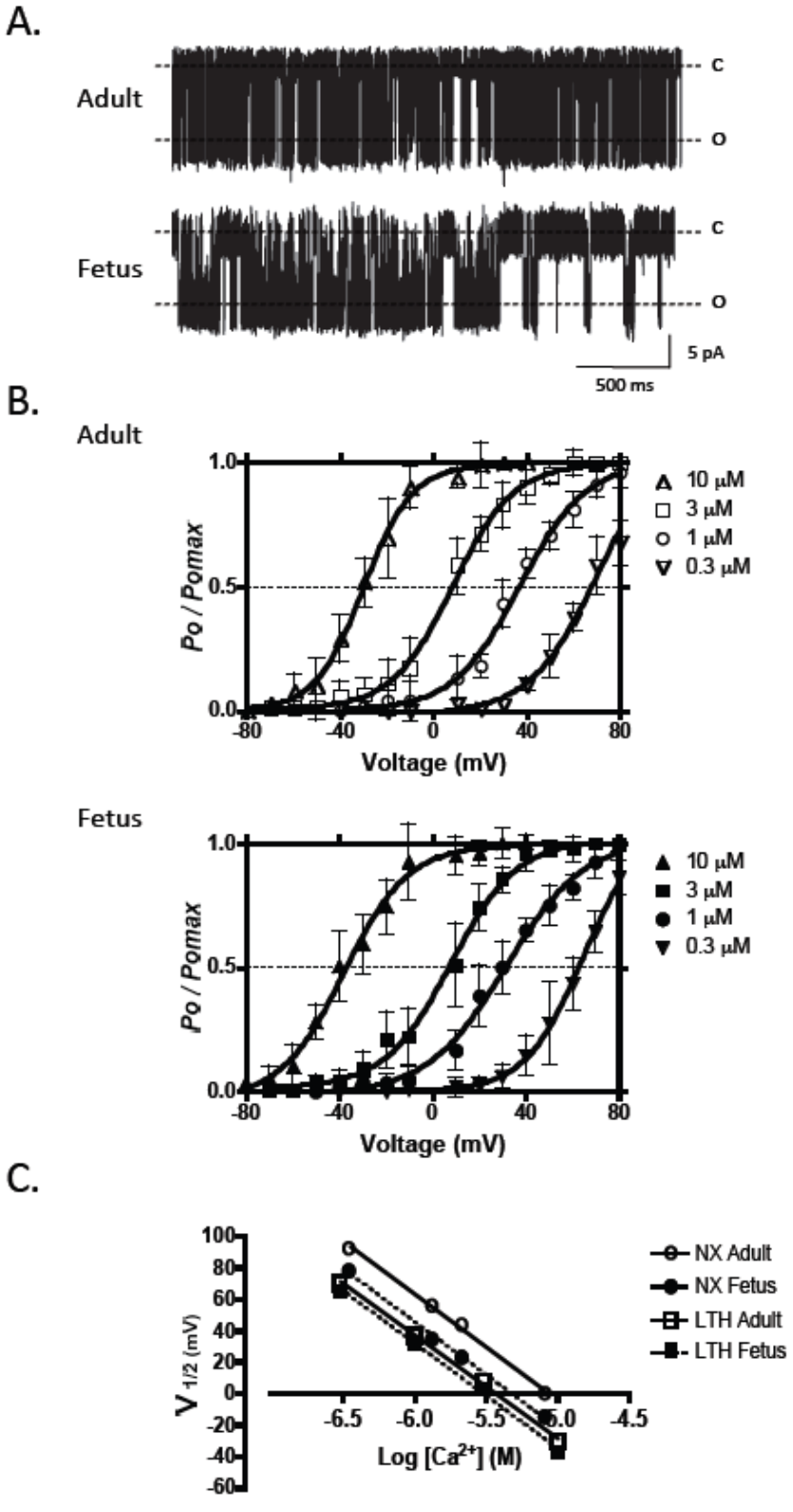
A.
Adult
C
O
Fetus
C
O
5 pA
500 ms
B.
Adult
Po / Pomax
1.0
0.5
0.0
-80
-40
0
40
80
Voltage (mV)
10 μM
3 μM
1 μM
0.3 μM
Fetus
Po / Pomax
1.0
0.5
0.0
-80
-40
0
40
80
Voltage (mV)
10 μM
3 μM
1 μM
0.3 μM
C.
V 1/2 (mV)
100
80
60
40
20
0
-20
-40
-60
-6.5
-6.0
-5.5
-5.0
-4.5
Log [Ca2+] (M)
NX Adult
NX Fetus
LTH Adult
LTH Fetus

Figure 2. BK channel open probabilities and calcium set points. A. Representative inside-out patch recordings of BK channel from LTH adult and fetal smooth muscle cells in symmetrical 140 mM KCl. In both cases, command potentials were -30 mV making BK channels experience +30 mV depolarizations. The bath $[Ca^{2+}]$ was 1.0 μM. Dotted lines represent the channels in closed (C) and open (O) states. B. Voltage activation curves at different membrane potentials in 10-mV increments for various $[Ca^{2+}]_i$. Data are channel open probability (P_o) expressed relative to maximum channel open probability ($P_o max$). Solid lines indicate best-fit curves to the Boltzmann equation: $P_o/P_o max = 1\{1+\exp[(V_{1/2}-V_m)/K]\}$, where $V_{1/2}$ is the membrane potential (V_m) required for half-maximal activation of the channel and K is the logarithmic voltage sensitivity (change in voltage required for an e-fold increase in activity). The voltage sensitivities estimated from the fitted curves were similar for all concentrations of Ca^{2+} tested and indicated that channel activity increased e-fold (~2.72 times) for 23.5 ± 1.8 mV (n = 4, adult) and 25.0 ± 2.1 mV (n = 4, fetus) depolarizations. C. Estimation of changes in $V_{1/2}$ for a 10-fold change in $[Ca^{2+}]_i$ ($\Delta V_{1/2}$) and estimation of the Ca^{2+} axis intercept (calcium set point, Ca_0) for both adult and fetal BK channels. $V_{1/2}$ values were obtained from B. The lines represent the best linear regression fits. LTH adult and fetal Ca_0 values were calculated to be 3.6 μM and 3.0 μM, respectively.

Table 2. *Summary of BK $V_{1/2}$ and differences in $V_{1/2}$ values in different phosphorylation states.*

	LTH		NX		NX-LTH $V_{1/2}$ diff	
Phosphorylation state	Adult	Fetus	Adult	Fetus	Adult	Fetus
Native	22.0 ± 6.5 (8)	20.5 ± 4.9 (6)	58.4 ± 5.4* (11)	51.5 ± 3.9* (16)	36.4	31.0
Dephosphorylated	25.3 ± 5.2 (8)	23.6 ± 6.1 (7)	67.3 ± 6.6* (12)	64.1 ± 4.9* (14)	42.0	40.5
PKA	-32.6 ± 6.2 (8)	-35.3 ± 5.6 (6)	3.3 ± 6.5* (14)	-1.2 ± 5.0* (15)	35.9	34.1
PKG	-22.8 ± 5.5 (9)	-25.9 ± 7.0 (6)	20.6 ± 4.5* (11)	14.9 ± 4.9* (11)	43.4	40.8

Data are means ± SE, based on a sample size of (n). $V_{1/2}$ values were obtained from BK channel voltage-activation curves at each phosphorylation state. Values for *Native controls, dephosphorylation, PKA, and PKG phosphorylation states* were obtained from Figure 3. NX-LTH $V_{1/2}$ diff values show BK $V_{1/2}$ differences between LTH and normoxic (NX) animal groups. Compared against LTH counterparts: * $P < 0.05$.

Effects of phosphorylation on BK channel activity. Under appropriately controlled conditions (*i.e.* identical BKα isoforms and BKα expression levels), we have shown that the Ca_0 is a surrogate measure of the extent of channel phosphorylation, with lower Ca_0 values correlating with greater extents of phosphorylation by either PKA or PKG (33). Because BK channels from LTH animals show similar Ca_0 values that are lower than those from normoxic controls (Table 1; 31), we hypothesized that LTH adult and fetal BK channels are both phosphorylated similarly and to a greater extent than the normoxic channels. To test these hypotheses, we compared BK channel voltage-activation from different phosphorylation states by applying exogenous alkaline phosphatase and protein kinases using inside-out patches. We plotted single-channel open probability, $P_o/P_{o\,max}$, against membrane potential and fitted the Boltzmann equation to data (Fig. 3).

To compare the voltage-activation of BK channels in the fully dephosphorylated state from each group, we added alkaline phosphatase (Apase, 350 U/ml) to the bath on the cytoplasmic side of the plasma membrane. Apase right-shifted normoxic adult and fetal BK voltage-activation curves to the same extent (Fig. 3A). The voltage-activation curves of LTH adult and fetal myocytes were also right shifted to the same extent by Apase. However, the shift in their $V_{1/2}$ values was substantially less and about -40 mV to the left (*i.e.* more negative) relative to normoxic $V_{1/2}$ values (Fig 3A; Table 2). Despite the difference, BK channel voltage sensitivities did not differ among the four groups of myocytes. Bar graphs in Figure 3A represent Apase-induced changes of $V_{1/2}$ values ($\Delta V_{1/2}$) from their previous endogenous (native) state. Consistent with our first hypothesis, native LTH adult and fetal BK channels were similarly phosphorylated.

Unexpectedly, dephosphorylation with Apase right shifted both $V_{1/2}$ values only by ~ 3 mV, indicating that LTH BK channels were less phosphorylated relative to normoxic controls. The $\Delta V_{1/2}$ values from native state to dephosphorylated state for both LTH adult and fetus were about one-third and one-fourth of normoxic controls, respectively. Thus, compared to normoxic groups, the lower Ca^{2+} set point values of LTH groups (Table 1) are unlikely due to BK channels being more highly phosphorylated.

Nevertheless, to examine the effects of phosphorylation on BK channel voltage-activation, we first dephosphorylated the channels with 350 U/ml Apase, followed by removing Apase from the bath and exposing BK channels to purified catalytic subunit of protein kinase A (cPKA; 30 U/ml) in the presence of KT-5823 (PKG inhibitor, 1 μM), okadaic acid (OA, 1 μM), and ATP (0.5 mM). KT-5823 and OA were used to inhibit the endogenous, channel-associated PKG and phosphatase activities, respectively (32). cPKA left-shifted the voltage-activation curves of both LTH and normoxic BK channels by ~60 mV (Fig. 3B), but the $V_{1/2}$ values for LTH channels were about -35 mV to the left of those for normoxic channels (Table 2).

Similarly, we studied the effect of protein kinase G (PKG) phosphorylation on BK channel activity. Following Apase pre-treatment and subsequent washout, addition of exogenous PKG (2000 U/ml), KT-5720 (PKA inhibitor; 0.3 μM), OA, and ATP left shifted the voltage-activation curves of both LTH and normoxic BK channels by ~50 mV (Fig. 3C), but the $V_{1/2}$ values for LTH adult and fetal myocytes were about -40 mV to the left of that for normoxic myocytes (Table 2). The bar graphs show that PKA (Fig. 3B) and PKG (Fig. 3C) phosphorylation shifted the $V_{1/2}$ values of BK channels from all four groups to a similar extent toward more negative potentials.

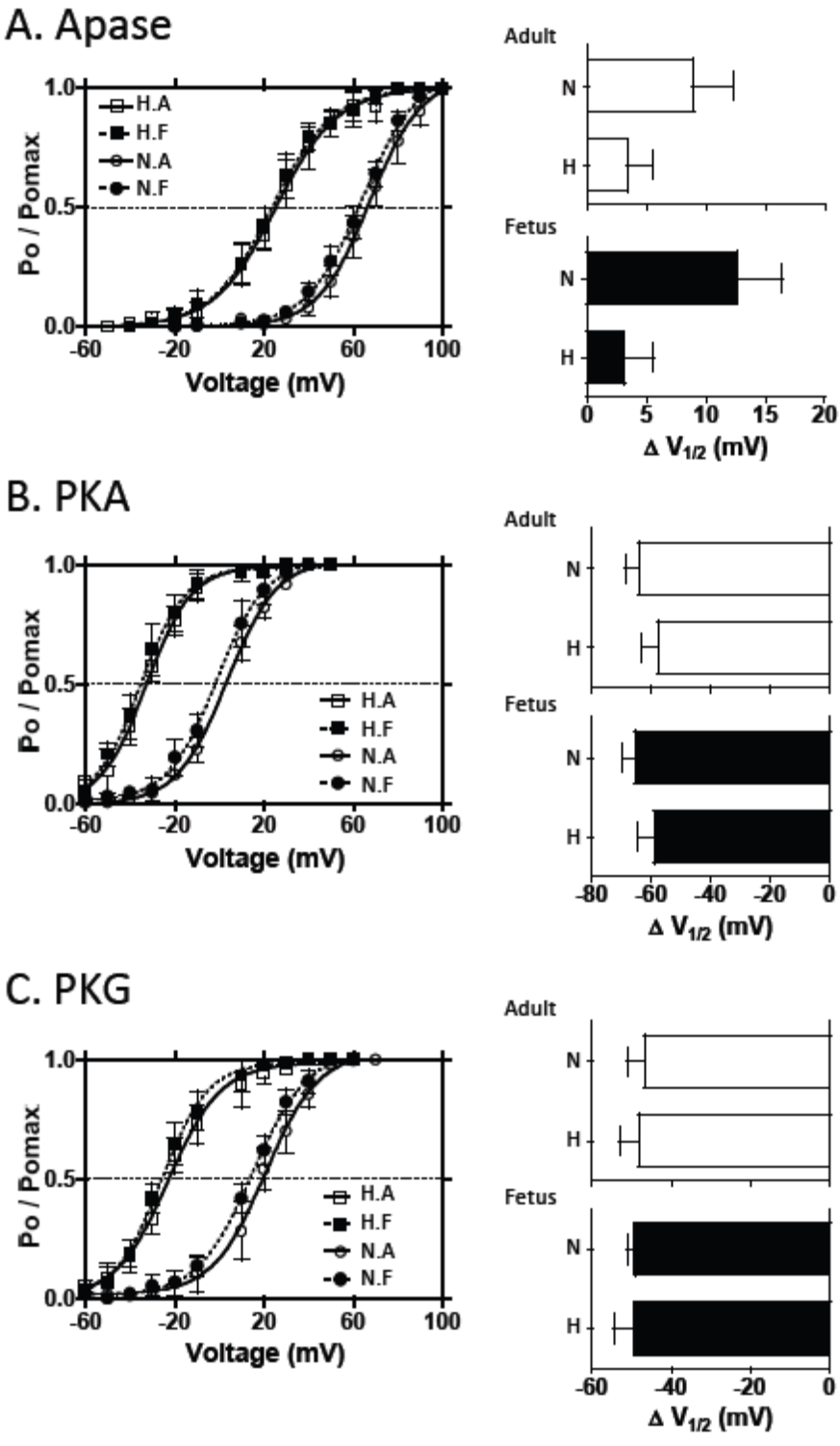
A. Apase
1.0
0.5
0.0
Po / Pomax
H.A
H.F
N.A
N.F
-60
-20
20
60
100
Voltage (mV)
Adult
N
H
Fetus
N
H
0
5
10
15
20
Δ V1/2 (mV)
B. PKA
1.0
0.5
0.0
Po / Pomax
H.A
H.F
N.A
N.F
-60
-20
20
60
100
Voltage (mV)
Adult
N
H
Fetus
N
H
-80
-60
-40
-20
0
Δ V1/2 (mV)
C. PKG
1.0
0.5
0.0
Po / Pomax
H.A
H.F
N.A
N.F
-60
-20
20
60
100
Voltage (mV)
Adult
N
H
Fetus
N
H
-60
-40
-20
0
Δ V1/2 (mV)

Figure 3. Effects of exogenous phosphorylation and dephosphorylation on BK channel activities. Single BK channel recordings of BK channels from inside-out micro patches were obtained in 3 μM free [Ca^{2+}] from the isolated myocytes of the four experimental animal groups: LTH (H) and normoxic (N) and adult (A) and fetus (F). A. Voltage-activation curves of BK channels with alkaline phosphatase (Apase, 350 U/ml) in the bathing medium. Bar graphs summarize the extent to which Apase treatment right shifts the activation curves in terms of change in $V_{1/2}$ values for adult (top) and fetal (bottom) groups. B. Voltage activation curves of BK channels in the presence of exogenous PKA. After phosphatase pretreatment, purified PKA catalytic subunit (cPKA, 30 U/ml) was added in the presence of KT5823, OA, and ATP. The extent to which PKA left shifts $V_{1/2}$ values is summarized on the bar graphs. C. Voltage activation curves of BK channels in the presence of exogenous PKG. Following phosphatase pretreatment, purified PKG (2000 U/ml) was added in the presence of KT5720, OA, and ATP. Effect of PKG left-shift $V_{1/2}$ values is summarized on the right bar graphs. Solid lines show the best-fit curves to the Boltzmann equation from which $V_{1/2}$ values were calculated.

Taken together, inducing changes in phosphorylation status consistently segregated voltage-activation curves for both LTH age groups from their comparable normoxic controls. In each of the three defined phosphorylation states, $V_{1/2}$ values for BK channels from LTH myocytes were consistently -35 to -40 mV more negative relative to those from normoxic myocytes (Table 2), demonstrating that intrinsic functional differences exist between LTH and normoxic BK channels.

Gating kinetics. Despite BK channels from LTH adult and fetal myocytes being from developmentally different populations, they exhibited similar Ca^{2+} affinities (Ca_o; Fig. 2C) and voltage-activation ($V_{1/2}$; Fig. 3). However, single-channel BK channel recordings (Fig. 2A) suggest different gating kinetics. Therefore, we compared gating kinetics by measuring open and closed dwell times of LTH and normoxic adult and fetal BK channels from single-channel, inside-out preparations. Figure 4A shows representative traces of single BK channel recordings from the four groups in their native state (*i.e*. endogenous controls). BK channel dwell times were plotted as the square root of event fraction versus the logarithmic open or closed dwell times. The histograms to the right were set to 50 bins per decade and the plots were best fitted to 3-component exponential functions to display open (Fig. 4B) or closed components (Fig. 4C). By summing the products of the component mean dwell times (τ_1, τ_2, τ_3) and their respective weight factors (ω_1, ω_2, ω_3; Figs 4B and 4C shown in parentheses), we calculated the weighted mean open (τ_o) and closed (τ_c) times, which are represented as $\tau = (\omega_1\tau_1 + \omega_2\tau_2 + \omega_3\tau_3)/(\omega_1 + \omega_2 + \omega_3)$, where $(\omega_1 + \omega_2 + \omega_3) = 1$. The τ_o and τ_c of BK channels in the native state from LTH fetus were more than three times longer than that of the other three groups (Table 3).

Table 3. *Summary of weighted mean open and closed dwell-times.*

	τ_O				τ_C			
	LTH		NX		LTH		NX	
Phosphorylation state	Adult	Fetus	Adult	Fetus	Adult	Fetus	Adult	Fetus
Native	3.84 (8)	13.81 (7)	1.84 (5)	2.09 (6)	8.32	27.03	6.64	6.69
Dephosphorylated	2.77 (6)	9.65 (6)	1.66 (5)	1.63 (6)	8.59	21.07	26.37	19.88
PKA	1.31 (5)	1.83 (7)	1.73 (6)	1.48 (7)	14.61	4.98	8.71	5.48
PKG	1.33 (6)	0.92 (5)	1.45 (5)	1.85 (5)	6.19	13.89	2.06	28.83

Dwell-times were obtained from square-root vs logarithmic time plots (Figs 4B, C) best fitted to an exponential function with three components. Mean time constants (τ) were multiplied by corresponding weighing factor (see Supplement Table 1, including P values) and the three products were summed to yield weighted mean open (τ_o) and closed (τ_c) times for different phosphorylation states: native control; dephosphoryated (alkaline phosphatase, Apase); and phosphorylation by added PKA and PKG following pre-treatment with Apase. Sample sizes (n) are shown in parentheses.

To determine the extent to which the longer dwell times of LTH fetal BK channels may be attributable to differential phosphorylation, we examined the effects of BK channel de-phosphorylation and phosphorylation on dwell times. We treated inside-out patches in Apase to dephosphorylate or in PKA or in PKG to phosphorylate BK channels (identical to the procedures for Fig. 3). Table 3 summarizes the compiled weighted mean open (τ_o) and closed dwell times (τ_c) for BK channels from each of four animal groups in three defined phosphorylation states: dephosphorylated; PKA-; and PKG-phosphorylated. Changes in phosphorylation state did not influence normoxic BK weighted mean open dwell times significantly, while both protein kinases A and G decreased open dwell times in LTH groups. Moreover, dephosphorylation with Apase had little effect on LTH BK open or closed dwell times. Consistent with findings in Figure 3, these results indicated that BK channels from LTH adult and fetus in the native state were essentially de-phosphorylated compared to native state normoxic controls.

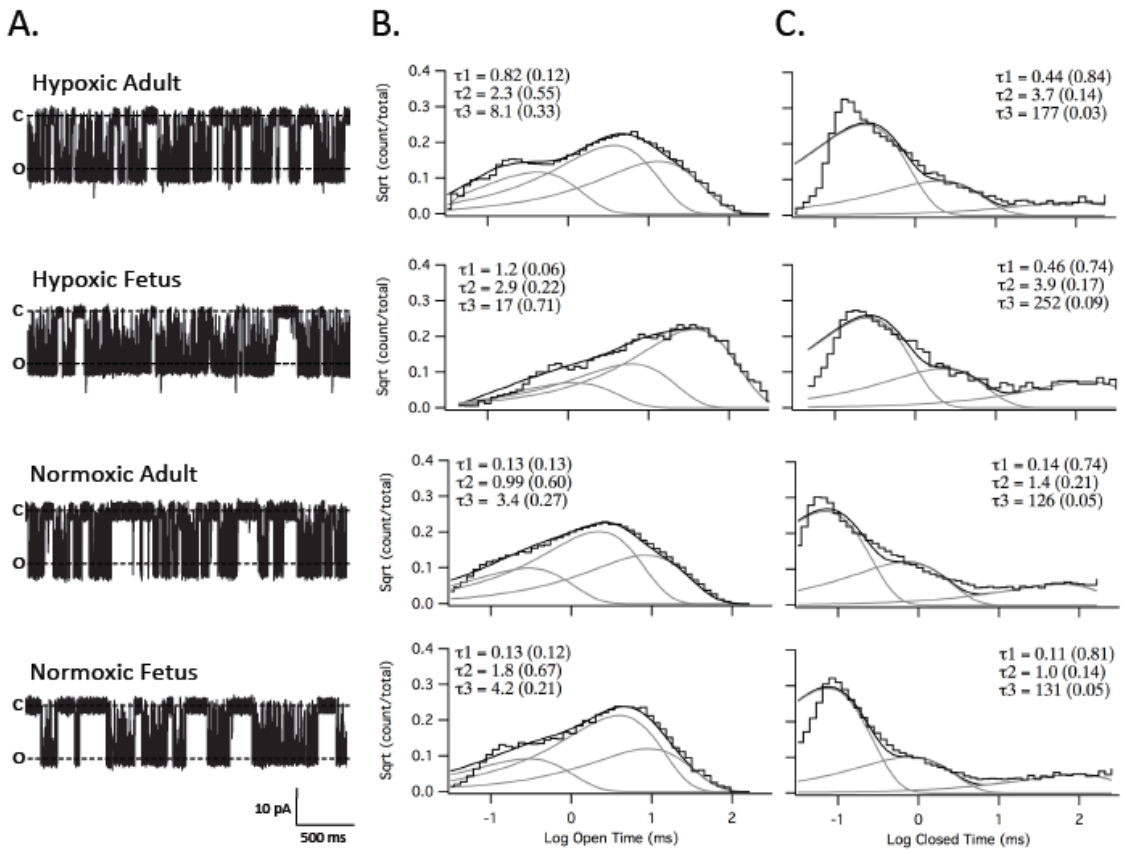

Figure 4. BK channel dwell time analysis. A. Representative inside-out patch recordings of BK channels from hypoxic (LTH) adult and fetal, and normoxic adult and fetal myocytes in symmetrical 140 mM KCl solutions with 3 μM free Ca^{2+}. Recordings were done at +60 mV depolarizing potential. B. and C. Plots of open and closed dwell times. Channel open and closed dwell times were plotted on a logarithmic time abscissa as a function of the square-root of the number of events per bin on the ordinate axis. The bin density is 50 bins per decade. Both the open (B) and closed (C) plots were best fitted to exponential functions with three components using QuB software (see Methods). The lines for the sum and each component exponential fit are shown. The time constants (τ) and their relative weight contributions (in parentheses) of each component to the composite fit are listed.

Table 4. *Summary of BKβ and BKα surface densities and BKα clusteriing.*

	LTH		NX	
	Adult	Fetus	Adult	Fetus
A. Flow cytometry:				
Geometric mean (FL)	299 ± 17*	546 ± 68	452 ± 27	206 ± 13*
Mean cell count/sample	1.2 x 10^4	3 x 10^4	3 x 10^4	6.5 x 10^5
Relative Surface area (pF)[a]	16.1 ± 1.3	9.4 ± 1.7	15.7 ± 0.6	9.1 ± 0.6
BKb-1 Surface density (FL/pF)	18.6	58.1	28.8	22.6
B. Channels per micropatch:				
Mean BK channel per patch	2.1 ± 0.2	2.6 ± 0.3	2.2 ± 0.2	2.6 ± 0.2
Mean tip resistance (MΩ)	15.2 ± 0.1	15.9 ± 0.1	15.3 ± 0.1	15.5 ± 0.1
BK per patch, minus empties	2.3 ± 0.2*	3.7 ± 0.3	2.5 ± 0.2	2.6 ± 0.2*
% patches with no BK channels	8.3	31.7	7.0	1.6
% patches with 1 BK channel	27.8	7.1	27.9	29.0
% BK channels clustered[b]	33.3	50.0	37.2	53.2
C. BK clustering:				
Total BKα (10^3)[c]	9.2 ± 1.1	6.0 ± 1.1	9.8 ± 1.3	5.8 ± 1.1
BKα surface density (10^2)[d]	8.0 ± 1.2	6.6 ± 1.0	7.6 ± 1.0	6.8 ± 0.9
BKα clusters/total BKα (10^{-3})[e]	1.4 ± 0.2*	3.8 ± 0.4	1.4 ± 0.2*	3.4 ± 0.2
D. Cluster co-localization:				
No. BKα clusters (10^3)[f]	11.6 ± 2.8	20.0 ± 0.4	12.5 ± 4.3	15.6 ± 4.8
No. ChTx clusters (10^2)[g]	7.5 ± 0.9	9.2 ± 1.9	5.8 ± 1.7	10.0 ± 2.1
Co-localized clusters (10^3)[h]	2.6 ± 1.2*	7.8 ± 1.6	2.8 ± 0.8*	9.0 ± 1.6
% BKα clusters co-localized	31.9	39.0	32.0	53.8

Values expressed as mean ± SE, as appropriate, with n values indicated in accompanying text or Figures. **A.** Flow cytometry was used to measure BK β-1 surface expression (Fig. 5) and calculate relative β-1 surface density. **B.** Estimated BK channels on excised micro-patches. [a], measured in perforated-patch mode (Table 1); [b], % of channels associated with 3 or more other channels in patch. **C.** Extent of BK channel clustering. [c], from Fig. 8A; [d], from Fig. 8B; [e], from Fig. 8F. **D.** Co-localization of BK clusters with clusters of ChTx. [f], from Fig. 9A; [g], from Fig. 9B; [h], from Fig. 9F. *, compared to LTH fetus ($P < 0.05$).

Expression of cell surface BK α-1. Because increases in BK α-1 subunit expression have been associated with increases in channel gating kinetics (39), increases in channel Ca^{2+} affinity (*i.e.* lower Ca_0; 48), and left-shifted voltage activation (42), we tested the hypothesis that myocyte cell surface BK α-1 subunit expression was up regulated in LTH fetal myocytes. To test this proposition, we used flow cytometry with a primary antibody directed against a conserved, extracellular BK α-1 subunit epitope (Fig. 5). An epitope-blocking peptide was used as a negative control (Fig. 5E, F). The specificity of the antibody was tested in Western immunoblots, which showed BK α-1 expression in ovine fetal and adult pulmonary arteries, as previously reported by Resnik *et al*. (50), but not in ovine adult brain, which predominantly expresses the BK β-4 isoform (data not shown; 6, 7). To eliminate effects due to variation in cell size and surface area, we normalized cell surface BK β-1 expression (fluorescence units, FL) to relative surface area based on measured cell capacitances (*i.e*. pF; Table 1). We thereby converted flow cytometric data (FL) for surface BK β-1 into units of relative surface density (*i.e*. FL/pF; Table 4A). Our data indicate that BK β-1 surface density on LTH fetal myocytes was three times greater than on LTH adult cells and two times greater than on either normoxic group. Based upon this analysis, long-term hypoxia enhances BK β-1 surface expression on fetal myocytes relative to that of LTH adult myocytes and both normoxic control myocytes.

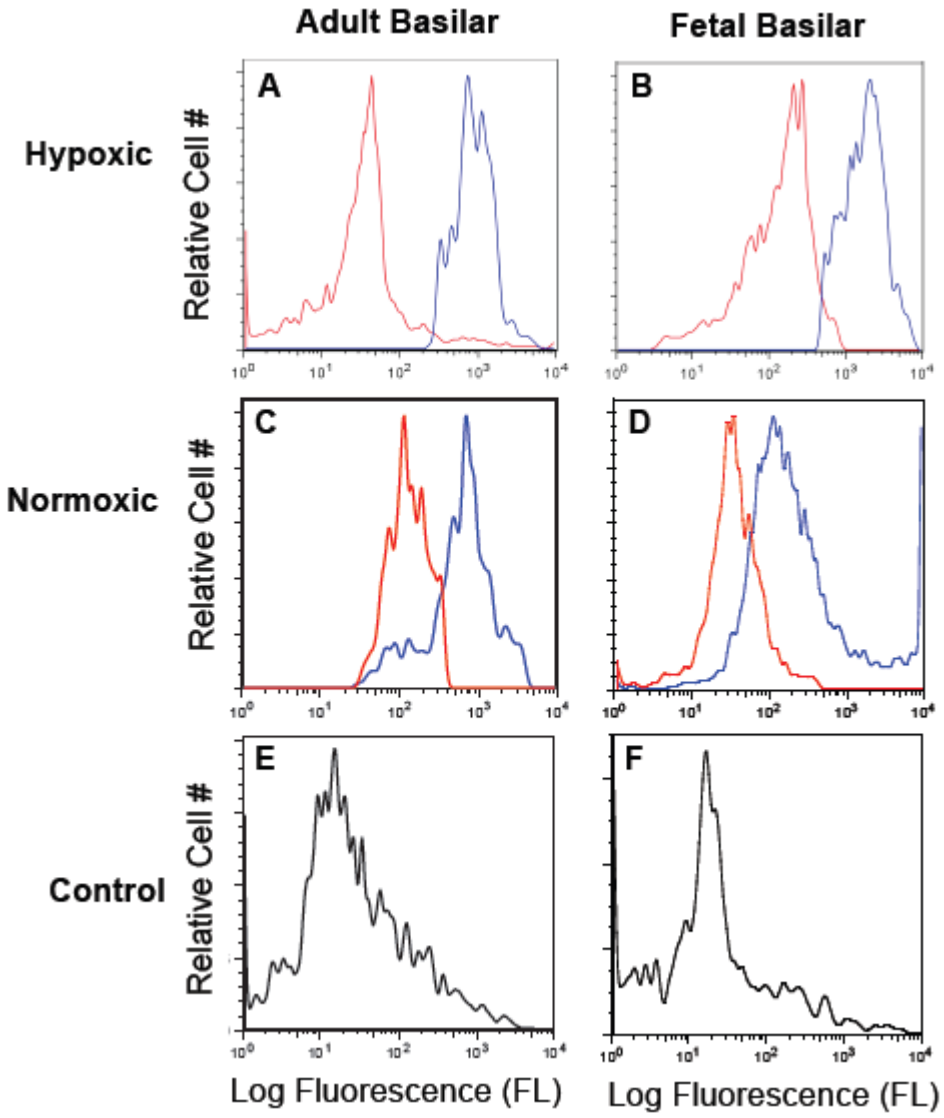

Figure 5. Representative flow cytometric distributions of cell surface BK channel β-l subunit. A-D. Isolated, intact basilar artery smooth myocytes were treated with either primary anti-BK β-l (blue trace) plus secondary antibody or with secondary antibody alone (red trace). E-F. Primary anti-BK β-l antibody was pre-incubated with 70-fold molar excess β-l epitopic peptide overnight on ice. Isolated, intact basilar artery smooth myocytes then were treated with the primary antibody and peptide mixture followed by secondary antibody to serve as antibody specificity controls (black trace). A. LTH adult (n = 8); B. LTH near-term fetus (n = 9); C. normoxic adult (n = 13); D. normoxic near-term fetus (n = 13); E. normoxic adult (n = 13); and F. normoxic fetus (n = 13).

Channel surface density. Because myocyte BK β-1 surface density was significantly greater in the LTH fetus than in the other three groups, we measured the corresponding BK channel surface density. For this purpose, we counted BK channels in excised membrane patches from micropipettes of similar tip diameter and resistance (15.5 ± 0.10 MΩ; n = 192) (2, 51). The data show that channel surface densities did not differ between treatment groups (Table 4B). However, frequency histograms of number of channels per excised patch (Fig. 6) suggest different patterns of BK surface distribution between groups. In the LTH fetus, many patches did not have channels (31.7%), few patches contained one channel (7.1%), while the largest percentage of patches had three or more BK channels (50.0%). The two adult groups had fewer patches containing three or more BK channels (33.3% and 37.2%), while the normoxic fetal group had an intermediate percentage (53.2%; Table 4B). These findings suggest that myocyte BK channels of the LTH fetus and the normoxic fetus are more clustered than those of the adult.

BKα expression and clustering. To further test the hypothesis that BK channels are more clustered in the fetal groups, we used confocal microscopy to measure BKα channel expression and extent of BKα clustering. The representative micrographs (Fig. 7) show that myocytes of the four treatment groups exhibited BKα in both dispersed and clustered forms. Such variation in expression is consistent with our electrophysiological recordings of excised patches (Fig. 6).

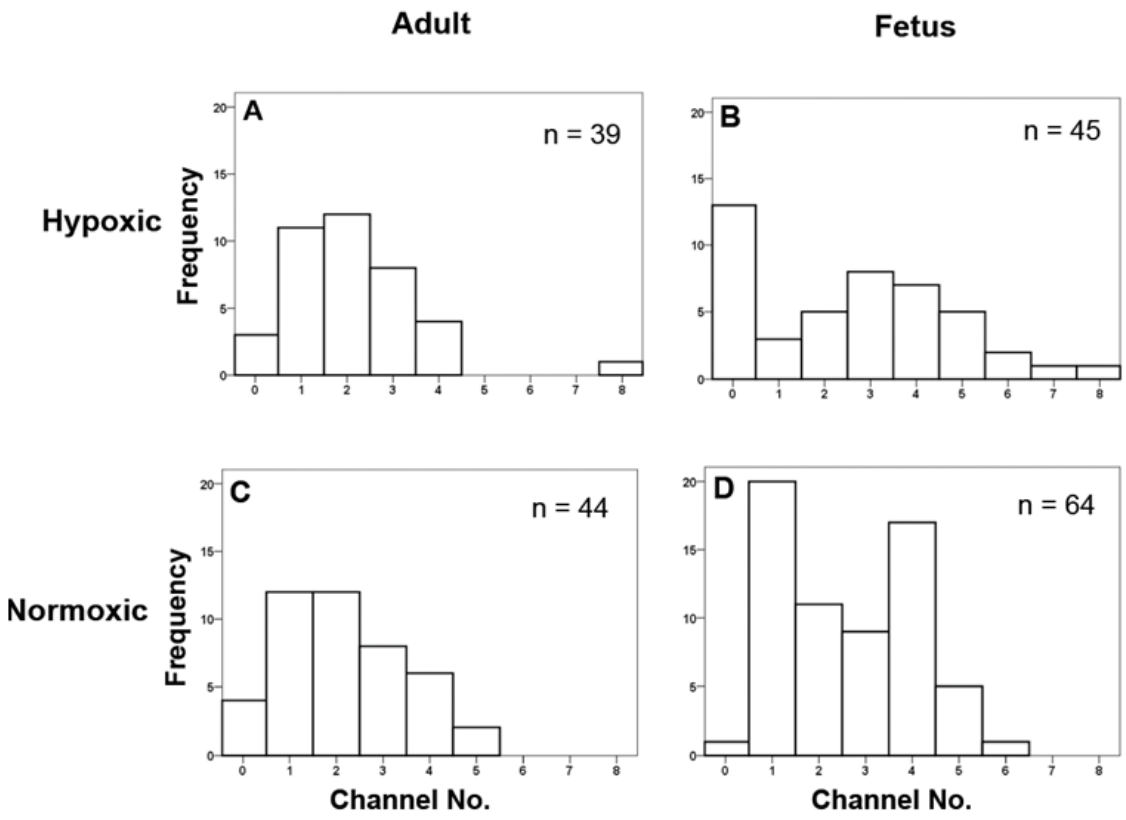

Figure 6. Number of BK channels in excised micro patches**.** The number of BK channels in inside/out patches was determined at +60 mV in symmetrical KCl solutions with 3 mM Ca^{2+} in the bath solution to ensure maximal channel activation. Patch electrode tip resistances averaged 15.5 ± 0.1 MW (n = 192). Frequency histograms of the number of BK channels per patch preparation with distribution curve overlays were displayed. A. LTH adult (n = 39); B. LTH near-term fetus (n = 45); C. normoxic adult (n = 44); and D. normoxic near-term fetus (n = 64).

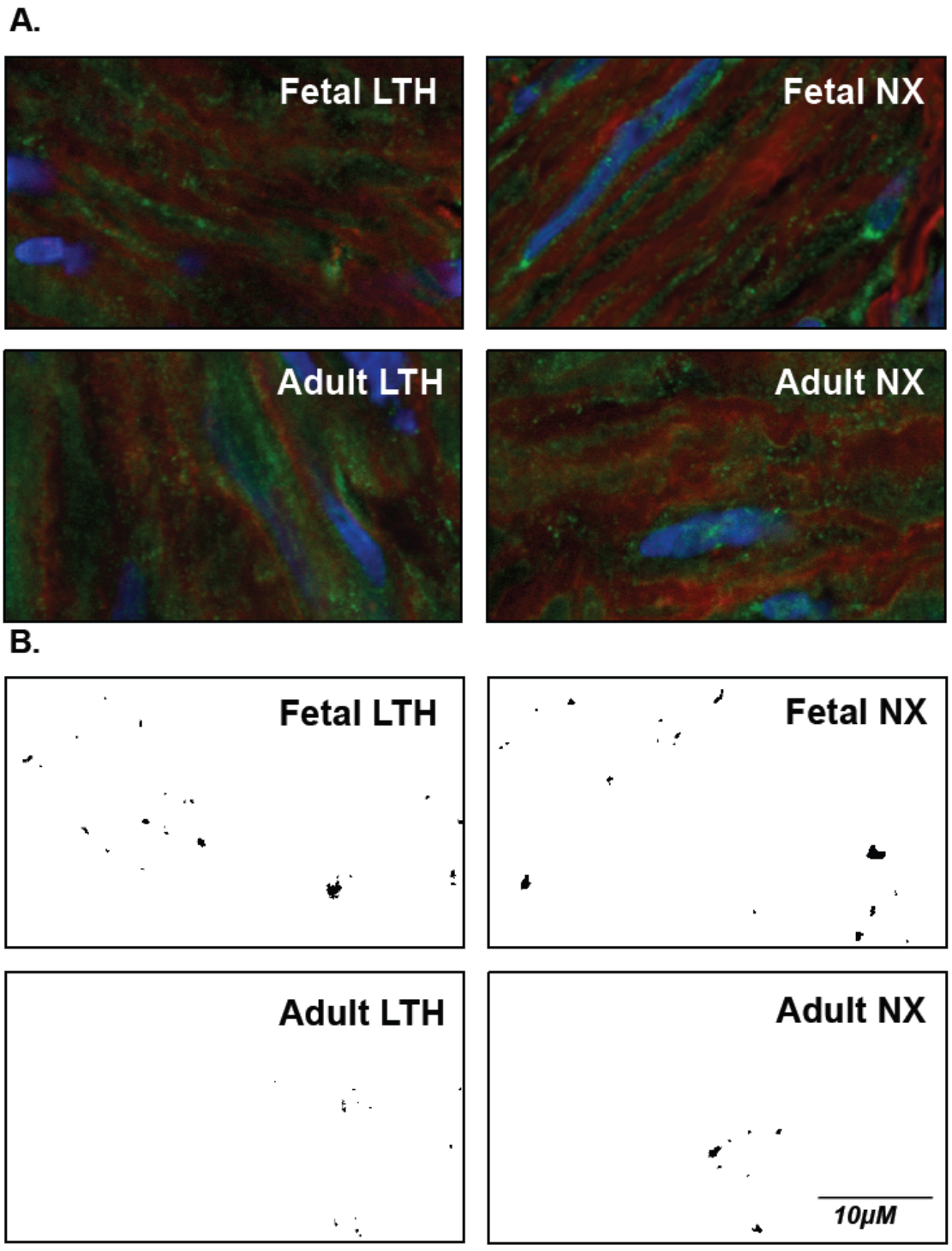
A.
Fetal LTH
Fetal NX
Adult LTH
Adult NX
B.
Fetal LTH
Fetal NX
Adult LTH
Adult NX
10μM

Figure 7. Representative confocal microscopic images of arterial myocytes reveal presence of dispersed and clustered BK channels. A. Representative color images from adult LTH, fetal LTH, adult NX (normoxic), and fetal NX. Viewed areas measure 20 x 40 mm. Green color indicates presence of BK channels. B. Green channel (BK fluorescence) intensities converted to binary image from same areas as above (A) after masking out all values below "threshold" (3.5x mean intensity). BK clusters show as black areas of different size and shape. Controls with secondary antibody alone or with primary antibody pre-absorbed with antigenic peptide revealed little to no detectable BKα fluorescence (data not shown).

Myocytes from normoxic and LTH adult groups expressed 35% ($P < 0.05$) and 31% ($P < 0.05$) more total BKα per cross-sectional area than their fetal counterparts, respectively (Fig. 8A; Table 4C). However, when BKα fluorescence was co-localized to the cell surface marker, AF-594 conjugated WGA, cell surface expression of BKα did not differ among the groups (Fig. 8B; Table 4C). Again, this is consistent with our findings from counting channels in micropatches (Table 4B).

In contrast to total expression and surface expression, the fetal groups exhibited significantly more BKα clusters than their corresponding adult groups across a range of intensity thresholds above mean BKα fluorescence (*e.g.* Fig. 8C-E). What is more, at higher intensity thresholds the ratio of fetal cluster numbers to adult clusters increased (Fig. 8E) suggesting that fetal groups have larger clusters than the adult counterparts. LTH and normoxic fetal groups expressed 2.7 ($P < 0.01$) and 2.4 ($P < 0.01$) times more BK clusters, respectively, than their corresponding adult groups (Fig. 8F; Table 4C) after normalizing the number of BK clusters (*e.g.* Fig. 8C) to total BKα fluorescence (Fig. 8A). These results confirm our hypothesis that BK channels on fetal myocytes are more clustered (Fig. 8F).

BK channels in vascular myocytes are known to localize on lipid rafts (1, 37). Therefore, we hypothesized that BK channel clusters co-localize with lipid rafts and that these fetuses would have greater lipid raft associated clusters as compared to adults independent of altitude. To address this hypothesis, we measured BK channel clustering by examining cholera toxin B subunit-Alex 594 conjugate (ChTx) as a marker of GM1-containing lipid rafts (38, 44), such as caveolae (20). Operationally, we defined lipid rafts as sites of ChTx clusters and correlated this with BKα fluorescence using the

methodology described for Figure 8. Although slightly more ChTx clusters occur in the fetal groups than in the adults (Fig. 9), the number of BK clusters that co-localize to ChTx clusters is two times higher in the fetal groups than their corresponding adult groups (Fig. 9; Table 4D; $P < 0.05$).

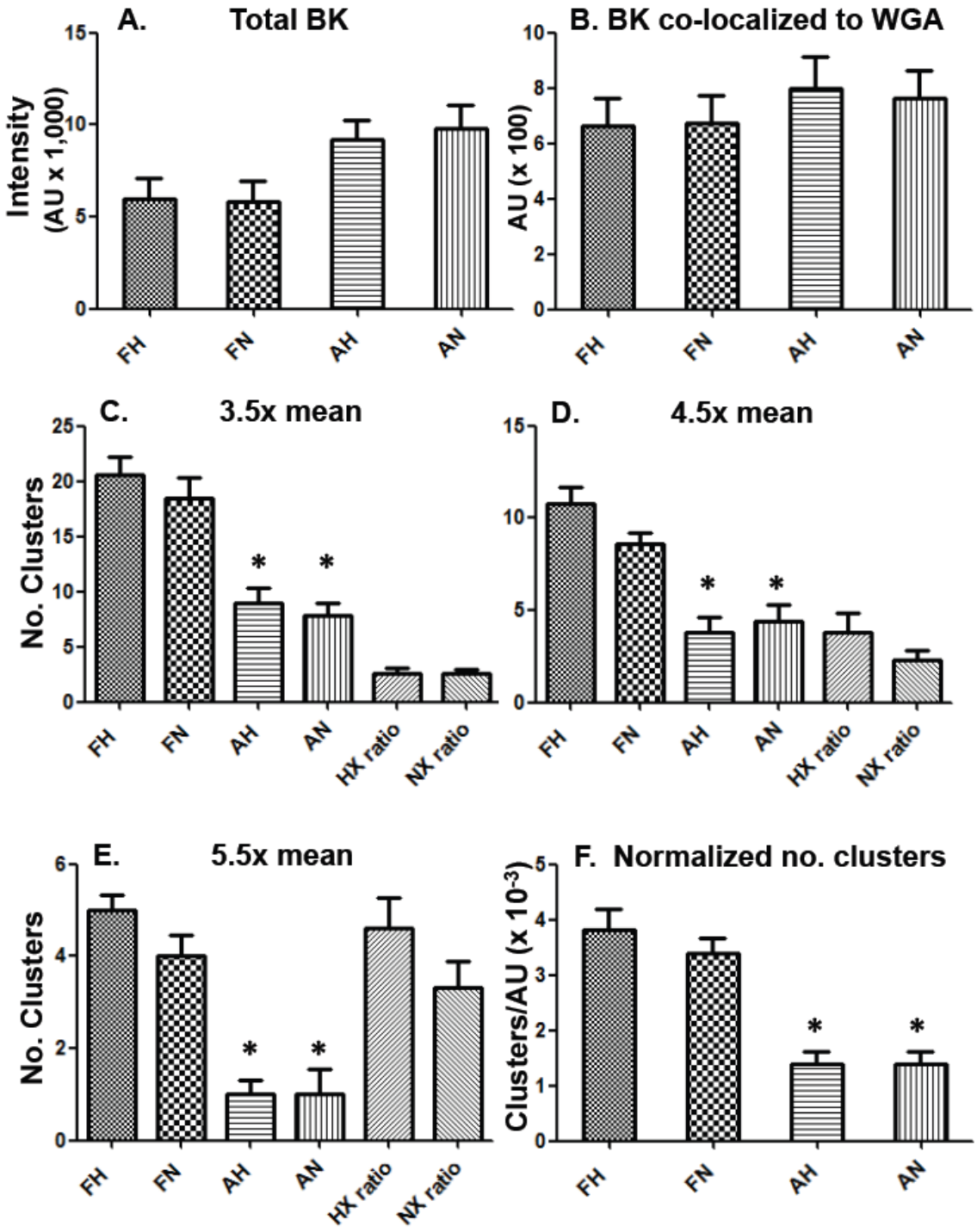
A.
Total BK
Intensity
(AU x 1,000)
15
10
5
0
FH
FN
AH
AN
B. BK co-localized to WGA
AU (x 100)
10
8
6
4
2
0
FH
FN
AH
AN
C.
3.5x mean
No. Clusters
25
20
15
10
5
0
*
*
FH
FN
AH
AN
HX ratio
NX ratio
D.
4.5x mean
15
10
5
0
*
*
FH
FN
AH
AN
HX ratio
NX ratio
E.
5.5x mean
No. Clusters
6
4
2
0
*
*
FH
FN
AH
AN
HX ratio
NX ratio
F. Normalized no. clusters
Clusters/AU (x 10-3)
5
4
3
2
1
0
*
*
FH
FN
AH
AN

Figure 8. Total BK channel density, BK surface density, and BK clustering measured in confocal images of intact basilar artery myocytes. A. Total BK fluorescence intensity in arbitrary units (AU; mean ± SEM; n = 5), where FH is fetal hypoxic (LTH), FN is fetal normoxic, AH is adult hypoxic, and AN is adult normoxic; B. BK co-localized with the surrogate surface membrane marker, wheat germ agglutinin (WGA; n = 6); C. Number of BK clusters measured at 3.5 times above mean intensity (n = 7); D. Number of BK clusters measured at 4.5 times above mean intensity (n = 6); E. Number of BK clusters measured at 5.5 times above mean intensity (n = 6); and F. Number of BK clusters at 3.5 times mean intensity per total BK intensity (n = 6). Imaged areas measured 20 x 40 mm. Number of animals in each group was either 3 or 4. Asterisks (*) denote significant difference with $P < 0.001$ relative to either fetal group. HX ratio and NX ratio refer to FH:AH and FN:AN, respectively.

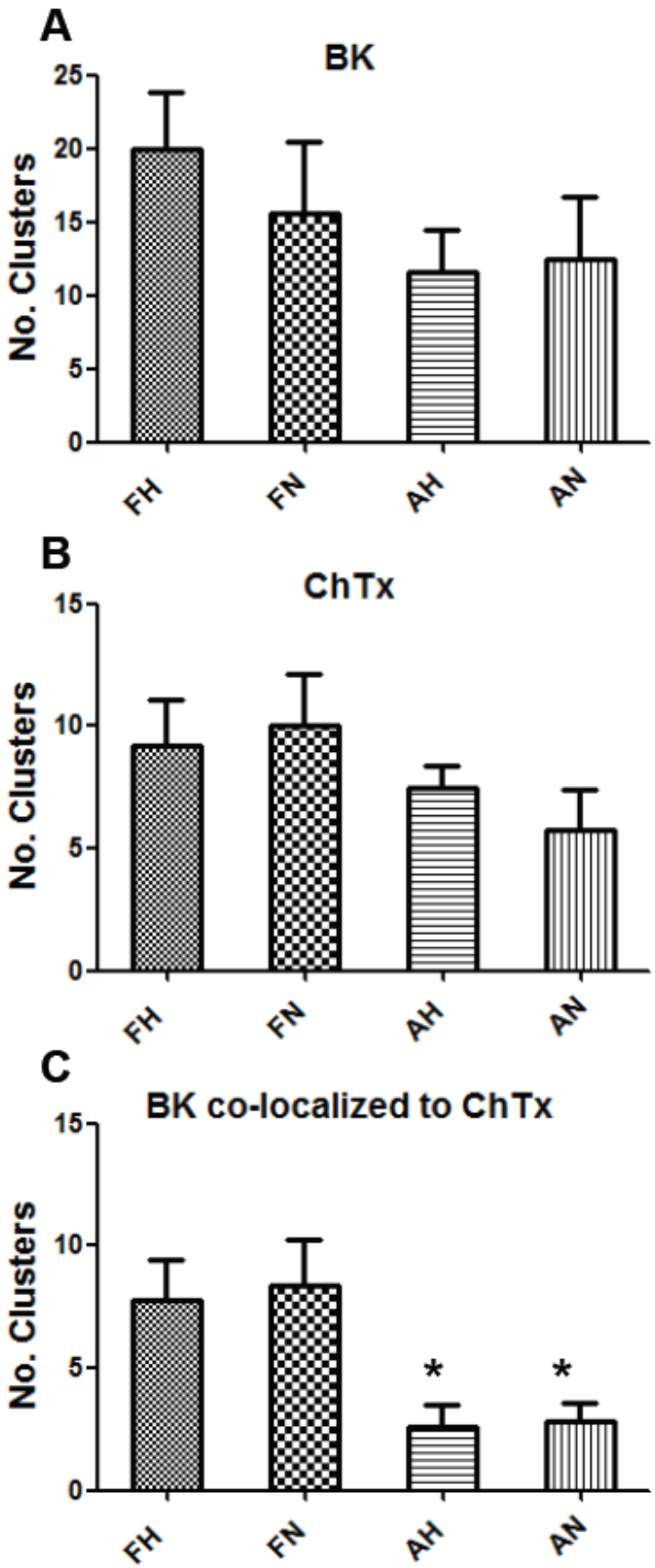
A
BK
No. Clusters
25
20
15
10
5
0
FH
FN
AH
AN
B
ChTx
No. Clusters
15
10
5
0
FH
FN
AH
AN
C
BK co-localized to ChTx
No. Clusters
15
10
5
0
*
*
FH
FN
AH
AN

Figure 9. BK channel clusters co-localized to cholera toxin clusters. A. Number of BK clusters measured at 3.5 times above mean intensity (mean ± SEM; n = 5), where FH is fetal hypoxic (LTH), FN is fetal normoxic, AH is adult hypoxic, and AN is adult normoxic; B. Number of cholera toxin (ChTx) clusters measured at 3.0 times above mean intensity (n = 5); and C. Number BK clusters co-localized with ChTx clusters. Imaged areas measured 20 x 40 mm. Number of animals in each group was 3. Asterisks (*) denote significant difference with $P < 0.05$ relative to either fetal group.

Perforated-patch whole-cell currents. Because BK clusters co-localize to lipid rafts more in both fetal groups than in the adults, we hypothesized that outward currents recorded from the two fetal groups would increase more relative to the adult groups while recording under conditions that permit spark activity (47). To test our prediction, we recorded whole-cell outward currents in perforated-patch mode (Fig. 10), which permits Ca^{2+} spark activity, and compared currents to conventional whole-cell mode (Fig. 1), which suppresses Ca^{2+} sparks. Cell membrane capacitances were similar to those from conventional whole-cell mode (Table 1). As predicted, outward current densities were higher in perforated-patch mode (Fig. 10) with LTH adult currents increasing by 38%, while LTH fetal currents increased by 189% (Table 1). In addition, normoxic fetal outward currents were higher than normoxic adults (Fig. 10; Table 1). These results suggest that both normoxic and LTH fetal BK channels may be more sensitive to endogenous Ca^{2+} sparks than adults (47, 55). Because of these significant age differences in BK co-localization to lipid rafts and channel activities, future work should examine sparks and spontaneous transient outward currents between adult and fetus in this ovine model.

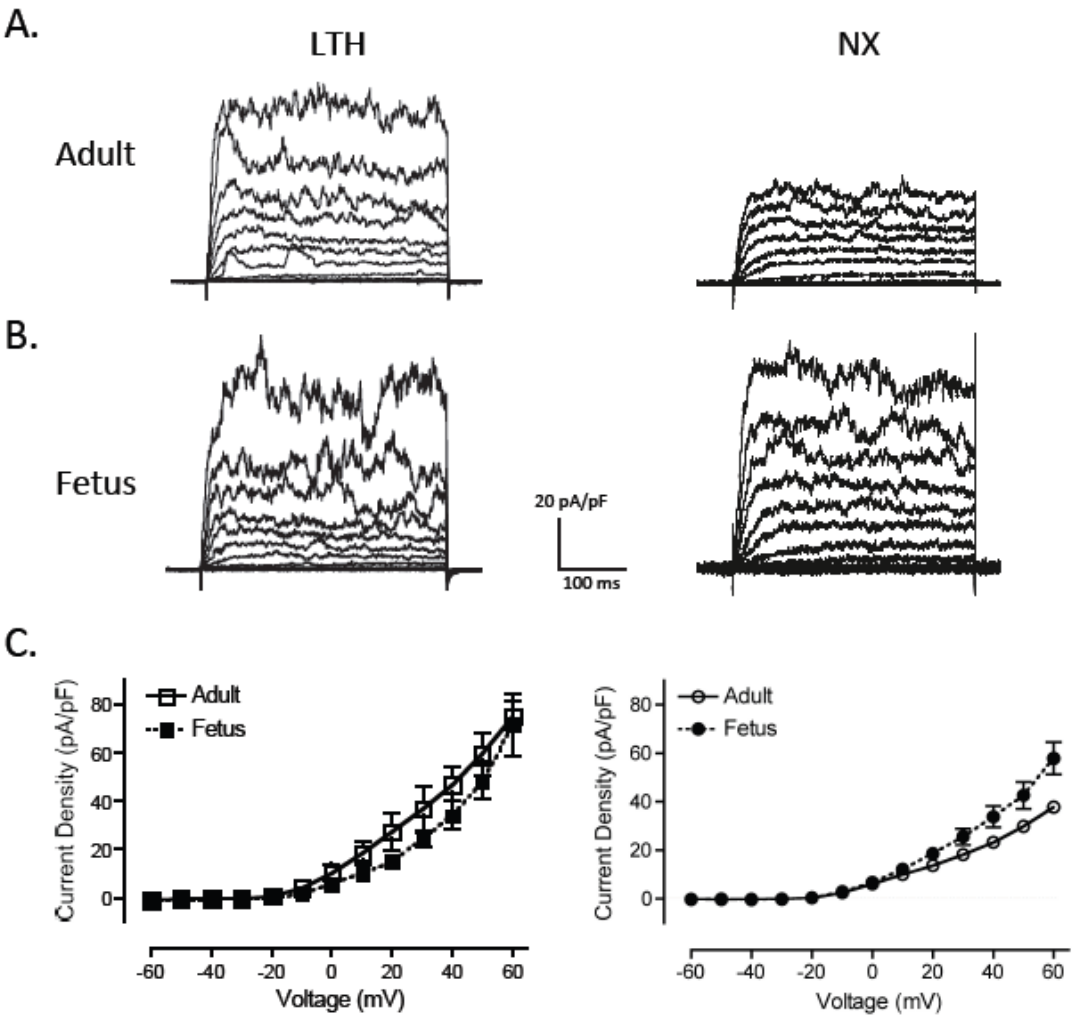

Figure 10. Perforated-patch, whole-cell outward current density recordings. A. and B. Representative whole-cell outward membrane current density traces are shown from isolated LTH and normoxic (NX) adult (A) and fetal (B) basilar artery myocytes. Currents were elicited by a series of 10-mV depolarizing steps (-60 to +60 mV) from a holding potential of -60 mV. Whole-cell current density was used to normalize whole cell currents for size differences between adult and fetal myocytes. C. Averaged steady-state current-voltage plot of outward current density in myocytes obtained from LTH (left) adult (n = 5) and fetal (n = 6) and normoxic (right; taken from reference 3) adult (n = 4) and fetal (n = 5) basilar arteries.

Discussion

Despite the physiological importance of adequate cerebral blood flow and the role of BK channels in its maintenance, few studies have measured directly the effects of long-term hypoxia on BK channels of the developing cerebral vasculature. Our findings indicate that basilar artery smooth muscle BK channels in LTH adult and near-term fetus are significantly more active than their normoxic counterparts. This acclimatization to high-altitude hypoxia involves lowering the Ca^{2+} set point independently of channel phosphorylation and, in the case of the LTH fetus, up regulating accessory BK β-1subunit expression. In addition, our findings indicate that the BK channels of both the LTH and normoxic fetuses are more clustered and co-localized to lipid rafts. Under conditions of perforated-patch recordings, the fetal channels may be more coupled to endogenous Ca^{2+} sparks than either of the two adult groups.

LTH increases BK activity independent of age. Several features distinguish LTH BK channels from normoxic controls, regardless of age group. The LTH BK channels show: (i) increased Ca^{2+} affinity (*i.e.* lower Ca^{2+} set points; Fig. 2; Table 1); (ii) $V_{1/2}$ values shifted -35 to -40 mV more negative in each of three defined phosphorylation states (Fig. 3; Table 2); (iii) lower extent of phosphorylation in the endogenous native state (Fig. 3A); and (iv) longer weighted mean open dwell times (Fig. 4; Table 3). In addition, the nearly dephosphorylated state of native LTH channels suggests that the BK channels have additional capacity to further increase Ca^{2+} affinity and left-shift activation curves should either PKA or PKG pathways be activated (32, 33). Together these channel features suggest that LTH acclimatization increases BK channel activity, possibly in order to lower vascular tone. This, in turn, would ensure adequate brain perfusion in the

face of lowered arterial oxygen levels. Such modulations during LTH underscore the role of cerebral smooth muscle BK channels in regulating vascular tone and CBF (30).

At high altitude, the physiological challenge of LTH is accentuated in the fetus by additional demands of cerebral growth and development and by being *in utero* at lower arterial PO_2 values. In response to these additional challenges, fetal acclimatization to LTH includes up-regulation of BK β-1 myocyte surface expression (Fig. 5; Table 4A). This increased fetal BK β-1 subunit expression may enhance BK channel coupling to Ca^{2+} sparks and increase cerebral blood flow (CBF), because decreased expression of BK β-1 uncouples BK channels from Ca^{2+} sparks, increases vascular tone (8, 34, 47, 55), and produces hypertension in mice (2). In comparison to the BK channels of the LTH adult, those of the fetus are two-times more clustered (Figs 6 and 8; Table 4C) and two-times more co-localized to sites of lipid rafts identified by cholera toxin clustering (Fig. 9). In keeping with this, we observed an estimated five-fold increase in BK current density in perforated-patch mode over conventional whole-cell mode in the LTH fetus, but less than a two-fold increase in the LTH adult (Table 1).

Previously, our group showed that LTH reduced NS1619-induced BK channel activation-mediated vasorelaxation of middle cerebral artery segments (35), which was attributed to either decreased BK channel expression or decreased sensitivity to Ca^{2+} (13). In contrast, the present studies showed that in basilar arteries neither BK channel expression (Figs 6 and 8B) nor channel affinity to Ca^{2+} decreased (Fig. 2; Table 1). Our findings are in keeping with others (26, 46, 60), who showed that cerebral blood flow is near normal in the LTH fetus. The findings of Long *et al.* (29) and Gilbert *et al.* (14) may stem from non-selective effects of NS1619 that can offset the relaxation effects of

BK channel activation when used on intact tissues (59). Such non-selective effects include inhibition of L-type Ca^{2+} channels (43) and stimulation of Ca^{2+} mobilization from ryanodine-sensitive Ca^{2+} stores (29, 64). Alternatively, these differences may arise from variations among different cerebrovascular branches.

Fetal BK activity increases in both treatment groups. Normoxic and LTH fetuses exhibit increased BK channel activity compared to their adult counterparts. To ensure adequate blood flow to the developing brain, the fetus appears to regulate vascular BK channel activity rather than raising the level of BKα expression (Tables 4B and C; Figs 6 and 8). In both normoxic and LTH, the fetus increased BK channel activity due to (i) increased channel affinity to Ca^{2+} (Table 1) and (ii) increased channel clustering (Fig. 8) on lipid rafts (Fig. 9). In the normoxic fetus, the increase in BK channel Ca^{2+} affinity (Table 1) was driven by increased channel phosphorylation (32). In the LTH fetus, where the challenge of adequate CBF is more severe, a different strategy was observed: BK channel Ca^{2+} affinity was increased (Table 1), but not due to increased channel phosphorylation. In addition, increased BK channel activity was associated with (i) a three-fold up regulation of BK b-1 surface expression (Fig. 5; Table 4A), (ii) a three-fold increase in open and closed dwell times (Fig. 4; Table 3), and (iii) a left shift of the voltage-activation relationship (Fig. 3; Table 2). Furthermore, (iv) the LTH fetal channels were relatively dephosphorylated (Fig. 3A), which provides the channels with a capacity of up to a 10-fold increase in Ca^{2+} affinity, depending upon extent of PKA or PKG signaling pathway stimulation (4, 32). This suggests that the cerebral arteries of LTH fetus may be more relaxed than those of the normoxic fetus, and possibly more prone to rupture and produce cerebral hemorrhage.

Perspective. The main branch cerebral arteries, including the basilar, play a critical role in regulating and maintaining CBF (22). During increased flow demand, a significant pressure drop from these vessels to smaller cerebral arteries occurs (12), and a substantial portion of the change in cerebral vascular pressure results from dilation and contraction of these large arteries that supply the brain (28). Such changes in vessel diameter serves to moderate hydrostatic pressure changes in smaller cerebral arteries that feed pial arteries and penetrating arterioles that oxygenate and deliver brain nutrients.

In premature and fetal growth restricted (FGR) puppies (22) and in premature lambs (3), however, the large cerebral arteries of may not regulate effectively the CBF, as opposed to full-term newborns. Such dysregulation primarily is due to undeveloped sympathetic adrenergic innervation that normally provides central control of vasoconstriction (10, 61). Increased risk of cerebral hemorrhage in LTH near-term fetuses and premature infants occurs in response to sudden increases in arterial pressure. We suggest that neonatal hemorrhagic stroke in LTH newborns may occur due to diminished sympathetic vasoconstriction (9) in the face of vasorelaxation stemming from increased BK channel activation, as reported here. Thus, the present study underscores the important role of the basilar artery in regulating vascular tone and CBF, and suggests that failure of these vessels to regulate downstream pressure in smaller cerebral arteries may result in their rupture with dire consequences. Our findings of increased cerebrovascular BK channel activity in both LTH fetus and adult compared to their normoxic counterparts suggest, at least, a partial physiological basis by which sheep successfully acclimatize to long-term high altitude; whereas many mammals do not.

Author Contributions

XT performed conventional whole-cell patch-clamp experiments, confocal microscopy analysis, and helped to write the manuscript. MTL performed perforated-patch and single-channel experiments, analysis, and helped to write the manuscript. GUT performed flow cytometric experiments, analysis, and helped to write the manuscript. SW advised on confocal microscopy and helped to write the manuscript. LDL worked with DAH to formulate the hypothesis and aspects of the study, provided sheep used in study, and helped to write the manuscript. DAH designed and directed the study and wrote the majority of the manuscript. The authors approve the final version of the manuscript, and have no interests to disclose.

Acknowledgements

This work was supported in part by National Institutes of Health Grants HD-003807-41 and HD031226-20 (to LDL) and HD06946 (to SW). A portion of this study was performed in the Loma Linda University School of Medicine Advanced Imaging and Microscopy Core that is supported by the National Science Foundation under Major Research Instrumentation, Division of Biological Infrastructure Grant No. 0923559 (to SW) and the Loma Linda University School of Medicine. We are indebted to Monica Romero for assistance with confocal microscopy. We appreciate the help of Dr. Pooja Mujumdar with aspects of data presentation and statistical analysis.

References

1. Alioua A, Lu R, Kumar Y, Eghbali M, Kundu P, Toro L, Stefani E. Slo 1 caveolin-binding motif, a mechanism of caveolin-Slo 1 interaction regulating Slo 1 surface expression. *J Biol Chem* 283: 4809-4817, 2008.

2. Amberg, GC, Bonev, AD, Rossow, CF, Nelson, MT, Santana, LF. Modulation of the molecular composition of large conductance, Ca^{2+} activated K^+ channels in vascular smooth muscle during hypertension. *J Clin Invest* 112: 717-724, 2003.

3. Behringer EJ, Leite LD, Buchholz NE, Keeney MG, Pearce WJ, Vanterpool CK, Wilson SM, Buchholz JN. Maturation and long-term hypoxia alters Ca^{2+}-induced Ca^{2+} release in sheep cerebrovascular sympathetic neurons. *J Appl Physiol* 107: 1223-34, 2009.

4. Berkefeld H, Fakler B, Schulte U. Ca^{2+}-activated K^+ channels: from protein complexes to function. *Physiol Rev* 90: 1437-1459, 2009.

5. Braddock M, Campbell CJ, Zuder D. Current therapies for wound healing: electrical stimulation, biological therapeutics and the potential for gene therapy. *Int J Dermatol* 38: 808-817, 1999.

6. Behrens R, Nolting A, Reimann F, Schwarz M, Waldschutz R, Pongs O. hKCNMB3 and hKCNMB4, cloning and characterization of two members of the large-conductance calcium-activated potassium channel beta subunit family. *FEBS Lett* 474: 99–106, 2000.

7. Brenner R, Jegla TJ, Wickenden A, Liu Y, Aldrich RW. Cloning and functional characterization of novel large conductance calcium-activated potassium channel beta subunits, hKCNMB3 and hKCNMB4. *J Biol Chem* 275: 6453–6461, 2000a.

8. Brenner R., Peréz GJ, Bonev AD, Eckman DM, Kosek JC, Wiler SW, Patterson AJ, Nelson MT, Aldrich RW. Vasoregulation by the β1 subunit of the calcium-activated potassium channel. *Nature* 407: 870-876, 2000b.

9. Buchholz J, Duckles SP. Chronic hypoxia alters prejunctional alpha(2)-receptor function in vascular adrenergic nerves of adult and fetal sheep. *Am J Physiol Regul Integr Comp Physiol* 281: R926-R934, 2001.

10. Cassaglia PA, Griffiths RI, Walker AM. Sympathetic nerve activity in the superior cervical ganglia increases in response to imposed increases in arterial pressure. *Am J Physiol Regul Integr Comp Physiol* 29: R1255-R1261, 2008.

11. Coleman CN. Hypoxia in tumors: a paradigm for the approach to biochemical and physiological heterogeneity. *J Natl Cancer Res* 80: 310-317, 1988.

12. Dieckhoff D, Kanzow E. On the location of the flow resistance in the cerebral circulation. *Pflugers Arch* 310: 75-85, 1969.

13. Ferriero, DM. Neonatal brain injury. *N Engl J Med* 351: 1985-1995, 2004.

14. Gilbert RD, Pearce WH, LD Longo LD. Fetal cardiac and cerebrovascular acclimatization responses to high altitude, long-term hypoxia. *High Alt Med Biol* 4*:* 203-213, 2003.

15. Giordano FJ. Oxygen, oxidative stress, hypoxia, and heart failure. *J Clin Invest* 115: 500-508, 2005.

16. Goddard-Finegold J, Mizrahi EM. Understanding and preventing perinatal, intracerebral, peri- and intraventricular hemorrhage. *J Child Neurol* 2: 170-185, 1987.

17. Goyal R, Mittal A, Chu N, Shi L, Zhang L, Longo LD. Maturation and the role of PKC-mediated contractility in ovine cerebral arteries. *Am J Physiol Heart Circ Physiol* 297: H2242-H2252, 2009.

18. Hackett PH, Roach RC. High altitude cerebral edema. *High Alt Med Biol* 5: 136-146, 2004.

19. Hamill OP, Marty A, Neher E, Sakmann B, Sigworth FJ. Improved patch-clamp techniques for high-resolution current recording from cells and cell-free membrane patches. *Pflugers Arch* 391: 85-100, 1981.

20. Hao Pang, Phuong U. Le and Ivan R. Nabi. Ganglioside GM1 levels are a determinant of the extent of caveolae/raft-dependent endocytosis of cholera toxin to the Golgi apparatus. *J Cell Sci* 117: 1421-1430, 2004.

21. Harris AL. Hypoxia - a key regulatory factor in tumour growth. *Nat Rev Cancer* 2: 38-47, 2002.

22. Heistad DD, Marcus ML, Abboud FM. Role of large arteries in regulation of cerebral blood flow in dogs. *J Clin Invest* 62: 761-768, 1978.

23. Horn R & Marty A. Muscarinic activtion of ionic currents measured by a new whole-cell recording method. *J Gen Physiol* 92: 145-159, 1988.

24. Hunter CJ, Blood AB, White CR, Pearce WJ, Power GG. Role of nitric oxide in hypoxic capillary flow response to hypoxia. *J Physiol (Lond)* 549: 625-633, 2003.

25. Jensen JB, Wright AD, Lassen NA, Harvey TC, Winterborn MH, Bradwell AR. Cerebral blood flow in acute mountain sickness. *J Appl Physiol* 69: 430-433, 1990.

26. Kamitomo, M, Alonso JG, Okai T, Longo LD, Gilbert RD. Effects of long-term, high-altitude hypoxemia on ovine fetal cardiac output and blood flow distribution. *Am J Obstet Gynecol* 169: 701-707, 1993.

27. Kirby BS, Bruhl A, Sullivan MN, Francis M, Dinenno FA, Earley S. Robust internal elastic lamina fenestration in skeletal muscle arteries. *PLoS One* 8: e54849, 2013.

28. Kontos HA, Wei EP, Navari RM, Levasseur JE, Rosenblum WI, Patterson JL. Responses of cerebral arteries and arterioles to acute hypotension and hypertension. *Am J Physiol* 234: H371-H383, 1978.

29. Korper S, Nolte F, Rojewski MT, Thiel E, Schrezenmeier H. The K^+ channel openers diazoxide and NS1619 induce depolarization of mitochondria and have differential effects on cell Ca^{2+} in CD34 cell line KG-1a. *Exp Hematol* 31: 815-823, 2003.

30. Ledoux J, Werner ME, Brayden JE, Nelson MT. Calcium-activated potassium channels and the regulation of vascular tone. *Physiology (Bethesda)* 21: 69-79, 2006.

31. Lin MT, Hessinger DA, Pearce WJ, Longo LD. Developmental differences in Ca^{2+}-activated K^+ channel activity in ovine basilar artery. *Am J Physiol Heart Circ Physiol* 285: H701-H709, 2003.

32. Lin MT, Longo LD, Pearce WJ, Hessinger DA. Ca^{2+}-activated K^+ channel-associated phosphatase and kinase activities during development. *Am J Physiol Heart Circ Physiol* 289: H414-H425, 2005.

33. Lin MT, Hessinger DA, Pearce WJ, Longo LD. Modulation of BK channel calcium affinity by differential phosphorylation in developing ovine basilar artery myocytes. *Am J Physiol Heart Circ Physiol* 291: H732-H740, 2006.

34. Lohn M, Lauterbach B, Haller H, Pongs O, Luft FC, Gollasch M. β1-Subunit of BK channels regulates arterial wall [Ca^{2+}] and diameter in mouse cerebral arteries. *J Appl Physiol* 91: 1350-1354, 2001.

35. Long W, Zhang L, Longo LD. Fetal and adult cerebral artery K(ATP) and K(Ca) channel responses to long-term hypoxia. *J Appl Physiol* 92: 1692-1701, 2002.

36. Longo LD, Pearce WJ. Fetal cerebrovascular acclimatization responses to high-altitude, long-term hypoxia: a model for prenatal programming of adult disease? *Am J Physiol Regul Integr Comp Physiol* 288: R16-R24, 2005.

37. Lu T, Zhang DM, Wang XL, He T, Wang RX, Chai Q, Katusic ZS, Lee HC. Regulation of coronary arterial BK channels by caveolae-mediated angiotensin II signaling in diabetes mellitus. *Circ Res* 106:1164-73, 2010.

38. Massol RH, Larsen JE, Fujinaga Y, Lencer WI, Kirchhausen T. Cholera Toxin Toxicity Does Not Require Functional Arf6- and Dynamin-dependent Endocytic Pathways. *Mol Biol Cell* 15: 3631–3641, 2004.

39. Navarro-Antolín J, Levitsky KL, Calderón E, Ordóñez A & López-Barneo J (2005). Decreased expression of maxi-K channel beta 1-subunit and altered vasoregulation in hypoxia. *Circulation* 112, 1309-1315, 2005.

40. Nelson DA, Tan TT, Rabson AB, Anderson D, Degenhardt K, White E. Hypoxia and defective apoptosis drive genomic instability and tumorigenesis. *Genes Dev* 18: 2095-2107, 2004.

41. Nelson KB. Can we prevent cerebral palsy? *N Engl J Med* 349: 1765-1769, 2003.

42. Orio P, Latorre R. Differential effects of beta 1 and beta 2 subunits on BK channel activity. *J Gen Physiol* 125: 395-411, 2005.

43. Park WS, Kang SH, Son YK, Kim N, Ko JH, Kim HK, Ko EA, Kim CD, Han J. The mitochondrial Ca^{2+}-activated K^{+} channel activator, NS 1619 inhibits L-type Ca^{2+} channels in rat ventricular myocytes. *Biochem Biophys Res Commun* 362: 31-6, 2007.

44. Parton RG. Ultrastructural localization of gangliosides; GM_1 is concentrated in caveoli. *J Histochem Cytochem* 42: 155-166, 1994.

45. Patton C, Thompson S, Epel D. Some precautions in using chelators to buffer metals in biological solutions. *Cell Calcium* 35: 427-431, 2004.

46. Pereyra Peña, JL, Tomimatsu T, Hatran DP, McGill LL, Longo LD. Cerebral blood flow and oxygenation in the ovine fetus: responses to superimposed hypoxia at both low and high altitude. *J Physiol (Lond)* 578: 359-370, 2007.

47. Plüger S, Faulhaber J, Fürstenau M, Löhn M, Waldschütz R, Gollasch M, Haller H, Luft FC, Ehmke H, Pongs O. Mice with disrupted BK channel β1 subunit gene feature abnormal Ca^{2+} spark/STOC coupling and elevated blood pressure. *Circ Res* 87: 53-60, 2000.

48. Qian X, Magleby KL. b1 subunits facilitate gating of BK channels by acting through the Ca^{2+}, but not the Mg^{2+}, activating mechanisms. *Proc Natl Acad Sci (USA)* 100: 10061-10066, 2003.

49. Rasband, WS. ImageJ, U. S. NIH, Bethesda, MD, http://imagej.nih.gov/ij/. 1997-2012

50. Resnik E, Herron J, Fu R, Ivy DD, Cornfield DN. Oxygen tension modulates the expression of pulmonary vascular BK_{Ca} channel a and b subunits. *Am J Physiol Lung*

Cell Mol Physiol 290: L761-L768, 2006.

51. Sakmann B, Neher E. *Single-Channel Recording*. New York: Plenum, 1995, p. 627-650.

52. Samaranayake H, Saunders JC, Greene MI, Navaratnam DS. Ca^{2+} and K^{+} (BK) channels in chick hair cells are clustered and colocalized with apical-basal and tonotopic gradients. *J Physiol* 560: 13-20, 2004.

53. Sanchez M, McManus OB. Paxilline inhibition of the alpha-subunit of the high-conductance calcium-activated potassium channel. *Neuropharmacol* 35: 963-8, 1996.

54. Schmedtje JF, Ji YS. Hypoxia and molecular cardiovascular medicine. *Trends Cardiovasc Med* 8: 24-33, 1998.

55. Semenov I, Wang B, Herlihy JT, Brenner R. BK channel b_1-subunit regulation of calcium handling and constriction in tracheal smooth muscle. *Am J Physiol Lung Cell Mol Physiol* 29: L802-L810, 2006.

56. Severinghaus JW, Chiodi H, Eger EI II, Branstater B, Hornbein TF. Cerebral blood flow in man at high altitude. Role of cerebrospinal fluid pH in normalization of flow in chronic hypocapnia. *Circ Res* 19: 274-282, 1966.

57. Soleymanlou N, Jurisica I, Nevo O, Ietta F, Zhang X, Zamudio S, Post M, Caniggia I. Molecular Evidence of Placental Hypoxia in Preeclampsia. *J Clin Endocr Metab* 90: 4299-4308, 2005.

58. Stoll BJ, Hansen NI, Bell EF, *et al*. Neonatal outcomes of extremely preterm infants from the NICHD Neonatal Research Network. *Pediatrics* 126: 443-456, 2010.

59. Szewczyk A, Kajma A, Malinska D, Wrzosek A, Bednarczyk P, Zabocka B, Doowy K. Pharmacology of mitochondrial potassium channels: dark side of the field. *FEBS Letters* 584: 2063-2069, 2010.

60. Tomimatsu, T, Pereyra-Peña JL, Hatran DP, Longo LD. Maternal oxygen administration and fetal cerebral oxygenation: Studies on near-term fetal lambs at both low and high altitude. *Am J Obstet Gynecol* 195: 535-541, 2006.

61. van Lieshout JJ, Secher NH. Point:Counterpoint: Sympathetic activity does/does not influence cerebral blood flow. Point: Sympathetic activity does influence cerebral blood flow. *J Appl Physiol* 105: 1364-6, 2008.

62. Vargas M, Ororio J, Moraga D, Sepulveda M, Del Solar J, Hudson C, Cortes G, Leon A. Acute mountain sickness at 3500 and 4250 m. A study of symptom incidence and severity. *Rev Med Chile* 127: 166-172, 2001.

63. Volpe A. Brain injury in the premature infant: neuropathology, clinical aspects, pathogenesis and prevention. *Clin Perinatol* 24: 567-587, 1997.

64. Yamamura H, Ohi Y, Muraki K, Watanabe M, Imaizumi Y. BK channel activation by NS-1619 is partially mediated by intracellular Ca^{2+} release in smooth muscle cells of porcine coronary artery. *Brit J Pharmacol* 132: 828-834, 2001.

CHAPTER THREE

PROTEIN KINASE C ACTIVATES BK CHANNELS IN FETAL, BUT NOT ADULT, MIDDLE CEREBRAL ARTERIES

XIAOXIAO TAO[1], LIJUN SHI, [2,3], LAWRENCE D. LONGO[1,2], DAVID A. HESSINGER[1]

[1]Departments of Physiology and Pharmacology, [2]Center for Perinatal Biology, Loma Linda School of Medicine, Loma Linda, California 92350 and [3]Department of Human Sport Science, Beijing Sport University, Beijing 100084, China

Abstract

In cerebral arteries, K^+ channels play a major role in modulating membrane potential, voltage-gated Ca^{2+}-channel activity, intracellular Ca^{2+} concentration ($[Ca^{2+}]_i$), and vascular tone. We have shown that Ca^{2+}-activated, large-conductance K^+ (BK) channels and ATP-sensitive (K_{ATP}) channels predominate among cerebral K^+ channels in regulating $[Ca^{2+}]_i$ and these channels are more active in the ovine fetus than adult. Protein Kinase C (PKC) causes cerebral vasoconstriction, but little is known about the effects of PKC on K^+ channel activity in cerebral vascular smooth muscle. To measure the effects of PKC on cerebrovascular K^+ channels of middle cerebral arteries (MCAs) from near-term fetal (～140 day) and nonpregnant adult sheep, we simultaneously measured phorbol 12,13-dibutyrate (PDBu; PKC agonist)-induced responses of vascular tension and $[Ca^{2+}]_i$ in the absence and presence of selective K^+ channel blockade, PDBu (3×10^{-6} M) increased tension in fetal and adult MCA to ～20% K_{max} and ～55% K_{max}, respectively ($P<0.05$). Among tested K^+ channel blockers (iberiotoxin, glibenclamide, 4-aminopyridine, and $BaCl_2$), only iberiotoxin, a BK blocker, increased PDBu-induced contraction and $[Ca^{2+}]_i$, and this was only in the fetus. Zero extracellular Ca^{2+} or nifedipine (10^{-5}M), an L-type Ca^{2+}-channel blocker, eliminated this effect. We hypothesized that in fetal MCA, PKC stimulation by PDBu regulates vascular tone by activating BK channels to inhibit Ca^{2+} influx through the L-type Ca^{2+}-channel and thus inhibit $[Ca^{2+}]_i$ increase. In inside-out membrane patches, PKC activated BK channel activity. Also, PDBu hyperpolarized the resting membrane potential of fetal, but not adult, myocytes. These results are consistent with our hypothesis.

Introduction

Protein kinase C (PKC) regulates a variety of cell functions, including growth and differentiation, gene expression, and membrane activities (27). In cerebral arteries, PKC plays an important role in the regulation of vascular tone under both physiological and pathological conditions (10, 23, 38). In addition to increasing calcium sensitization in vascular smooth muscle cells (SMCs; 15, 23, 37), PKC may also affect vascular ion channels (26, 33, 35).

By modulating membrane potential in vascular smooth muscle, K^+ channels regulate voltage-gated Ca^{2+}-channel activity, intracellular Ca^{2+} concentration ($[Ca^{2+}]_i$), and vascular tone. Several types of K^+ channel activities occur in cerebral artery SMCs, including large-conductance Ca^{2+}-activated (BK), ATP-sensitive (K_{ATP}), voltage-dependent (K_v), and inward rectifier (K_{IR}) (12, 26). Membrane potential, $[Ca^{2+}]_i$, cytoplasmic ATP concentrations, protein kinases and phosphatases, and second messengers may regulate these channel activities. PKC can modulate vascular contractility by acting on different K^+ channels, including K_{ATP} (5), K_v (4, 8) and K_{IR} (11, 14) channels.

In general, among vascular SMC ion channels, BK channels predominate in regulating vascular tone (26). In ovine middle cerebral arteries (MCAs), both BK and K_{ATP} channels appear to play major roles in the regulation of this tone (20). PKC inhibits BK channel activation in pulmonary (1), coronary (25), and rat tail artery (34) SMCs. However, in pulmonary vascular SMCs, PKC activates BK channels via phosphorylation of PKG (2). Although PKC activation induces vasoconstriction in cerebral arteries, (23, 38), there are no studies of which we are aware that have investigated the effects of PKC

on K^+ channel activity in cerebral vascular SMCs, much less during development. Because the BK channels of near-term fetal cerebral arteries have three-fold more channel-associated PKG activity than channels from adult (19), we hypothesized that PKC activation by PDBu in fetal cerebral vessels will activate BK channels to a greater extent than in the adult, and will inhibit Ca^{2+} influx through L-type Ca^{2+} channels, thereby modulating vascular tone. Our findings from simultaneous measures of vessel tension and $[Ca^{2+}]$ and patch-clamp electrophysiology support this hypothesis.

Methods

Experimental animals and tissues. For these studies, we used main branch middle cerebral arteries from near-term fetal (~140 gestational day) and nonpregnant female adult sheep (≤2 yr) obtained from Nebeker Ranch (Lancaster, CA). We obtained isolated cerebral artery segments from both the nonpregnant ewes and fetuses after anesthetizing and sacrificing ewes with 100 mg/kg intravenous pentobarbital sodium. We have shown that this method has no significant effect on vessel reactivity (30). To avoid the involvement of eondothelial-mediated effects, we removed the endothelium by carefully inserting a small wire three times (22). Cerebral arteries then were used immediately for simultaneous measurements of $[Ca^{2+}]_i$ and tension (20, 21). To confirm endothelium removal, we contracted the vessel with 10^{-5} M 5-hydroxytryptamine and, at the plateau, added 10^{-6} M ADP. Vessels that relaxed >20% after this treatment were rejected from further study. Unless otherwise noted, all chemical compounds were purchased from Sigma-Aldrich (St. Louis, MO).

Contractility and intracellular calcium measurements. We cut the MCAs into rings 2 mm in length and mounted them on two tungsten wires (0.13-mm diameter; A-M Systems, Carlsborg, WA). We attached one wire to an isometric force transducer (Kent Scientific, Litchfield, CT), and the other to a post attached to a micrometer used to vary resting tension in a 5-ml tissue bath mounted on a Jasco CAF-110 intracellular Ca^{2+} analyzer (Jasco, Easton, MD). Briefly, we measured vessel inside diameter, wall thickness, length, and KCl (0.12 M)-induced force, and calculated tension, per cross-sectional area, as previously described (20, 21, 30). MCA rings were equilibrated under 0.3 g passive tension at 25°C for 40 min before loading with the acetoxymethyl ester of

fura 2 [fura 2(AM); Teflabs, Austin, TX], a fluorescent Ca^{2+} indicator used to measure ratiometric changes in $[Ca^{2+}]_i$ (13). We measured fura 2 fluorescence ratio ($F_{340/380}$) and force simultaneously at 38°C (21). In tissues such as cerebral arteries, the presentation of the ratio is less ambiguous than the transformation of fluorescence into $[Ca^{2+}]_i$ (21). During all contractility experiments, we continuously digitized, normalized, and recorded contractile tensions and the fluorescence ratio using an online computer. For all vessels, we expressed the contractile response for tension and fluorescence ratio as percent K_{max}.

Effects of PKC activation on K^+ channels and changes with development. Because relatively little is known about the role of PKC in modulating the several K^+ channels in fetal SMCs, we quantified $[Ca^{2+}]_i$, and vascular tension in the presence of selective K^+-channel blockers. For all studies, following initial K^+ (120 mM) depolarization to determine K_{max}, we measured responses to the PKC activator, phorbol 12,13-dibutyrate (PDBu), in the absence or presence of appropriate K^+-channel blocker. To avoid interactions between different K^+-channel blockers, we tested each segment with only one type of K^+-channel inhibitor. PDBu was dissolved in dimethyl sulfoxide (DMSO). The maximal bath DMSO concentration attained during any experiment was less than 0.1%, which had no independent effect on vessel tension. To examine the effect of PKC activity on BK channels in fetal and adult cerebral arteries, we first stimulated the vessel with 3×10^{-6} M PDBu in one segment to determine the $\%K_{max}$. Then, on the other segment from the same artery, the vessel was pretreated with iberiotoxin (10^{-9} to 10^{-6} M IbTX; a highly selective blocker of BK channels) for 15 min, and then PDBu was added in the presence of IbTX. To examine the possible effect of PDBu on K_{ATP} activity, we pretreated the segments with glibenclamide (a selective

blocker of ATP-sensitive K^+ channels) for 15 min, and then quantified PDBu-induced $[Ca^{2+}]_i$ and vascular tone in the presence of glibenclamide. We also examined the effect of different concentrations of glibenclamide (10^{-9} to 10^{-4} M) alone. Similarly, to examine the potential effect of PKC on K_v or K_{IR} channels, we measured PDBu-induced $[Ca^{2+}]_i$ and tension after administration of 4-aminopyridine (4-AP) or barium chloride ($BaCl_2$), respectively. We also examined the effect of 4-AP (10^{-8} to 10^{-2} M) or $BaCl_2$ (10^{-9} to 10^{-4} M) alone. We selected the concentration of PDBu and of each K^+-channel blocker used in the present study according to previous studies of our laboratory (20, 23).

Role of extracellular Ca^{2+}. To determine the role of extracellular Ca^{2+} concentration in the PDBu-induced responses following BK channel blocker, we measured $[Ca^{2+}]_i$ and vessel tension in response to IbTX alone or with PDBu after vessels had been exposed to nominally calcium-free (1mM EGTA to chelate Ca^{2+}) Krebs buffer for 15 min ($n = 4$). Again, we evaluated the contractile response of tension and fluorescence ratio by measuring the maximum peak height and expressing it as percent K_{max} (21).

Current clamp recordings of resting membrane potentials. We used a cell-attached, whole-cell, current-clamp method (24) to record resting membrane potentials from freshly isolated SMCs. To record membrane potentials, the current was held at 0 pA. After recording a steady baseline membrane potential for at least 60 s, PDBu (3×10^{-6} M) was added to the bath. Pipette resistances were between 10–15 MΩ seal resistances were between 8–10 GΩ. Voltages were not corrected for junction potentials. The pipette solution (in mM) was: 150 KCl, 2 EGTA, 2 MgCl2 10 HEPES pH 7.3 with KOH. The

bath solution (in mM): 145 NaCl, 5 KCl, 1 CaCl2, 1MgCl2, 10 HEPES, 10 Glucose, pH 7.35 with NaOH

Single-channel recordings. We recorded single-channel currents from inside-out membrane patches of isolated arterial myocytes (17). Patch pipettes were made using a programmable Flaming-Brown pipette puller with fire polishing. The area of contact with each membrane also was similar because patch pipettes so produced had similar tip resistances (≈15 MΩ). We filtered currents at 2 KHz and digitized at 10 KHz. The number of channels in any given excised patch (N) was estimated from all-points histograms. Channel activity, NP_o, was calculated by using equation 1.

$$NP_o = \sum_{i=0}^{N} i \cdot Ai / \sum_{i=0}^{N} Ai, \qquad \text{Equation 1}$$

where i is the number of open channels (0 is the number for closed state), and A_i is the area associated with each channel state, as determined from curve-fit individual peak areas. Single-channel open probability (P_o) was calculated from NP_o/N. We obtained the values for N using high [Ca^{2+}] and/or high depolarization to ensure that no more than three coincidental open events occurred during recordings (>20 s) at a P_o higher than 0.8. We discarded preparations showing more than three channels. The bath solution contained (in mM): KCl (140), Mg^{2+} (1), HEPES (10), and EGTA (5) adjusted to pH 7.2 with KOH with free Ca^{2+} concentrations (~3 μM) measured fluorometrically using Fura-2. The single-channel pipette solution was the same as the bath solution with ~3 μM free Ca^{2+}.

Statistical analysis. All values were calculated as means ± SE. In all cases, n refers to the number of vessel segments, which corresponds to the number of animals studied. The n values for the different experiments are given in Table 1. For testing

differences between two groups, we used a simple unpaired Student's *t*-test. Comparison among multiple groups was made by using one-way ANOVA for multiple comparisons. A P value < 0.05 was considered to indicate a significant difference.

Results

PDBu increased tension without changing $[Ca^{2+}]_i$. To identify the effects of PKC activation on K^+ channels in fetal and adult MCA, we measured the effects of 3×10^{-6} M PDBu on contractile and $[Ca^{2+}]_i$ responses in the absence and presence of various K^+ channel inhibitors at the doses known to be maximally effective (20). In fetal MCAs, PDBu by itself induced steady-state tension to increase ~20% K_{max} within 20 min, at which time it remained steady, while $[Ca^{2+}]_i$ remained at baseline levels or decreased slightly (Fig.1A; Table 1). In adult MCAs, PDBu induced a significantly greater increase in vascular tension, to ~55% K_{max} at 40 min, while $[Ca^{2+}]_i$ decreased slightly (Fig. 1B, Table 1). Fig. 1C summarizes these PDBu-induced responses in both tension and fluorescence ratio as percent K_{max}.

To establish the specificity of PDBu effects on MCA responses, we used 4α-PMA (3×10^{-6} M), an inactive chemical homologue of PDBu as a negative control for phorbol ester activation of PKC. Administration of 4α-PMA was without significant effect on either vessel contractility or $[Ca^{2+}]_i$ in either age group (n=3 each; data not shown).

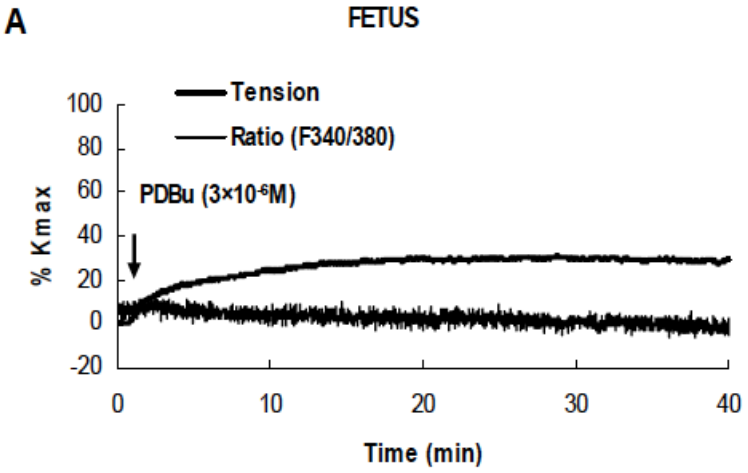
A
FETUS
Tension
Ratio (F340/380)
PDBu (3×10-6M)
% Kmax
100
80
60
40
20
0
-20
0
10
20
30
40
Time (min)

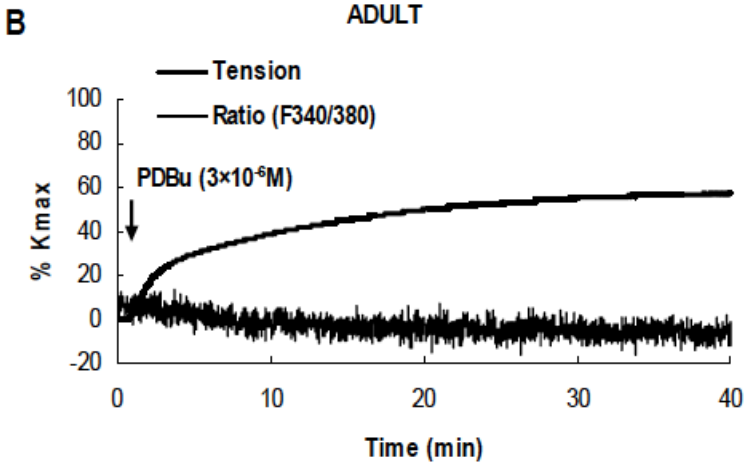
B
ADULT
Tension
Ratio (F340/380)
PDBu (3×10-6M)
% Kmax
100
80
60
40
20
0
-20
0
10
20
30
40
Time (min)

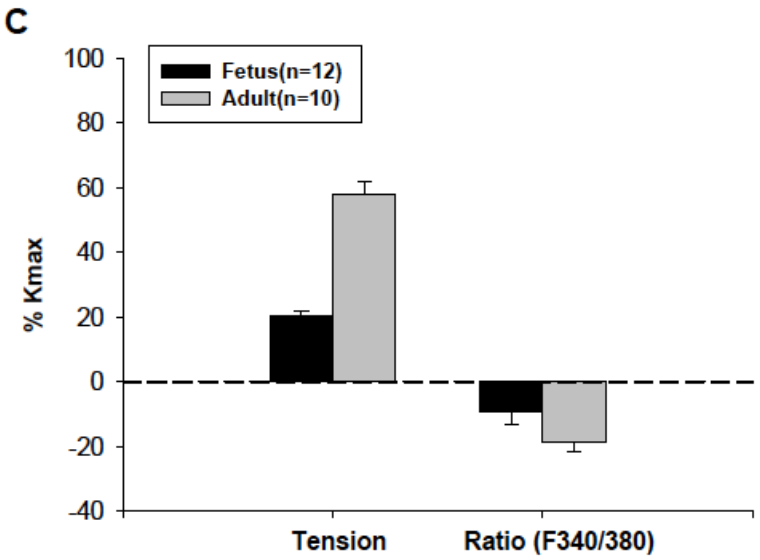
C
Fetus(n=12)
Adult(n=10)
% Kmax
100
80
60
40
20
0
-20
-40
Tension
Ratio (F340/380)

Figure 1. PDBu-induced tension and intracellular Ca^{2+} concentration (% K_{max}) in ovine fetal and adult middle cerebral arteries (MCA). A: Time-course of 3 x 10^{-6} M PDBu - induced contraction and fluorescence ratio ($F_{340/380}$) of $[Ca^{2+}]_i$ in fetal MCA. B: Time-course of PDBu-induced contraction and fluorescence ratio ($F_{340/380}$) of $[Ca^{2+}]_i$ in adult MCA. C: Bars indicate the average PDBu-induced tension and intracellular Ca^{2+} concentration (% K_{max}) in ovine fetal (black) and adult (gray) MCA. Error bars represent ± SE. *, $P<0.01$ compared with control 3 x 10^{-6} M PDBu. The fluorescence ratio ($[Ca^{2+}]_i$) shows a slight decrease in response to PDBu treatment in both developmental age groups.

BK channel inhibition increased both tension and $[Ca^{2+}]_i$. To measure the effect of BK channel inhibition on the basal vessel tension and $[Ca^{2+}]_i$, we performed dose responses of IbTX in half-log doses (10^{-9} to 10^{-6} M). In the fetal artery, 3 x 10^{-7} M IbTX and above increased tension and $[Ca^{2+}]_i$ significantly and dose-dependently (Fig. 2A and B; Fig. 3A and B). In adult MCA, consistent with the results of our previous studies (20), IbTX also increased both tension and $[Ca^{2+}]_i$ significantly and dose-dependently, but with lower sensitivity and lower maximum effect (Fig. 3A and B). The dose-response relationships of IbTX alone (IbTX-transient) are shown in Figs. 3A and B. The maximum IbTX-transient for both tension (Fig. 3A) and $[Ca^{2+}]_i$ (Fig. 3B) were significantly greater in the fetus than in the adult ($P<0.01$), as was the pD2 value (negative logarithm of the mean effective concentration at half-maximal response) or "sensitivity" to IbTX ($P<0.05$).

BK inhibition predisposed PDBu-induced transients in fetus. To compare the contribution of BK channel inhibition in fetal and adult MCAs, we tested the effects of IbTX on PDBu-induced tension and fluorescence ratio. As shown in Figs. 2A-D, in both age groups, IbTX alone at 10^{-8} M was without effect on basal MCA tension or $[Ca^{2+}]_i$. However, in fetal MCA, following IbTX incubation for 15 min, the tension induced by PDBu in the presence of IbTX increased sharply and transiently within the first 2-3 min (referred to as "PDBu-induced transient") and reaching a maximum at ~32% K_{max}. Then, the elevated tension dropped rapidly (within 5 min), but in the following 40 min a steady-state tension developed and reached ~25% K_{max} (Fig. 2A). Shortly after PDBu administration, the fluorescence ratio also increased significantly, within the first 2-3 min, with the maximum ratio reaching 12% K_{max}. In parallel with the change of vessel

tension, the fluorescence ratio quickly fell to baseline level, but in the following 40 min steady-state tension increased again to ~10% K_{max} (Fig. 2B). In adult vessels, however, in the presence of 10^{-8} M IbTX, the PDBu did not produce PDBu-induced transient increases in tension nor fluorescence ratio, and neither steady-state tension nor fluorescence ratio were significantly altered (Figs. 2C and D), as compared to PDBu-treated only (Fig. 1B) ($P<0.05$).

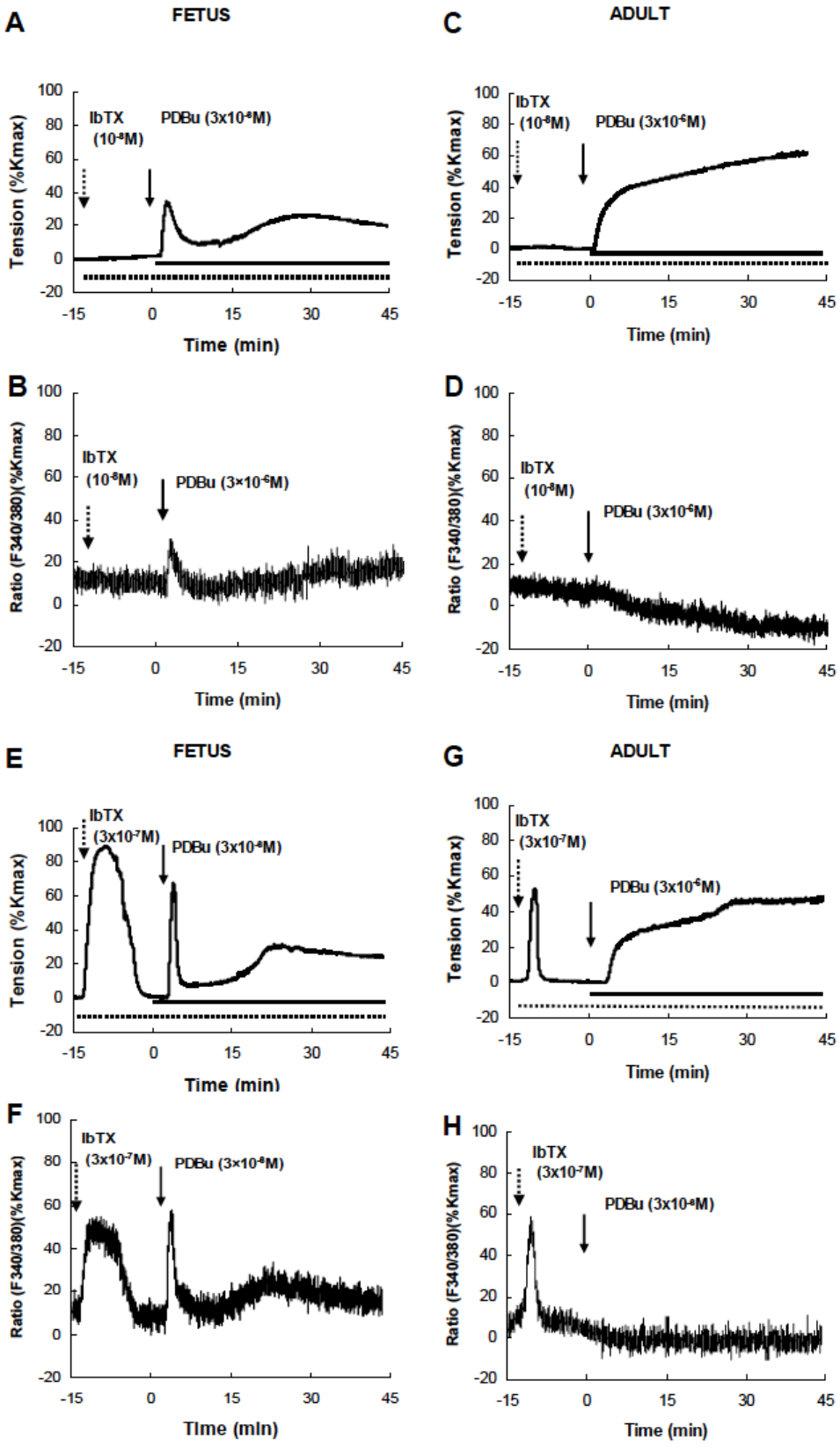
A
FETUS
C
ADULT
IbTX
(10-8M)
PDBu (3x10-6M)
Tension (%Kmax)
Time (min)
B
D
Ratio (F340/380)(%Kmax)
E
FETUS
G
ADULT
IbTX
(3x10-7M)
F
H
TIme (mIn)

Figure 2. PDBu-induced tension and intracellular Ca^{2+} concentration ($\%K_{max}$) in ovine fetal and adult MCA in the presence of iberiotoxin (IbTX). Time-course of 3 x 10^{-6} M PDBu-induced contraction (A) and fluorescence ratio ($F_{340/380}$) of $[Ca^{2+}]_i$ (B) in fetal MCA in the presence of IbTX (10^{-8} M). Time-course of PDBu-induced contraction (C) and fluorescence ratio ($F_{340/380}$) of $[Ca^{2+}]_i$ (D) in adult MCA in presence of IbTX (10^{-8} M). Time-course of PDBu-induced contraction (E) and fluorescence ratio ($F_{340/380}$) of $[Ca^{2+}]_i$ (F) in fetal MCA in the presence of IbTX (3 x 10^{-7} M). Time-course of PDBu-induced contraction (G) and fluorescence ratio ($F_{340/380}$) of $[Ca^{2+}]_i$ (H) in adult MCA in the presence of IbTX (3 x 10^{-7} M). IbTX, iberiotoxin.

To determine the dose effectiveness of BK channel inhibition on the increase of PDBu-induced tension and $[Ca^{2+}]_i$, we repeated the above experiments using IbTX from 10^{-9} to 10^{-6} M in half-log doses. The results of 3 x 10^{-7} M IbTX are shown in Figs. 2E-H, and the complete dose responses are shown in Fig. 3. In fetal MCA, IbTX increased vessel tension significantly to about 80% K_{max}, after which it returned to the basal level within 15 min (Fig. 2E). After its decrease to near control, PDBu was added in the presence of IbTX, which produced a rapid, but transient increase of tension with peak height ~70% K_{max}, followed by a delayed steady-state or sustained increase to ~30% K_{max} (Fig. 2E). In concert with tension changes, the fluorescence ratio increased rapidly following IbTX to ~55 % K_{max}, after which it returned to the basal level within 15 min (Fig. 2F). When PDBu was added in the presence of IbTX, the fluorescence ratio rapidly, but transiently, increased to ~50% K_{max}. In the following 40 min, the ratio increased gradually to ~15% K_{max} (Fig. 2F). In the adult MCA, the PDBu induced increase in tension and fluorescence ratio did not change significantly after higher (3 x 10^{-7} M) IbTX treatment, although IbTX alone increased the vessel tension and $[Ca^{2+}]_i$ significantly (Figs. 2G and H).

Figure 3 shows the dose-response relationships of the PDBu-induced responses in the presence of IbTX [(PDBu-induced transient (Figs. 3C and D) and PDBu-induced steady state (Figs. 3E and F)] in fetal and adult MCAs. The PDBu-induced transient responses (Figs. 3C and D) and the PDBu-induced steady-state responses (Figs. 3E and F) were IbTX concentration-dependent in fetal, but not adult, MCA.

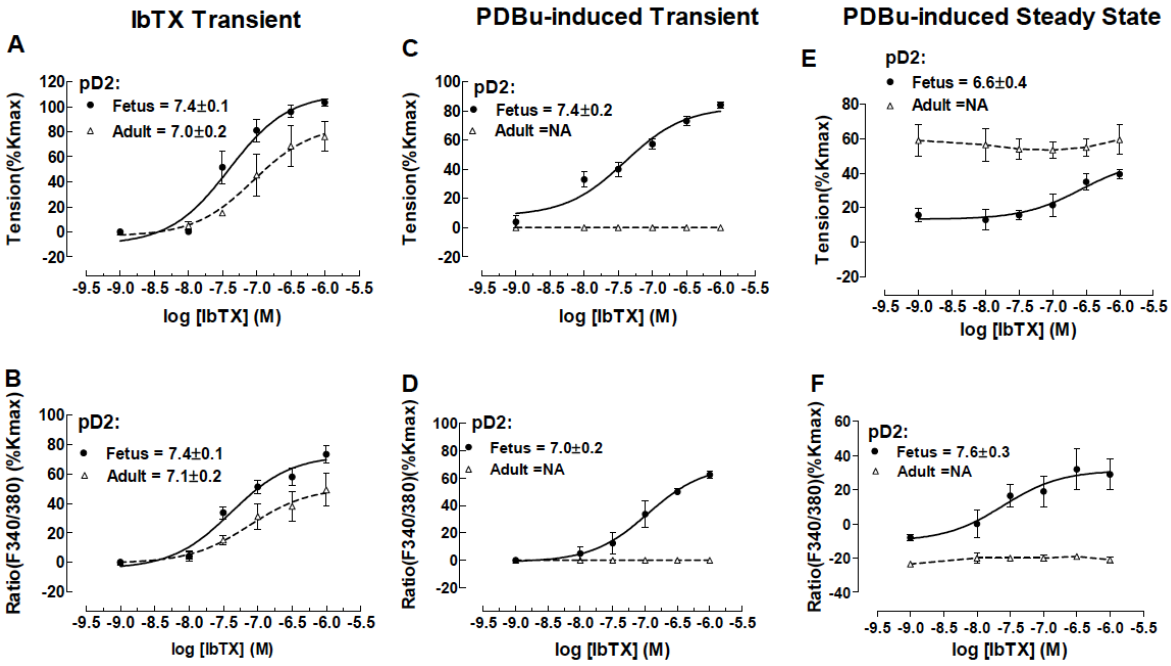

Figure 3. Dose-response relationships of iberiotoxin and of iberiotoxin followed by 3 x 10^{-6} M on PDBu-induced tension and fluorescence ratio (% K_{max}) in ovine fetal and adult MCA. Dose-response relationships of IbTX on IbTX-induced transients in fetal and adult MCA contraction (A) and fluorescence ratio ($F_{340/380}$) of $[Ca^{2+}]_i$ (B). PDBu-induced transient contraction (C) and fluorescence ratio (D) responses following different doses of IbTX pretreatment. PDBu-induced steady-state responses of tension (E) and fluorescence ratio (F) following different doses of IbTX pretreatment. •, solid line refer to, fetus (*n*=4); Δ, dashed line refer to adult (*n*=4); NA, not applicable.

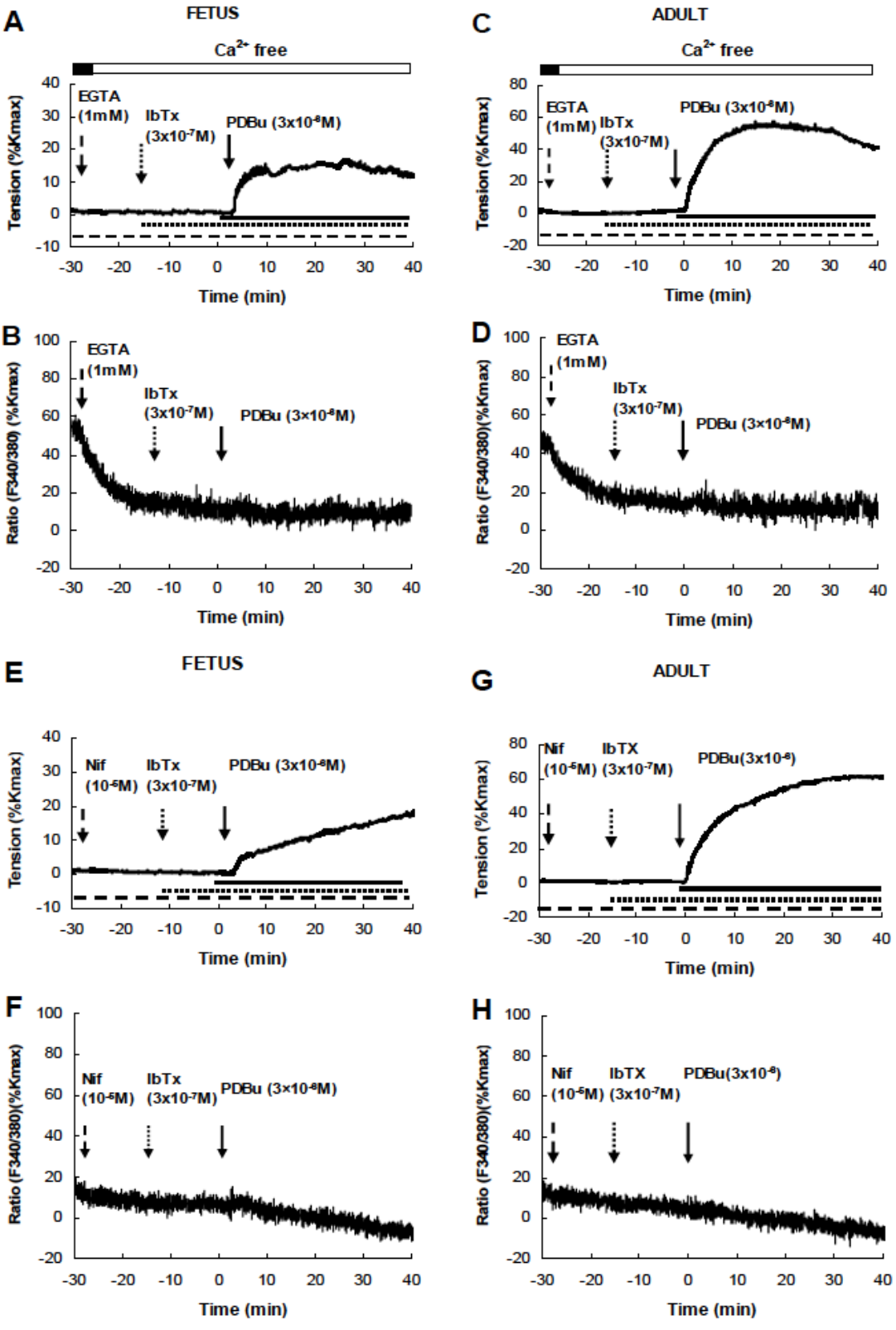
A
FETUS
Ca2+ free
EGTA (1mM)
IbTx (3x10-7M)
PDBu (3x10-6M)
Tension (%Kmax)
Time (min)
C
ADULT
Ca2+ free
EGTA (1mM)
IbTx (3x10-7M)
PDBu (3x10-6M)
Tension (%Kmax)
Time (min)
B
EGTA (1mM)
IbTx (3x10-7M)
PDBu (3x10-6M)
Ratio (F340/380) (%Kmax)
Time (min)
D
EGTA (1mM)
IbTx (3x10-7M)
PDBu (3x10-6M)
Ratio (F340/380)(%Kmax)
Time (min)
E
FETUS
Nif (10-5M)
IbTx (3x10-7M)
PDBu (3x10-6M)
Tension (%Kmax)
Time (min)
G
ADULT
Nif (10-5M)
IbTX (3x10-7M)
PDBu(3x10-6)
Tension (%Kmax)
Time (min)
F
Nif (10-5M)
IbTx (3x10-7M)
PDBu (3x10-6M)
Ratio (F340/380)(%Kmax)
Time (min)
H
Nif (10-5M)
IbTX (3x10-7M)
PDBu(3x10-6)
Ratio (F340/380)(%Kmax)
Time (min)

Figure 4. The effect of iberiotoxin pretreatment on PDBu-induced tension and fluorescence ratio (% K_{max}) in ovine fetal and adult MCA, under the condition of nominally Ca^{2+}-free extracellular medium, or L-type Ca^{2+} channel blockade by nifedipine. Arterial segments were first treated with either EGTA (10^{-3} M) or nifedipine (10^{-5} M) for 15 min, and then treated with IbTX in the presence of either EGTA or nifedipine for another 15 min before adding PDBu (3 x 10^{-6} M), in the continued presence of EGTA (or nifedipine) with IbTX. PDBu-induced contraction (A) and fluorescence ratio ($F_{340/380}$) of $[Ca^{2+}]_i$ (B) in fetal MCA in the presence of IbTX under the condition of nominally Ca^{2+}-free extracellular medium. Time-course of PDBu-induced contraction (C) and fluorescence ratio ($F_{340/380}$) of $[Ca^{2+}]_i$ (D) in adult MCA in the presence of IbTX under the condition of nominally Ca^{2+}-free extracellular Ca^{2+} medium. PDBu-induced contraction (E) and fluorescence ratio ($F_{340/380}$) of $[Ca^{2+}]_i$ (F) in fetal MCA in presence of IbTX under the blockade of L-type Ca^{2+} channel by nifedipine. Time-course of PDBu-induced contraction (G) and fluorescence ratio ($F_{340/380}$) of $[Ca^{2+}]_i$ (H) in adult MCA in presence of IbTX under the blockade of L-type Ca^{2+} channel by nifedipine. In contrast to the responses in the presence of 1.6 mM extracellular Ca^{2+} (Fig. 2), the increase of fluorescence ratio ($[Ca^{2+}]_i$) in the presence of IbTX and IbTX +PDBu in the fetal MCA was eliminated by EGTA or nifedipine . IbTX, iberiotoxin. Nif, nifedipine.

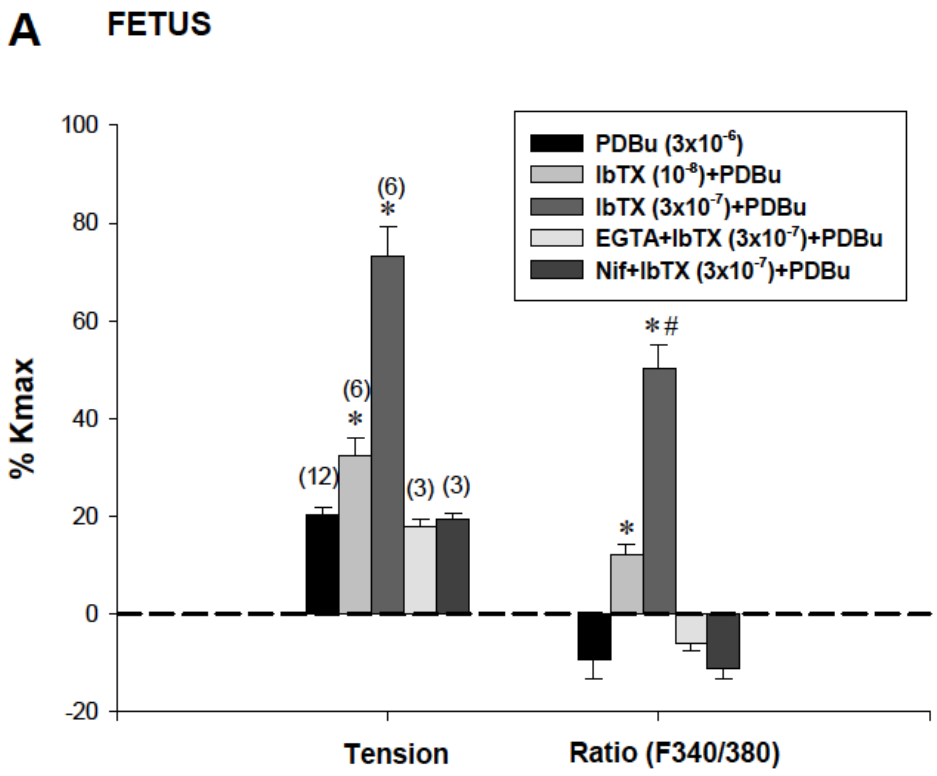
A
FETUS
PDBu (3x10-6)
IbTX (10-8)+PDBu
IbTX (3x10-7)+PDBu
EGTA+IbTX (3x10-7)+PDBu
Nif+IbTX (3x10-7)+PDBu
% Kmax
100
80
60
40
20
0
-20
(12)
(6)
*
(6)
*
(3)
(3)
*
*#
Tension
Ratio (F340/380)

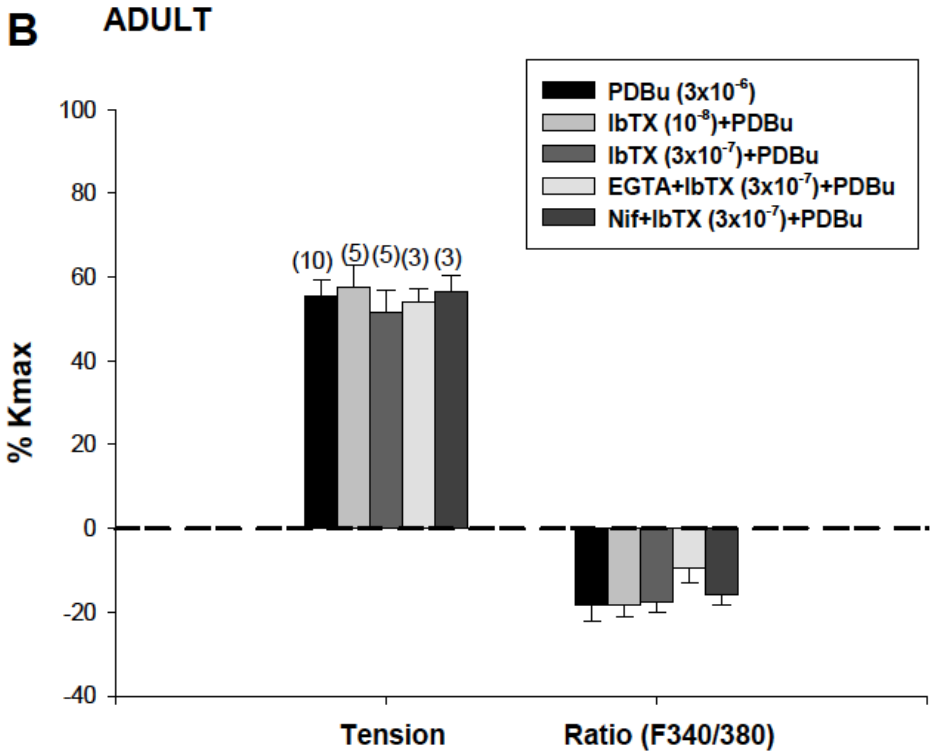
B
ADULT
PDBu (3x10-6)
IbTX (10-8)+PDBu
IbTX (3x10-7)+PDBu
EGTA+IbTX (3x10-7)+PDBu
Nif+IbTX (3x10-7)+PDBu
% Kmax
100
80
60
40
20
0
-20
-40
(10)
(5)
(5)
(3)
(3)
Tension
Ratio (F340/380)

Figure 5**.** Average peak responses of tension and fluorescence ratio induced by PDBu under various treatment in ovine fetal (A) and adult (B) MCA. Error bars represent ± SE. * $P < 0.01$ compared with control PDBu (3×10^{-6} M). #, $P < 0.01$ compared with IbTX (10^{-8} M) + PDBu (3×10^{-6} M). Numbers in parentheses refer to number of individual experiments for each protocol for adult and fetus, as tension and intracellular Ca^{2+} concentration ($[Ca^{2+}]_i$) were measured simultaneously. The *n* values (given with tension) also apply to corresponding fluorescence ratios. IbTX, iberiotoxin; Nif, nifedipine (10^{-5} M); EGTA (10^{-3} M).

Table 1. Peak responses of vascular tension and fluorescence ratio to various treatments.

	Fetus		Adult	
	ΔMaximum tension (g)	**ΔMaximum ratio $F_{340/380}$**	**ΔMaximum tension (g)**	**ΔMaximum ratio $F_{340/380}$**
K_{max} (120 mM)	1.51±0.07 (12)	0.22±0.02	2.51±0.24 (10)	0.19±0.02
PDBu (3 x 10^{-6} M)	0.31±0.03 (12)	-0.02±0.01	1.64±0.05 (10)	-0.03±0.01
PDBu (3 x 10^{-6} M) % K_{max}	20.16±1.56 (12)	-9.46±3.92	55.36±3.95 (10)	-18.44±3.19
IbTX (10^{-8} M) + PDBu	32.34±3.65 (6)*	12.27±2.14*	57.49±5.21 (5)	-18.27±2.82
IbTX (3 x 10^{-7} M) + PDBu	73.08±6.21 (6)*	50.12±5.05*	51.54±5.28 (5)	-17.57±2.50
EGTA (1 mM) + IbTX (3 x 10^{-7} M) + PDBu	17.91±1.52 (6)	-5.88±1.63	53.98±3.19 (3)	-9.56±3.63
Nifedipine (10^{-5} M) + IbTX (3 x 10^{-7} M) + PDBu	19.29±1.24 (3)	-11.13±2.10	56.48±3.98 (3)	-16.02±2.25
Gli (3 x 10^{-7} M) + PDBu	18.39±2.29 (7)	-9.96±3.51	52.28±5.64 (5)	-21.5±2.85
4-AP (10^{-3} M) + PDBu	21.34±2.68 (3)	-9.75±0.49	57.50±5.57 (3)	-19.53±1.88
$BaCl_2$ (10^{-5} M) + PDBu	18.93±2.16 (3)	-10.09±0.12	52.77±5.15 (3)	-18.68±1.19

Values are means ± SE expressed in absolute terms and as % maximal tension achieved to 120 mM K^+ (K_{max}; see METHODS for details). Tension and intracellular Ca^{2+} concentration ($[Ca^{2+}]_i$) were measured simultaneously; *n* values given with tension also apply to fluorescence ratio. Changes in maximum tension and in fluorescence ratio, $F_{340/380}$, from baseline; 4-AP, 4-aminopyridine; Gli, glibenclamide; IbTX, iberiotoxin. Numbers in parentheses, number of individual experiments for each protocol for fetus and adult. *P< 0.01 compared with control 3 x 10^{-6} M PDBu. See text for exact drug doses and timing.

Table 2. Patch-clamp electrophysiology

	Fetus		Adult	
	Before	**After**	**Before**	**After**
A. PKC single-channel:				
$V_{0.5}$ (mV)	24.40 ± 1.94 (6)	4.09 ± 2.11*	35.72 ± 2.32 (5)	15.17 ± 2.65*
$\Delta V_{0.5}$ (mV)	20.31		20.55	
Slope	11.28 ± 2.03	11.71 ± 2.16	11.66 ± 1.83	11.06 ± 2.63
Conductance (pS)	323.3 ± 4.8	324.0 ± 13.2	326.0 ± 7.4	320.0 ± 8.6
B. PDBu current-clamp:				
RMP (mV) at 150s	-41 ± 1.39 (10)	-48 ± 1.66*	-53 ± 1.76 (5)	-56 ± 1.20

Values are means ± SE expressed in absolute terms. Numbers in parentheses are number of individual experiments for each protocol of fetus and adult. Data are means ± SEM. *, $P < 0.05$ compared with before application of 5 U PKC catalytic subunit and 3 x 10^{-6} M PDBu respectively. A. PKC effects on BK single-channel activity. $V_{0.5}$, potential at which channels are half activated; $\Delta V_{0.5}$, change in half-activating potential after addition of 5 U PKC; Slope, voltage sensitivity. B. PDBu effects on myocyte resting membrane potentials (RMPs) in current-clamp mode. Potentials recorded before and 150 s after addition 3 x 10^{-6} M PDBu.

Fetal PDBu-induced transients required Ca^{2+} entry. To determine the extent to which the PDBu-induced transients of tension and $[Ca^{2+}]_i$ in the presence of IbTX were due to Ca^{2+} influx from bathing medium, we suspended the MCAs in nominally Ca^{2+}-free media containing 1 mM EGTA for 15 min, and then, added 3 x 10^{-7} M IbTX for 15 min. Then, PDBu was added in the presence of IbTX in the nominal absence of $[Ca^{2+}]_o$. As shown in Fig. 4 and Table 1, under these conditions, in neither fetal nor adult MCA was a significant increase in tension or fluorescence ratio observed in response to IbTX alone, nor were responses to subsequent addition of PDBu significantly different from responses in the absence of IbTX in Ca^{2+}-containing medium (Fig. 1).

To determine the extent to which the fetal increase in tension and $[Ca^{2+}]_i$ were, in fact, secondary to Ca^{2+} influx through L-type Ca^{2+} channels, we first administered nifedipine (10^{-5} M) and then, after 15 min, determined the responses to IbTX (3 x 10^{-7} M); and another 15 min later, determined the responses to PDBu in the presence of IbTX and nifedipine (*n*=3). Under these circumstances, in fetal and adult MCA, there was no significant increase in either tension or $[Ca^{2+}]_i$ in response to either IbTX alone or with PDBu (Figs. 4E-H). Figure 5 summarizes the average peak height responses of both tension and fluorescence ratio induced by PDBu under various treatments in fetal (Fig. 5A) and adult MCA (Fig. 5B). As is evident, the difference in responses for the two age groups is striking.

PKC increased single-channel BK activity. As judged by the appearance of transient tension and $[Ca^{2+}]_i$ increases in the presence of IbTX (Figs 2 and 3), PDBu appeared to activate BK channel activity, but only in fetal vascular segments. This suggested that PDBu activated fetal BK channels via a PKC-dependent process. To test

this hypothesis, we measured the direct effect of PKC on BK channel activity using excised MCA membrane patch preparations in inside-out, single-channel mode under voltage-clamp control (Fig. 6A). PKC activated BK channels from both adult and fetal preparations by left-shifting their voltage-activation curves toward more negative membrane potentials (*i.e.* left-shifting; Fig. 6B). Although PKC left shifted the $V_{0.5}$ values of adult and fetal channels to similar extents ($DV_{0.5}$ = −20 mV; Table 2A), under basal conditions (*i.e*. before addition of the PKC and ATP) the $V_{0.5}$ values for fetal channels were consistently more negative by ~11 mV than adult ($P<0.05$). Addition of either PKC or ATP alone produced negligible effects on channel activity (not shown). BK channel voltage sensitivities appeared similar before and after PKC treatment for both adult and fetal SMCs (Fig. 6B) and did not differ significantly between age groups, as slopes of the fitted curves were not significantly different (Table 2A).

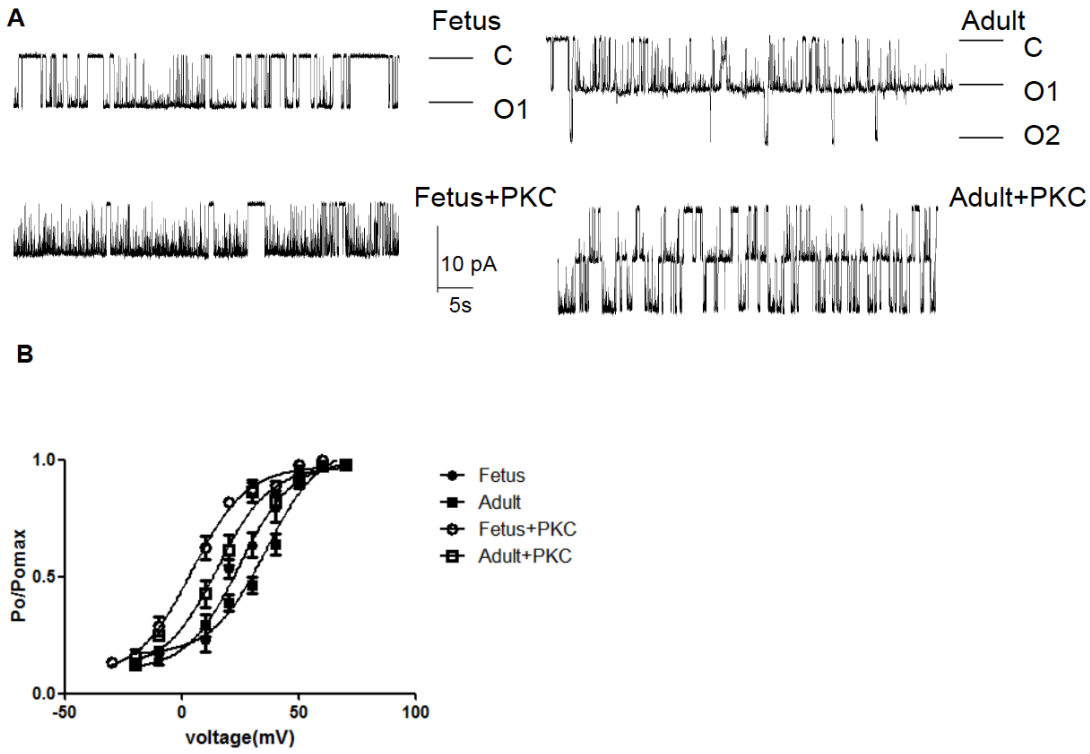

Figure 6. Effects of protein kinase C (PKC) on single-channel BK currents. A. Representative inside-out single-channel recordings from BK channels of ovine fetal and adult MCA myocytes before and after PKC (5 U/ml) treatment with ATP (5 x 10^{-4} M) present. Recording potential was 30 mV for both fetal and adult myocytes with 3 x 10^{-6} M calcium. B. Current/voltage relationship of PKC effects on fetal and adult MCA myocytes. Data are channel activities (Po) expressed relative to maximum channel activity (Po max). Solid lines indicate best-fit curves to the Boltzmann equation: $\boldsymbol{P}_o/\boldsymbol{P}_{o,max} = 1/\{1 + \exp[(\boldsymbol{V}_{½} - \boldsymbol{V}_m)/\boldsymbol{K}]\}$, where $\boldsymbol{V}_{½}$ is the membrane potential ($\boldsymbol{V}_m$) required for half-maximal activation of the channels and $\boldsymbol{K}$ is the logarithmic voltage sensitivity (change in voltage required for an $\boldsymbol{e}$-fold increase in activity). Data are means ± SEM.

PDBu hyperpolarized myocyte resting membrane potentials. Because PDBu activates endogenous PKC activity in MCAs, as evidenced by sustained Ca^{2+}-independent contraction (Figs 1 - 3), and because PKC activates BK channels (Fig. 6), we hypothesized that PDBu should hyperpolarize myocyte membrane potentials via activation of BK channels. To test this prediction, we measured resting membrane potentials by on-cell current clamp from isolated, intact smooth myocytes before and following the addition of 3×10^{-6} M PDBu (Fig. 7). Resting membrane potentials from fetal cells before PDBu were ~+12 mV less polarized than from adult ($P < 0.01$; Table 2B), which is consistent with our previous measurements from basilar artery SMCs (17). Within 30 sec of adding PDBu the membrane potentials of both adult and fetal cells decreased (hyperpolarized). However, this hyperpolarizing effect of PDBu only persisted about 30 s in the adult cells.

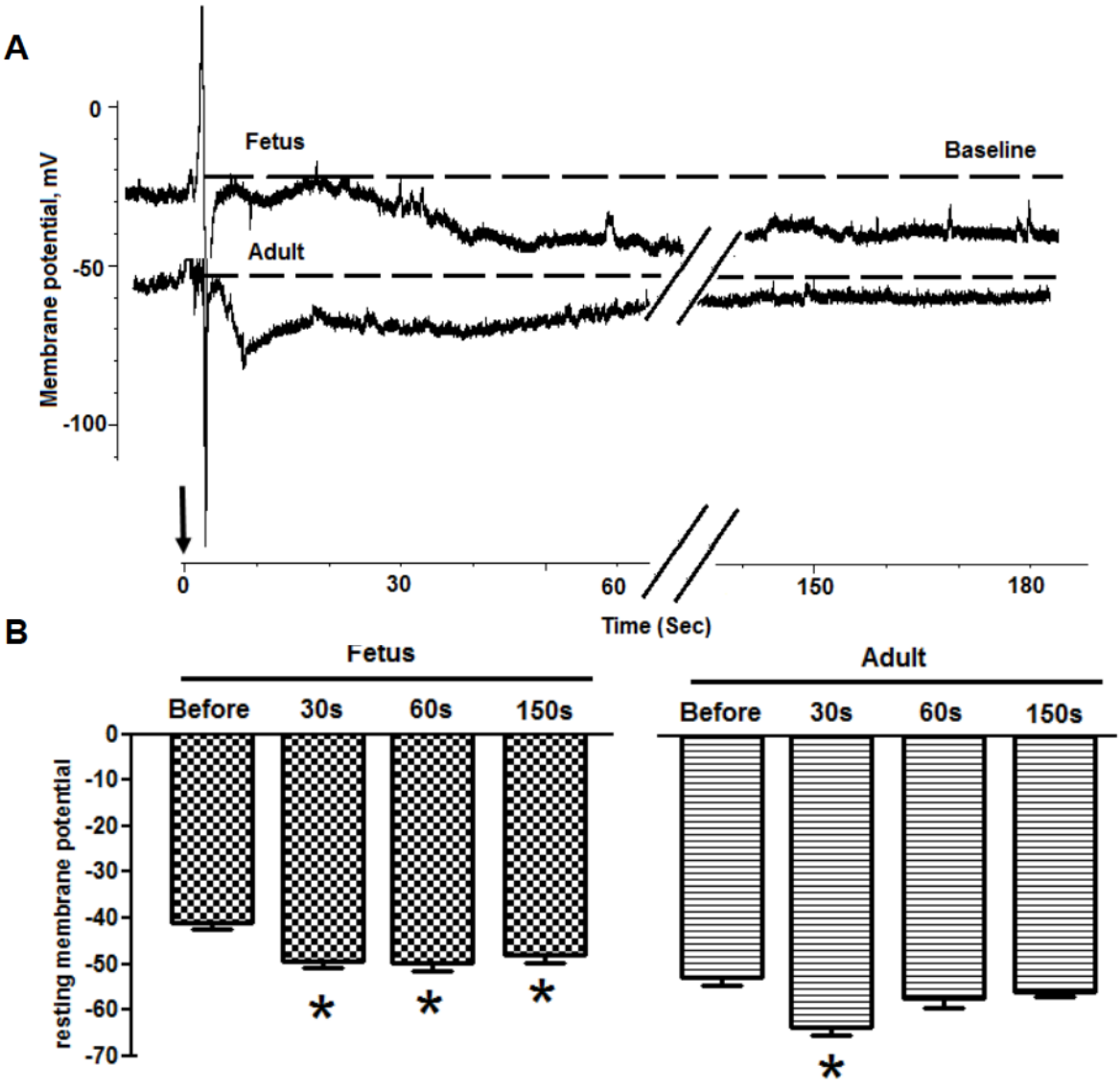

Figure 7. Effects of PDBu on myocyte resting membrane potentials. A. Representative continuous recordings of membrane potential (mV) from fetal and adult MCA myocytes following exposure to 3 x 10^{-6} M PDBu. Rapid initial hyperpolarizations in both groups during initial 10 sec were followed by slower returns to baseline in adult cells, while fetal hyperpolarizations persisted longer. B: Resting membrane potentials of fetal and adult MCA myocytes before and 30, 60, and 150 s after adding 3 x 10^{-6} M PDBu. Data are means ± SEM. *, $P<0.05$ difference from baseline before addition of PDBu.

Other K^+ channel inhibitors did not alter PDBu effects. Glibenclamide in half-log doses (10^{-9} to 10^{-6} M) to inhibit K_{ATP} channels, 4-AP in half-log doses (10^{-8} to 10^{-3} M) to inhibit K_v channels, and 10^{-5} M $BaCl_2$ to inhibit K_{IR} channels showed no effects on tension or $[Ca^{2+}]_i$ on either adult or fetal MCAs (data not shown). However, 3 x 10^{-3} M 4-AP slightly increased both tension and $[Ca^{2+}]_i$ and 10^{-2} M 4-AP markedly increased both variables in the fetus and adult (data not shown). To examine further the role of these K^+ channel inhibitors in PDBu-induced vessel tension and $[Ca^{2+}]_i$, we pretreated MCA segments with individual channel inhibitor for 15 min, and then determined the PDBu-induced vessel responses in the presence of the inhibitor. Neither tension nor fluorescence ratio changed significantly in either fetal or adult MCAs pretreated with 3 x 10^{-7} M glibenclamide, 10^{-3} M 4-AP, or 10^{-5} M $BaCl_2$, as summarized in Table 1.

Discussion

Our findings confirmed our previous work (26) that PDBu increases vessel tone with no significant increase in $[Ca^{2+}]_i$ in both adult and fetal MCA (Fig. 1). In addition, we showed that the selective BK channel blocker, IbTX, dose-dependently increases vessel tension and $[Ca^{2+}]_i$, and these effects are greater and more sensitive in fetal vessels (Fig. 3A and B). Moreover, IbTX pre-disposed PDBu to induce transient responses in fetal MCA tension and $[Ca^{2+}]_i$, but not in adult (Figs 2, 3C and D). Removing extracellular Ca^{2+} or inhibiting L-type Ca^{2+}-channels blocked the IbTX-induced transients of the adult and fetus, as well as the fetal PDBu-induced transients in the presence of IbTX (Fig. 4). Other K^+ channel inhibitors produced no apparent effects before or after application of PDBu. These results suggest that in fetal MCAs, PDBu-induced PKC stimulation activates BK channels to inhibit voltage-dependent Ca^{2+} channels by hyperpolarizing the myocyte membrane. We verified this hypothesis using patch-clamp electrophysiology to show that PDBu produces a sustained hyperpolarization only in fetal myocytes (Fig 7). In addition, we showed that direct application of PKC to the cytoplasmic face of inside-out membrane patches activated BK channel currents by left-shifting the voltage/activation curves of fetal preparations more than adult (Fig. 6). These findings are consistent with the Ca^{2+} and tension effects measured on intact vascular segments.

PDBu alters contractile and $[Ca^{2+}]_i$ responses. The effect of PKC on vascular contractility is well documented. PKC can feedback-inhibit phospholipase C to attenuate agonist-induced increases in inositol 1,4,5 trisphosphate ($Ins(1,4,5)P_3$), $[Ca^{2+}]_i$, and contraction (10). In addition, PKC activation *per se* can induce a slow and sustained

contraction that is $[Ca^{2+}]_i$ independent; possibly due to increased sensitivity of the contractile apparatus to Ca^{2+} (10, 23, 32). PKC also may modulate vascular smooth muscle Ca^{2+} sensitivity to α-adrenergic and other agonists (29).

Phorbol esters, such as PDBu, appear to activate PKC by substituting for diacylglycerol (DAG) (31). At normal basal $[Ca^{2+}]_i$ levels, DAG activates PKC by increasing its affinity for Ca^{2+} and phosphatidylserine (28). In the present study, PDBu significantly increased cerebral vascular contractility in both age groups, which is consistent with our previous studies (23, 38). In fetal and adult MCA, PDBu increases the maximum amplitudes of vessel tension by ~20% K_{max} and ~55% K_{max}, respectively. To confirm the selectivity of PDBu's effects, we showed that 4α-PMA, an inactive PDBu chemical homologue, had no effect on vessel contractility. In addition, PDBu either produced no change or slightly decreased $[Ca^{2+}]_i$, which is consistent with reports that PKC activation stimulates Ca^{2+} extrusion (6, 7). Our finding that PDBu increases tension with little or no increase in fluorescence ratio suggests PKC increases myofilament Ca^{2+} sensitivity in fetal and adult cerebral arteries.

PDBu effects in fetus involves BK channels. K^+ channel activity is the major determinant of the resting membrane potential. When K^+ channels are activated, the associated K^+ efflux causes hyperpolarization, which inhibits voltage-gated Ca^{2+} channels, decreases $[Ca^{2+}]_i$, and promotes vascular relaxation (16, 26). Although different vascular beds express several classes of K^+ channels at varying densities, in most arteries BK channels predominate in setting vascular tone and the resting membrane potential (26). Because of their large conductance, high density, and localization to sites of Ca^{2+} sparks, BK channels play a key role in regulating the resting membrane potential, and

provide an important repolarizing, negative-feedback mechanism to balance voltage-dependent Ca^{2+} entry. BK channel activation produces membrane hyperpolarization and subsequent vasorelaxation (26).

Several protein kinases modulate BK channel activity. In general, PKC inhibits SMC BK channels, whereas cAMP-dependent protein kinase A (PKA) and cGMP-dependent protein kinase G (PKG) activate BK channels (18, 33). Although several studies have investigated the effect of PKC on BK channels, in cerebral arterial smooth muscle the relationship between PKC and BK channel modulation is relatively unknown. In coronary artery smooth muscle, PKC blocks BK channel activation (25). PKC also inhibits BK channels in rat tail artery (34) and in cultured rat mesenteric artery (36). Nevertheless, in pulmonary artery, PKC activates BK channels to dampen pulmonary vessel contractility (2). In the present study, application of the highly selective BK channel inhibitor, IbTX, elicited vessel contraction and increased $[Ca^{2+}]_i$, suggesting that these channels are active under basal conditions and play a key role in maintaining normal cerebral vascular tone.

From the dose-response relationships of IbTX-transients (Figs 3A and B), the maximum IbTX-transients for both tension and $[Ca^{2+}]_i$ were significantly greater in the fetus than in the adult. This suggests that BK channels are more active in fetal MCAs than in adult, which is consistent with our previous studies in basilar arteries (17). The pD2, an index of tissue "sensitivity", was also greater in the fetus than in the adult. In previous studies, we demonstrated that resting membrane potentials of fetal basilar artery myocytes were significantly more depolarized than those of adults (18). The present study confirms this observation in MCA myocytes (Fig. 7). Because fetal cerebral

arteries are more depolarized, our results suggest that lower doses of IbTX are needed to activate voltage-gated L-type Ca^{2+} channels. It is also possible that the greater sensitivity of the fetal BK channels to IbTX is related to the fact that there are more L-type Ca^{2+} channels in fetal vessel SMCs than in the adult (3).

In vascular smooth muscle, PKC is coupled directly to plasma membrane L-type Ca^{2+} channels to increase Ca^{2+} influx or is coupled indirectly by inhibiting BK channels that activate the Ca^{2+} channels (9). In our study, PDBu produced no increase of $[Ca^{2+}]_i$ in either developmental age group. Following 10^{-8} M IbTX treatment, however, PDBu produced transient increases in tension and fluorescence ratio, but only in the fetus. This suggests that PDBu promotes BK channel activation in fetal MCAs. Consistent with this hypothesis, we found that PDBu hyperpolarized isolated fetal myocytes in the absence of IbTX, but not in adult cells. Furthermore, we have shown that PKC added in inside-out membrane preparations activates BK channels. Another finding of the present study was that the increase of $[Ca^{2+}]_i$ and vascular tension following IbTX, with or without PDBu, was eliminated in the presence of zero extracellular Ca^{2+} or L-type Ca^{2+} channel blockade. This suggests that the increased $[Ca^{2+}]_i$ resulted from Ca^{2+} influx through voltage-gated, L-type Ca^{2+} channels.

BK channel properties change with development. One possible mechanism to account for these age differences relates to BK channel properties with development. For instance, in related studies, we have reported that in basilar artery smooth muscle cells, BK channel activity of the fetus was much greater than that of the adult (17). This increased activity was associated with a lower BK channel Ca^{2+} set point (Ca_0), and a greater affinity of the channel for Ca^{2+}(18), which allows fetal myocytes to hyperpolarize

the cell in response to smaller changes in sub-plasmalemmal [Ca^{2+}] than the adult SMC. In this manner, the lower BK channel Ca_0 may act as a protective mechanism to govern the membrane potential of fetal myocytes, which is already more depolarized than that of the adult. Subsequently, we demonstrated that the Ca_0 change during development resulted from different levels of BK channel phosphorylation (18). In fetal cerebral artery, BK channel-associated PKG activity is three times greater in BK channels from fetal than adult myocytes (19).

In pulmonary arterial smooth muscle, PKC indirectly activates BK channels by phosphorylating PKG, which suggests a unique signaling mechanism for vasodilatation (2). If PKC activates the BK channel in the present study through PKG-related phosphorylation, as in pulmonary arteries, then our observation of PDBu activating BK channels in fetal, but not adult, MCAs may be explained by the three-fold higher channel-associated PKG activity in the fetus (19). Thus, on the one hand, PKC activation elicits vessel contraction in fetal cerebral artery by increasing the myofilament Ca^{2+} sensitivity through a Ca^{2+}-independent pathway (see diagram in Fig. 8). On the other hand, PKC may activate BK channels to facilitate vessel relaxation due to hyperpolarization, while stemming Ca^{2+} influx. The possible opposing effects of PKC in the fetus (Fig. 8) may explain why the PDBu-induced tension was ~20% K_{max} in fetal MCAs in contrast to ~55% K_{max} in adult. Our findings suggest that the weaker vasoconstriction effects of PKC activation in fetal MCAs may be due, in part, to a combination of PKC activating BK channels, as reported here, possibly due to higher levels of channel-associated PKG activity (19) and the higher affinity for Ca^{2+} of fetal BK channels (17, 18). A hierarchal interaction of protein kinases for BK channels invites further study.

Conclusions and Perspective

During the course of development from fetus to newborn to adult, the cerebral blood vessels undergo striking changes, both structurally and functionally. These include the levels of specific PKC isozymes and PKC-related mechanisms of contraction. Besides the role of PKC in increasing calcium sensitivity in SMCs, its vascular actions may, in part, be attributed to effects on K^+ channels. In the present study, based on the pharmacological selectivity of the K^+-channel inhibitors, we conclude that, while PKC produces contraction of cerebral arteries in both fetus and adult, its effect on BK channel activity differed significantly between the two age groups. Figure 8 encapsulates our results, which suggest that in fetal, but not adult, cerebral arterial smooth muscle, PDBu-induced PKC stimulation activates BK channels. Although the mechanism of PKC's effect on BK channel activity is, as yet, unclear, we speculate that PKC's activation of cerebral artery BK channels may reflect a mechanism to protect fetal vessels from Ca^{2+} overload during PKC-mediated cerebral artery contraction due to its more depolarized resting membrane potential (Fig. 7). Further studies are needed to clarify the role of PKC, including the role of PKC isozymes and other protein kinases, on BK channel function.

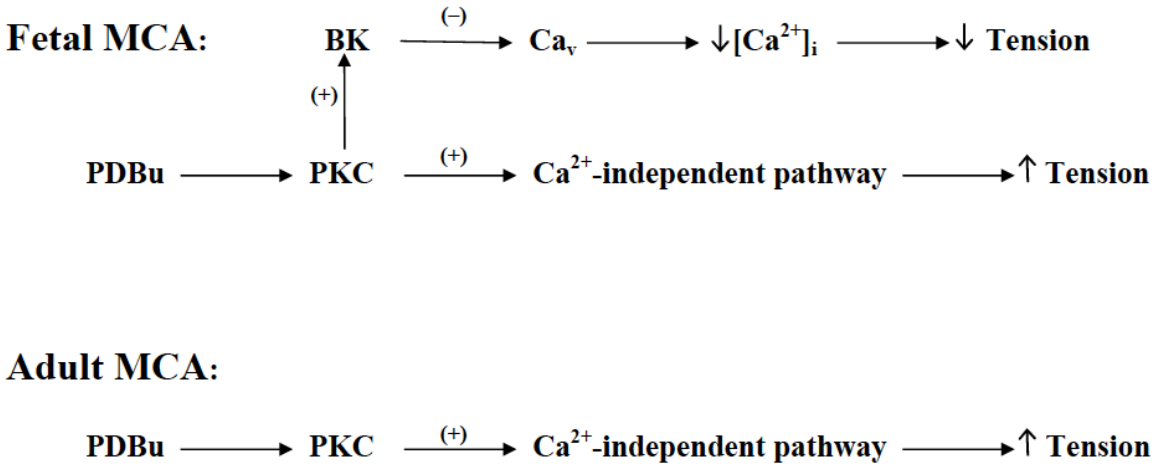

Figure 8. Contrasting schematic diagrams of proposed PDBu-induced pathways in fetal and adult middle cerebral arteries (MCA). As depicted, in adult MCA, PDBu activates PKC to increase tension via a Ca^{2+}-independent pathway. In contrast, in fetal MCA, PDBu-activated PKC can activate the BK channel to inhibit the L-type Ca^{2+} channel (Ca_v) via a sustained membrane hyperpolarization to decrease Ca^{2+} influx and $[Ca^{2+}]_i$, and therefore tension, while at the same time stimulating the Ca^{2+}-independent pathway and increasing tension as outlined above.

References

1. Barman SA. Potassium channels modulate canine pulmonary vasoreactivity to protein kinase C activation. *Am J Physiol Lung Cell Mol Physiol* 277: L558–L565, 1999.

2. Barman SA, Zhu S, and White RE. PKC activates BKCa channels in rat pulmonary arterial smooth muscle via cGMP-dependent protein kinase. *Am J Physiol Lung Cell Mol Physiol* 286: L1275–L1281, 2004.

3. Blood AB, Zhao Y, Long W, Zhang L, Longo LD. L-type Ca^{2+} channels in fetal and adult ovine cerebral arteries. *Am J Physiol Regulatory Integrative Comp Physiol* 282: R131–R138, 2002.

4. Boland LM and Jackson KA. Protein kinase C inhibits Kv1.1 potassium channel function. *Am J Physiol Cell Physiol* 277: C100–C110, 1999.

5. Bonev AD, Nelson MT. Vasoconstrictors inhibit ATP-sensitive K^+ channels in arterial smooth muscle through protein kinase C. *J Gen Physiol* 108: 315–323, 1996.

6. Broad LM, Cannon TR, Short AD, Taylor CW. Receptors linked to polyphosphoinositide hydrolysis stimulate Ca^{2+} extrusion by a phospholipase C-independent mechanism. *Biochem J* 342: 199–206, 1999.

7. Carafoli E. Calcium pump of the plasma membrane. *Physiol Rev* 71: 129–153, 1991.

8. Chrissobolis S, Sobey CG. Inhibitory effects of protein kinase on inwardly rectifying K^+- and ATP-sensitive K^+ channel-mediated responses of the basilar artery. *Stroke* 33:1692–1697, 2002.

9. Cobine CA, Callaghan BP, Keef KD. Role of L-type calcium channels and PKC in active tone development in rabbit coronary artery. *Am J Physiol Heart Circ Physiol* 292:3079-3088, 2007.

10. Danthuluri NR and Deth RC. Phorbol ester-induced contraction of arterial smooth muscle and inhibition of α-adrenergic response. *Biochem Biophys Res Commun* 125: 1103–1109, 1984.

11. Fakler B, Brandle U, Glowatzki E, Zenner H-P, Ruppersberg JP. Kir 2.1 inward rectifier K^+ channels are regulated independently by protein kinases and ATP hydrolysis. *Neuron* 13: 1413–1420, 1994.

12. Faraci FM, Sobey CG. Role of potassium channels in regulation of cerebral vascular tone. *J Cereb Blood Flow Metab* 18: 1047–1063, 1998.

13. Grynkiewicz G, Poenie M, Tsien RY. A new generation of Ca^{2+} indicators with greatly improved fluorescence properties. *J Biol Chem* 260: 3440–3450, 1985.

14. Henry P, Pearson WL, Nichols CG. Protein kinase C inhibition of cloned inward rectifier (HRK1/KIR 2:3) K^+ channels expressed in *Xenopus oocytes*. *J Physiol* 495: 681–688, 1996.

15. Jiang MJ, Morgan KG. Intracellular calcium levels in phorbol ester-induced contractions of vascular muscle. *Am J Physiol* 253: H1365–H137, 1987.

16. Kitazono T, Faraci FM, Taguchi H, Heistad DD. Role of potassium channels in cerebral blood vessels. *Stroke* 26: 1713–1723, 1995.

17. Lin MT, Hessinger DA, Pearce WJ, Longo LD. Developmental differences in Ca^{2+}-activated K^+ channel activity in ovine basilar artery. *Am J Physiol Heart Circ Physiol* 285: H701–H709, 2003.

18. Lin MT, Hessinger DA, Pearce WJ, Longo LD. Modulation of BK channel calcium affinity by differential phosphorylation in developing ovine basilar artery myocytes. *Am J Physiol Heart Circ Physiol* 291: H732-H740, 2006.

19. Lin MT, Longo LD, Pearce WJ, Hessinger DA. Ca^{2+}-activated K^+ channel - associated phosphatase and kinase activities during development. *Am J Physiol Heart Circ Physiol* 289: H414–H425, 2005.

20. Long W, Zhang L, Longo LD. Cerebral artery K_{ATP}- and K_{Ca}-channel activity and contractility: changes with development. *Am J Physiol Regul Integr Comp Physiol* 279: R2004–R2014, 2000.

21. Long W, Zhao Y, Zhang L, Longo LD. Role of Ca^{2+} channels in NE-induced increase in $[Ca^{2+}]i$ and tension in fetal and adult cerebral arteries. *Am J Physiol Regul Integr Comp Physiol* 277: R286–R294, 1999.

22. Longo LD, Ueno N, Zhao Y, Pearce WJ, Zhang L. Developmental changes in a1-adrenergic receptors, IP3 responses, and NE-induced contraction in cerebral arteries. *Am J Physiol Heart Circ Physiol* 271: H2313–H2319, 1996.

23. Longo LD, Zhao Y, Long W, Miguel C, Windemuth RS, Cantwell A-M, Nanyonga AT, Saito T, Zhang L. Dual role of PKC in modulating pharmacomechanical coupling in fetal and adult cerebral arteries. *Am J Physiol Regul Integr Comp Physiol* 279: R1419–R1429, 2000.

24. Mason MJ, Simpson AK, Mahaut-Smith MP, Robinson HP. The interpretation of current-clamp recording in the cell-attached patch-clamp configuration. *Biophys J* 88: 739–50, 2005.

25. Minami K, Fukuzawa K, Nakaya Y, Xeng XR, Inoue I. Mechanism of activation of the Ca-activated K^+ channel by cyclic AMP in cultured porcine coronary artery smooth muscle cells. *Life Sci* 53: 1129–1135, 1993.

26. Nelson MT, Quayle JM. Physiological roles and properties of potassium channels in

arterial smooth muscle. *Am J Physiol Cell Physiol* 268: C799–C822, 1995.

27. Nishizuka Y. The family of protein kinase C for signal transduction. *JAMA* 262: 1826–1833, 1989.

28. Nishizuka Y. The role of protein kinase C in cell surface signal transduction and tumor production. *Nature* 308: 693–698, 1984.

29. Nishimura J, Moreland S, Moreland RS, van Breemen C. Regulation of the Ca^{2+} force relationship in permeabilized arterial smooth muscle. *Adv Exp Med Biol* 304: 111–127, 1991.

30. Pearce WJ, Hull AD, Long DM, Longo LD. Developmental changes in ovine cerebral artery composition and reactivity. *Am J Physiol Regul Integr Comp Physiol* 261: R458– R465, 1991.

31. Rasmussen H, Calle R, Ganesan S, Smallwood J, Throckmorton D, Zawalich W. *Protein Kinase C: Role in Sustained Cellular Responses*. Chichester, UK: Ellis Horwood, 1991.

32. Rasmussen H, Takuwa Y, and Park S. Protein kinase C in the regulation of smooth muscle contraction. *FASEB J* 1: 177–185, 1987.

33. Schubert R, Nelson M. Protein kinases: tuners of the BKCa channel in smooth muscle. *Trends in Pharmacol Sci* 22: 505–512, 2001.

34. Schubert R, Noack T, Serebryakov VN. Protein kinase C reduces the KCa current of rat tail artery smooth muscle cells. *Am J Physiol Cell Physiol* 276: C648–C658, 1999.

35. Standen NB, Quayle JM. K^+ channel modulation in arterial smooth muscle. *Acta Physiol Scand* 64: 549–557, 1998.

36. Taguchi K, Kaneko K, and Kubo T. Protein kinase C modulates Ca^{2+}-activated K^+ channels in cultured rat mesenteric artery smooth muscle cells. *Biol Pharm Bull* 23: 1450–1454, 2000.

37. Walsh MP, Andrea JE, Allen BG, Clement-Chomienne O, Collins EM, Morgan KG. Smooth muscle protein kinase C. *Can J Physiol Pharmacol* 72: 1392–1399, 1994.

38. Zhao Y, Zhang L, Longo LD. PKC-induced ERK1/2 interactions and downstream effectors in ovine cerebral arteries. *Am J Physiol Regul Integr Comp Physiol* 289: R164–R171, 2005

CHAPTER FOUR

INTEGRATIVE DISCUSSION AND CONCLUSION

Dissertation Findings and Discussion

We examined the major possible mechanisms for the left shift of the BK channel I-V relationship in native basilar artery myocytes from the two LTH groups. These mechanisms included: differential expression of the accessary BK β-1 subunit; differential phosphorylation of the BKα subunit; and splice variation of the BKα subunit. Using molecular cloning, heterologous expression, and patch-clamp electrophysiology techniques, we elucidated a mechanism that, at least in part, contributes to the differences we observed between channels from native normoxic and LTH myocytes.

The results of our molecular cloning revealed a single-nucleotide transversion in the BKα transcript at the possible transcription level (mRNA level) in myocytes isolated from LTH adult basilar arteries as compared to the normoxic "wild type". This nucleotide transversion occurred in the second codon position; thereby producing a change from a hydrophobic to hydrophilic charged amino acid, in which a valine was switched to a glutamate at position 86 of the BKa subunit. The resulting amino acid substitution was located within the intracellular S0-S1 loop region. In the near-term fetus, however, we did not find such switching. Additional experiments are yet needed to confirm and possibly extend this finding in the fetus.

To examine further the functional consequences of such single amino acid substitution, we performed single-channel, voltage-clamp studies on both normoxic and LTH BK transcripts. We observed that in transfected HEK293 cells, which normally do not express BK channels, the expressed normoxic and LTH adult BK isoforms

(transcripts) showed similar functional differences that characterized their counterpart channels in native normoxic and LTH myocyte preparations. Firstly, the LTH isoform exhibited a left shifted current/voltage (I-V) relationship toward more negative potentials, compared to the expressed normoxic isoform, thereby making the LTH isoform channels more voltage sensitive. This mirrored the I-V left shifting observed in the native LTH channels compared to native normoxic channels. Secondly, the LTH isoform channels exhibited a lower calcium set point (Ca_0) compared with the expressed normoxic isoform channels, which was also a distinguishing feature of BK channels between the LTH and normoxic myocytes. By using exogenous alkaline phosphatase alone to de-phosphorylate the channels or followed with protein kinase G to phosphorylate the channels, we showed that the differences between the LTH and normoxic isoforms were independent of channel phosphorylation status, as was the case for the respective native myocytes. Thus, the V87E substitution in the adult's acclimatization to high-altitude, long-term hypoxia (LTH) can account for the major qualitative functional differences between BK channels from normoxic and LTH basilar artery smooth muscle.

That such a relatively small sequence change in BKα could so dramatically affect channel function and, in particular, contribute teleologically to increase cerebral blood flow in response to "migration" to high-altitude, long-term hypoxia, raises questions of whether such channel changes may occur in other hypoxia-tolerant species. To examine this aspect, we undertook a bioinformatics search of GenBank BK channel sequences. We found that the presence of threonine in position 86 of BKα occurs infrequently across the phylogenetic tree, but when it does occur it is most often occurs in hypoxic-tolerant species. The result of our bioinformatics search is shown in the following listing:

Animals sharing T86 within a DEKEETV-like motif in BKα S0-S1 loop:

Key: Hypoxia-tolerant *Hypoxia-intolerant

High-altitude mammals

Fam. Bovidae

Sheep (*Ovis aries*)

Goat (*Capra hircus*)

Tibetan antelope (*Pantholops hodgsonii*)

*Cow (*Bos taurus*)

Diving mammals (Fam. Ungulata)

Walrus (*Odobenus rosmarus*) DEKEEAT

*African elephant (*Loxodonta africana*)

Subterranean mammals

Cape golden mole (*Chrysoshloris asiatica*)

Diving reptiles

Chinese soft shelled turtle (*Pelodiscus sinensis*)

Turtle (*Trachemys scripya*)

Painted turtle (*Chrysemys picta bellii*)

Alligator (*Alligator mississippiensis*) DEKEETV

Marine invertebrates - - + - -(=)

Sea anemone (*Aiptasia pallida*)

+ + +ET-

NQDDET-

+ + - - -(=)

Using confocal microscopy, we found that, while the adult myocytes expressed slightly more BKα than fetal myocytes, in both normoxic and LTH fetal basilar arteries, the BK channels were two to three-fold more clustered on the cell surface than their adult counterparts. We then used fluorescent cholera toxin binding subunit to identify and count lipid rafts on basilar artery myocytes. We found that while the fetal myocytes showed slightly more clusters of cholera toxin, the fetuses had more than twice as many BK channel clusters co-localized to clustered cholera toxin than the adults. This suggests that the BK channels of fetal cerebral myocytes are localized at sites of calcium "sparks" (caveolae) where their activation may be more coupled to spark activity. Further co-localization and functional experiments are needed to test this hypothesis, however.

In summary, LTH adults we observed left shifting of the BK channel I-V curve and increased affinity for intracellular calcium, independent of phosphorylation status. We found that these intrinsic functional differences in channel activity could be accounted for by position a V→E switching at position 87. In the both normoxic and LTH fetus, however, we observed that increased BK channel activity, compared to the normoxic adult controls was due to, in part, increased BK channel clustering and co-localization to lipid rafts, which are sites of increased calcium spark activity.

Understanding such LTH adaptive mechanisms in sheep may help us understand mal-adaptive responses to LTH in humans. However, the mechanism by which V→E switching in the LTH adult occurs is unknown at the present and begs further investigation. Attempts by us to replicate this process *in vitro* using cultured vascular segments under hypoxic conditions (1% oxygen) failed. Possible mechanisms of

switching may include: RNA editing (HIF; A-I); alternative splicing involving very short exons; or genetic predisposition involving SNPs; same switching in SCD).

Dissertation Conclusions

- In adult, LTH-induced V→E switching makes BK channels more active at RMPs and more sensitive to $[Ca^{2+}]_i$. This leads to vasodilation and increased cerebral blood flow.
- In fetus, BK channel clustering in lipid rafts may favor greater coupling to Ca^{2+} sparks to offset more depolarized RMP. This leads to vasodilation and increased cerebral blood flow.
- DEEKEETV motif may be a model for hypoxia-tolerant BKα subunit across a wide range of the Animal Kingdom. Its structure-function relation to the coupling of voltage and calcium sensing by BK channels also raises the level of interest of the S0-S1 loop in relation to the voltage-sensing S4 transmembrane domain.

Future Directions

1. To extend our current observations that fetal cerebrovascular BK channels co-localize as clusters at lipid rafts, and determine if such rafts are, indeed, sites of calcium spark activity and determine if fetal coupling of BK channel activity to spark activity is greater than in adults. This can best be done by measuring both calcium spark activity using confocal microscopy while measuring spontaneous transient outward currents (STOCs) in perforated-patch, whole-cell preparations.
2. To study the beta subunit co-localization with alpha subunit using co-immunoprecipitation or confocal microscopy.

3. *In vitro* cell culture or tissue/organ culture to study the mechanisms of V→E switching.
4. To examine other tissue types to see if they undergo BKα V→E switching.